SHRP-ID/UFR-91-524

Evaluation of Electrochemical Impedance Techniques for Detecting Corrosion on Rebar in Reinforced Concrete

D.D. Macdonald, Y.A. El-Tantawy,
R.C. Rocha-Filho, M. Urquidi-Macdonald
SRI International
Menlo Park, California

Strategic Highway Research Program
National Research Council
Washington, DC 1994

SHRP-ID/UFR-91-524
Contract ID008
Product No.: 4003

Program Manager: *K. Thirumalai*
Project Managers: *Ataur Bacchus and Marty Laylor*
Production Editor: *Marsha Barrett*

September 1991
Reprint March 1994

key words:
concrete
corrosion
electrode
impedance
rebar
ULFACIS
ZSCAN

Strategic Highway Research Program
National Academy of Sciences
2101 Constitution Avenue N.W.
Washington, DC 20418

(202) 334-3774

50/NAP/394

Acknowledgments

The research described herein was supported by the Strategic Highway Research Program (SHRP). SHRP is a unit of the National Research Council that was authorized by section 128 of the Surface Transportation and Uniform Relocation Assistance Act of 1987.

Contents

List of Figures

List of Tables

Abstract

The report examines the applicability of ultralow frequency ac impedance spectroscopy (ULFACIS) for characterizing corrosion of rebar in concrete. The study focuses on demonstrating that ULFACIS could be used to locate and characterize corrosion nondestructively in reinforced concrete structures. A key issue was to establish whether ULFACIS could be used to determine the polarization resistance, and hence the corrosion rate, of the steel rebar.

Impedance data were obtained for concrete test slabs containing three equally spaced rebars. The slabs contained ports exposing the rebar at regular distances so that high local corrosion rates could be induced by the addition of hydrochloric acid to simulate variations in corrosion rates along the rebar. The impedance function was successfully demonstrated to be sensitive to the presence and extent of rebar corrosion. Tests performed for one, two, and three corrosion sites showed that ULFACIS can be used to spatially resolve areas of corrosion activity on the rebar.

The researchers developed an electrical transmission line model to describe the experimental data. The fitting of this model showed that changes in the impedance function can be understood in terms of changes in the parameters of the transmission line. A procedure (ZSCAN) was developed for extracting the polarization resistance from the measured impedance data, so that the corrosion rate can be measured. ZSCAN was tested on theoretically generated and experimental data. The analytical techniques for measuring the polarization resistance provide a basis for the development of a practical corrosion rate "meter" for use in the field.

Executive Summary

The corrosion of steel reinforcing bar (rebar) in concrete represents a serious threat to the nation's infrastructural systems. This corrosion phenomenon developed rapidly after the widespread use of deicing salts on roads and bridges became commonplace in the 1960s and 1970s, particularly in the northeastern states. A particularly important problem is the in situ detection of corroding rebar before damage becomes evident as spalling of concrete from the rebar, or as rust weeps from the surface. This report explores an electrochemical technique, ultralow frequency ac impedance spectroscopy (ULFACIS), as a means of detecting, locating, and characterizing corroding steel rebar in concrete before damage becomes evident to an observer.

ULFACIS is based on a prior theoretical study that indicated that corrosion may be located by imposing a sinusoidal current at a monitoring point on the surface to measure the rebar/concrete impedance (ratio of voltage to current) as a function of frequency (typically from 10^{4} to 10^{-3} Hz). The ability of ULFACIS to locate corrosion was predicted on the basis that the distance traveled by the ac wave down the rebar increases as the frequency is lowered. At some characteristic frequency, the ac wave intersects the corroding region resulting in a sudden, but perceptible change in the measured impedance. The researchers surmised that the impedance could be used to estimate the true polarization resistance of the rebar from which the corrosion rate can be calculated. If so, ULFACIS could prove to be a powerful in situ technique for rapidly surveying concrete structures to detect corrosion and to assess the extent of damage before the structural integrity is compromised.

This exploratory work accomplished the following:

- Experimentally demonstrated that the electrical impedance of the rebar/ concrete system is sensitive to the presence of corrosion on rebar in reinforced concrete structures.

- Demonstrated that the electrical properties of rebar in concrete may be accurately modeled using transmission line electrical equivalent circuits consisting of passive elements (resistors and capacitators). This finding is extremely important because it provides a readily manipulated model that can be used to calculate the distance of corroding regions from the monitoring point from the frequency of the applied ac and the properties of the concrete.

- Confirmed the theoretical prediction that the phase angle at low frequencies (1.0 to 0.01 Hz) is the most sensitive indicator of the presence of corrosion.

- Demonstrated that, by scanning the reference electrode (which is used to detect the alternating voltage) across the surface, ULFACIS can be used to spatially resolve areas of corrosion activity on rebar and hence can form the basis of a practical method of surveying corrosion damage to concrete structures.

- Developed a procedure (ZSCAN) for extracting the corrosion rate of the rebar from measured impedance data. This procedure circumvents the hitherto unresolved problem for electrochemical techniques of the area being sampled depending on the frequency of the electrical perturbation or the time at which the response is probed.

Although this work was exploratory, in keeping with the philosophy of the IDEA Program, it has demonstrated the feasibility of practical techniques for the in situ locating and characterizing of corrosion on rebar ULFACIS), and for estimating rebar corrosion rate (using ZSCAN) in concrete structures before damage becomes externally evident. The development and field-testing of practical corrosion surveying instruments based on the exploratory work described herein will be carried out in Phase II.

1

INTRODUCTION

The corrosion of steel reinforcing bar in concrete represents a serious threat to the nation's infrastructural systems.[1-3] This corrosion phenomenon developed rapidly after the use of deicing salt, particularly on roads and highways in the northeast, became commonplace in the 1960s and 1970s. Furthermore, the use of calcium chloride ($CaCl_2$) to accelerate the setting of portland cement in cold climates guarantees the presence of chloride ion in numerous concrete structures, including bridges, roads, buildings, and canals. The fundamental cause of corrosion of rebar, which may eventually cost several tens of billions of dollars in this country, has been shown in numerous laboratory studies and field investigations to be chloride-induced depassivation of steel.

The work reported here was carried out to assess the ability of electrochemical techniques to detect corrosion on reinforcing bar (rebar) in concrete. Electrochemical techniques are being explored for this purpose in various laboratories, because of their unique abilities to detect metal oxidation processes remotely by using relatively simple equipment and analytical techniques. Their abilities in this regard arise from the fact that corrosion is an electrochemical oxidation process in which iron metal is converted into corrosion products (rust)

$$\begin{aligned} Fe &\rightarrow Fe^{2+} + 2e^- \\ &\Big|\xrightarrow[O_2]{H_2O} Fe(OH)_2,\ \alpha\text{-}FeOOH,\ \gamma\text{-}FeOOH,\ Fe_3O_4,\ \alpha\text{-}Fe_2O_3 \end{aligned} \qquad (1)$$

which is represented here by ferrous hydroxide [$Fe(OH)_2$], iron oxyhydroxides [α-FeOOH and γ-FeOOH], magnetite [Fe_3O_4], and hematite (α-Fe_2O_3). Under freely corroding conditions, as exists for rebar in concrete, the electrons released in the iron-oxidation

process are consumed by the reduction of oxygen that has diffused through the concrete to the steel surface

$$1/2O_2 + H_2O + 4e^- \rightarrow 4OH^- \qquad (2)$$

such that the overall reaction is best written as

$$\begin{array}{l} Fe + 1/2O_2 + H_2O \rightarrow Fe^{2+} + 2OH^- \\ \qquad\qquad\qquad\quad \downarrow O_2, H_2O \\ \qquad\qquad\quad Fe(OH)_2, \alpha\text{-}FeOOH, \gamma\text{-}FeOOH, Fe_3O_4, \alpha\text{-}Fe_2O_3 \\ \qquad\qquad\qquad\quad \underbrace{\qquad\qquad\qquad\qquad\qquad\qquad}_{\text{Rust}} \end{array} \qquad (3)$$

Because oxygen and water combine with dissolved Fe^{2+} to form a solid product (rust) that occupies a volume that is 2-3 times that of the steel that is destroyed, the concrete adjacent to the rebar is placed in tension. However, concrete has poor tensile strength so that the concrete spalls from the reinforcing thereby compromising the structural integrity of the structure.

Because corrosion is an electrochemical process involving the flow of electrons through the metal rebar and positive ions through the concrete between the oxidation and reduction sites, as depicted in Figure 1, it has long been recognized that electrochemical techniques may represent powerful methods for the *in situ* detection and the characterization of corrosion on rebar before it becomes evident as physical damage to the structure. Although various electrochemical techniques, including linear polarization (LP) and electrochemical impedance spectroscopy (EIS), have been used extensively by other workers for detecting corrosion of rebar in concrete, a thorough study of the effectiveness of these methods has not been performed.

One variant of EIS, ultralow frequency ac impedance spectroscopy (ULFACIS), was previously explored theoretically[4] by modeling the rebar in concrete as an electrical transmission line (Figure 2), in which R_m and R_s are the electrical resistances per unit length of the rebar and concrete cover, respectively, and Z is the impedance of the interface per unit length. This latter quantity describes the resistance to the transport of positive charge (in the form of Fe^{2+}) across the interface from the steel to the concrete and hence is a measure of the corrosion resistance of the steel when any capacitive contribution has been eliminated. It is this quantity (the polarization resistance, R_p, which is the value of Z under dc conditions) that we wish to determine with any electrochemical technique that might be used to characterize corroding rebar in concrete. However, our theoretical work[4] also suggested that ULFACIS might be used to locate remotely where corrosion is occurring on the rebar by taking advantage of a peculiar property of an electrical transmission line; an ac signal (current or voltage) extends farther down the line as the frequency is lowered. Thus, if the monitoring point is not over the region of the rebar that is corroding, lowering the frequency is successive steps will cause the ac perturbation to extend down the rebar so that

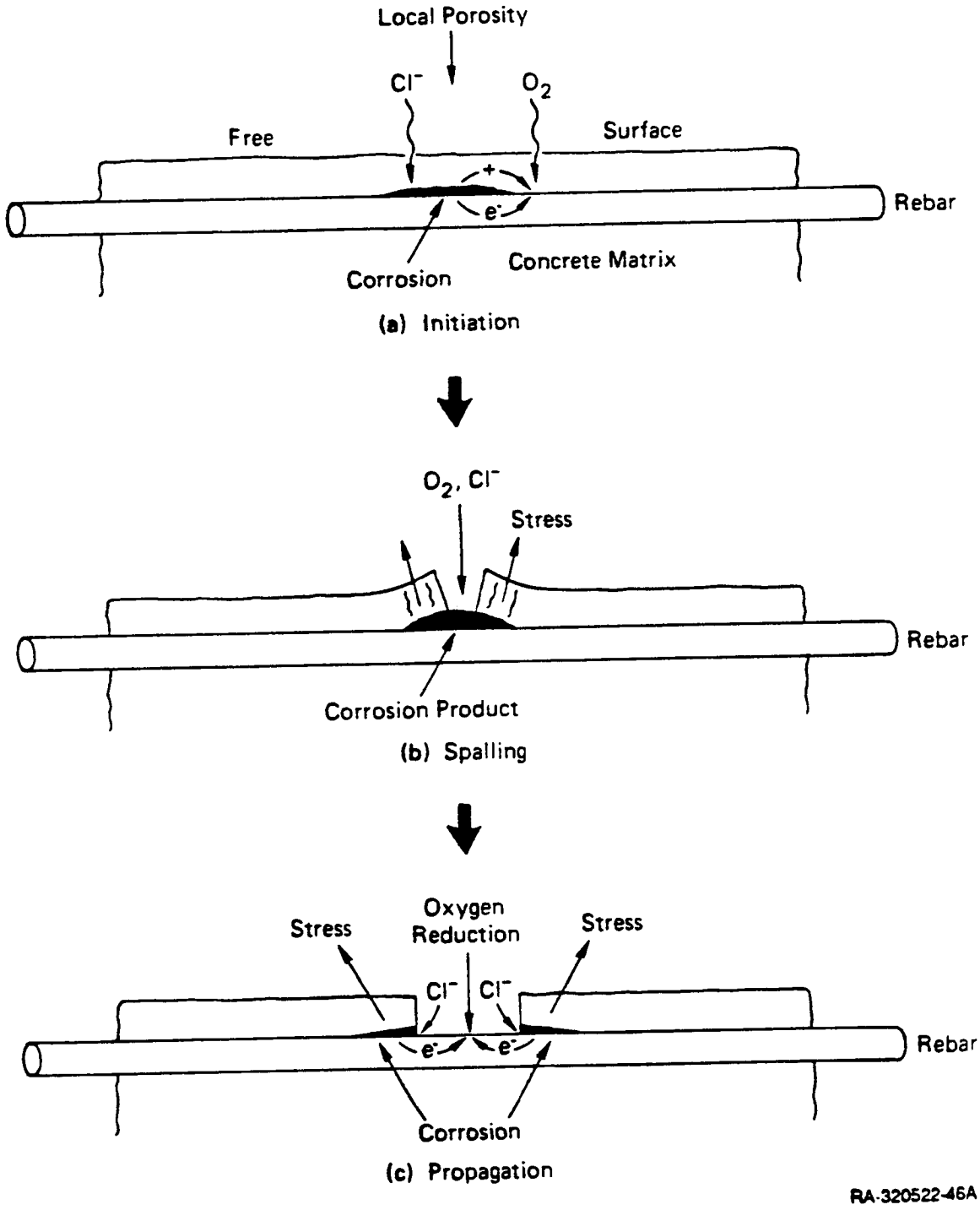

Figure 1. Schematic of events in the corrosion of rebar in reinforced concrete.

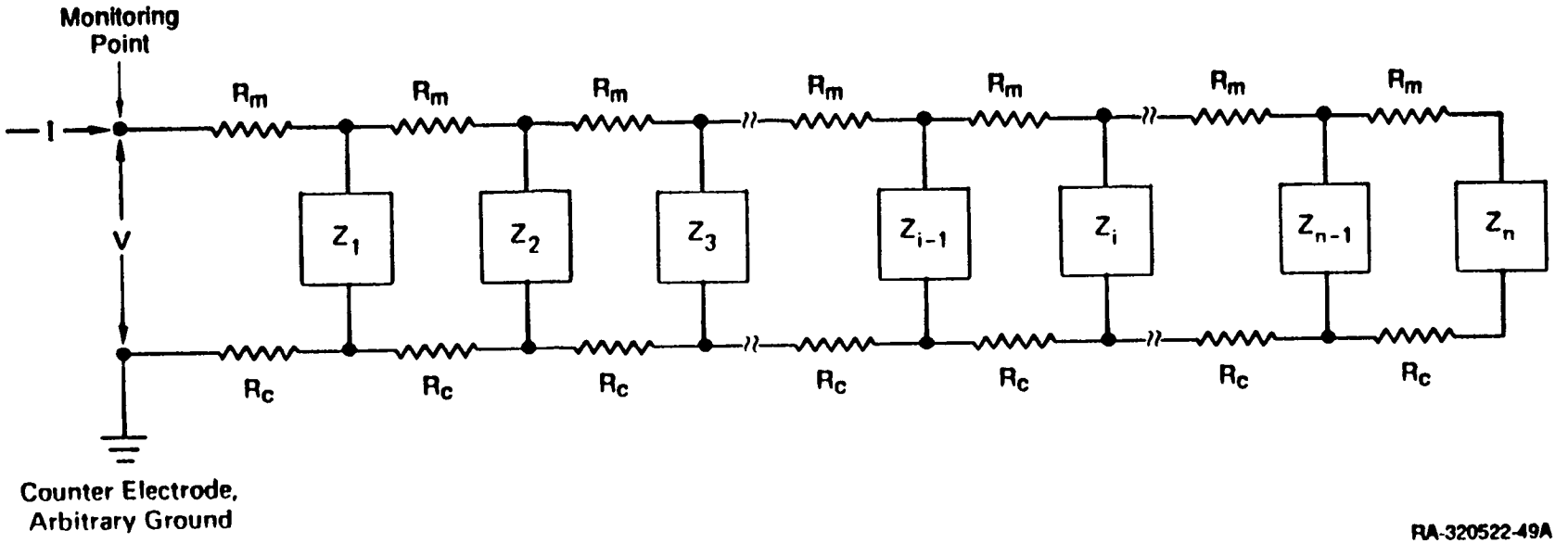

Figure 2. Discretized transmission line model for rebar in reinforced concrete.
R_m = resistance of rebar/segment; R_c = resistance of concrete/segment;
Z_i = rebar/concrete interfacial impedance/segment.

at some (low) frequency the wave will intersect the corroding region, which is characterized by a low interfacial impedance (Z). This, in turn, results in a change in the impedance of the line (rebar) at the monitoring point, signaling the presence of a corroding region. By knowing the electrical properties of the rebar and the concrete and the frequency dependence of the interfacial impedance (Z), it is theoretically possible calculate the distance from the monitoring point at which corrosion is occurring. If so, it should then be possible to map the regions of corrosive attack by monitoring the impedance of the rebar at preselected points along its length.

The work reported here was to determine the applicability of ultralow frequency ac impedance spectroscopy (ULFACIS) for characterizing the corrosion of rebar in concrete. This study was performed as part of the SHRP-IDEA program and, in keeping with the goals of that program, the work was exploratory. Our principal goal was to provide definitive answers to the following questions:

- Can ULFACIS be used to locate and characterize corrosion nondestructively in reinforced concrete structures?
- Can impedance spectroscopy be used to measure the polarization resistance of steel embedded in concrete and hence to calculate the steel corrosion rate?

The importance of the first question is due to the fact that by the time corrosion becomes apparent as rust stains on the concrete surface, extensive damage has already occurred, frequently requiring the complete removal of the concrete, cleaning and repassivation of the rebar, and replacement of the concrete cover. However, this procedure does not guarantee that corrosion will not occur at some other location at a later time. The importance of the second question results from the fact that rebar represents a distributed impedance system that can be modeled as an electrical transmission line (TL). As noted above, one characteristic of a TL is that the length of the rebar sampled in any electrochemical test is a function of time or frequency, such that as the time of sampling increases or the frequency decreases, the imposed signal travels farther down the line. Thus, the area being sampled is not well defined and, as we show later in this report, the sampled area at any given frequency depends on the concrete resistivity and the impedance of the rebar/concrete interface. The goal then is to develop a technique for extracting the polarization resistance from the impedance data.

The work reported in this study is inherently mathematical. To render our study understandable to a wide audience, we have included the mathematical analyses in a companion report, "Development of Ultralow Frequency AC Impedance Spectroscopy (ULFACIS) for Detecting and Locating Corrosion on Rebar in Reinforced Concrete" that was prepared in August, 1989. In the present summary report much of the mathematical detail is omitted with the goal of communicating the physical importance of the work to the highway engineer. In particular, we identify the advantages and disadvantages of impedance spectroscopy for characterizing corrosion of rebar in concrete, because this technique is now being applied extensively (and frequently in an uncritical manner) in both laboratory and field studies.

We re-emphasize that, in keeping with the goals of the SHRP-IDEA program, our 12-month project was exploratory and was not intended to produce an instrument for field use. However, we have succeeded in developing the necessary analytical techniques to measure the polarization resistance, and hence the corrosion rate, of corroding rebar with far greater precision than has hitherto been possible. The development of a practical corrosion rate "meter" for use in the field is a logical and achievable extension of this work.

2

EXPERIMENTAL STUDIES

An important premise at the outset of this work was that meaningful experimental studies on the use of ULFACIS to characterize the corrosion of rebar in concrete could only be carried out using test specimens that realistically simulate corroding rebar in the field. In this regard, we considered it important to employ a commercial concrete mix and to use actual rebar in a configuration that is typical of that found in the field but yet is simple enough that a meaningful analysis can be made. Of particular importance was that the test specimen be of sufficient dimension in the longitudinal direction to appear to be infinite as far as the experimental technique (ULFACIS) was concerned. Accordingly, test specimens eight feet in length were prepared, in contrast to the small block specimens that are frequently employed in laboratory studies.

As noted in the Introduction, corrosion of rebar is due to chloride depassivation of the steel. Chloride in the concrete originates from the use of deicing salt (NaCl) or from the addition of calcium chloride ($CaCl_2$) as a setting agent. In any event, chloride levels of a few tenths of one weight percent may be present, and we considered the simulation of these levels to be an important aspect of our work. In systems in which the chloride contaminant is not uniformly distributed, it is reasonable to expect the extent of corrosive attack to also be nonuniformly distributed.

Because the distance that an electrical perturbation signal extends down a transmission line (the rebar) is a function of frequency, and since the impedance of the transmission line will change more or less abruptly when the signal encounters a region of low interfacial impedance (high corrosion rate), it is also reasonable to expect that ULFACIS might be used to locate regions of high corrosion activity on embedded rebar. This expectation was supported by a recent theoretical study by Macdonald, McKubre, and Urquidi-Macdonald,[4] although those calculations indicated that discrimination between the corroding and passive regions could only be achieved at very low frequencies (sub-millihertz range). Furthermore, our initial theoretical studies assumed a sharp demarcation between corroding

and noncorroding areas, whereas in real systems, these regions are more likely to be separated by a "fuzzy" boundary over which the corrosion rate may change by several orders of magnitude. To simulate this variation in corrosion rate along a rebar, we equipped our experimental slabs with ports exposing the rebar at regular distances so that high, local corrosion rates could be induced by the addition of hydrochloric acid. We then explored the ability of ULFACIS to locate these regions of high corrosion rate by measuring the frequency dispersion of the impedance of the system.

PREPARATION AND SPECIFICATION OF CONCRETE SLABS

Four specimen slabs (237 x 53 x 18 cm) simulating those of bridge decks were prepared. A standard concrete mix prepared by RMC, LONESTAR of San Carlos, California, was employed, and the concrete was poured into suitable wood frames that were fabricated in SRI's workshop for that purpose. Each slab was prepared with a different chloride content, the $CaCl_2$ contents being 0, 0.5, 1.5, and 2 weight%. Each slab contained three rebars (type KS-4S-INDONESIA) laid along the length and with equal spacing between them (two successive rebars being ~12 cm apart). The rebars were located midway between the bottom and the top of the slab. On top of each middle bar (at equal distance along the length of the slab), three capped cavities were created (during pouring) to enable initiation of corrosion at various distances down the rebar (working electrode). Furthermore, eight conductivity probes fabricated from parallel stainless steel electrodes were inserted (during pouring of the concrete) in each slab to measure concrete resisitivity at various locations over the slab. Figure 3 illustrates a concrete slab with all measurement probes.

IMPEDANCE MEASUREMENTS

Electrochemical impedance measurements are made by imposing a small amplitude sinusoidal voltage or current at the monitoring point and measuring the response sinusoidal current and voltage, respectively. The amplitudes and the phase difference between the two signals are then analyzed to yield the impedance, which is a measure of the resistance to current flow in the system. Because the impedance contains both magnitude and phase information it is a complex number. However, if the frequency is made sufficiently high or low, the impedance approaches constant value which we refer to as the uncompensated resistance (R_u) and the interfacial resistance (R_{int}), respectively, as illustrated schematically in Figure 4, in which the imaginary component of the measured impedance is plotted against the real component as the frequency is changed. For corrosion monitoring purposes, the most important quantity is the apparent polarization resistance (R_p) given by

$$R_{p,app} = R_{int} - R_u \tag{4}$$

which can be used to calculate the true polarization resistance (R_p) provided that an appropriate electrical model is available for the system. In this work, we describe the electrical properties of rebar in concrete as an electrical transmission line and the method developed for extracting the true polarization resistance is described in the companion

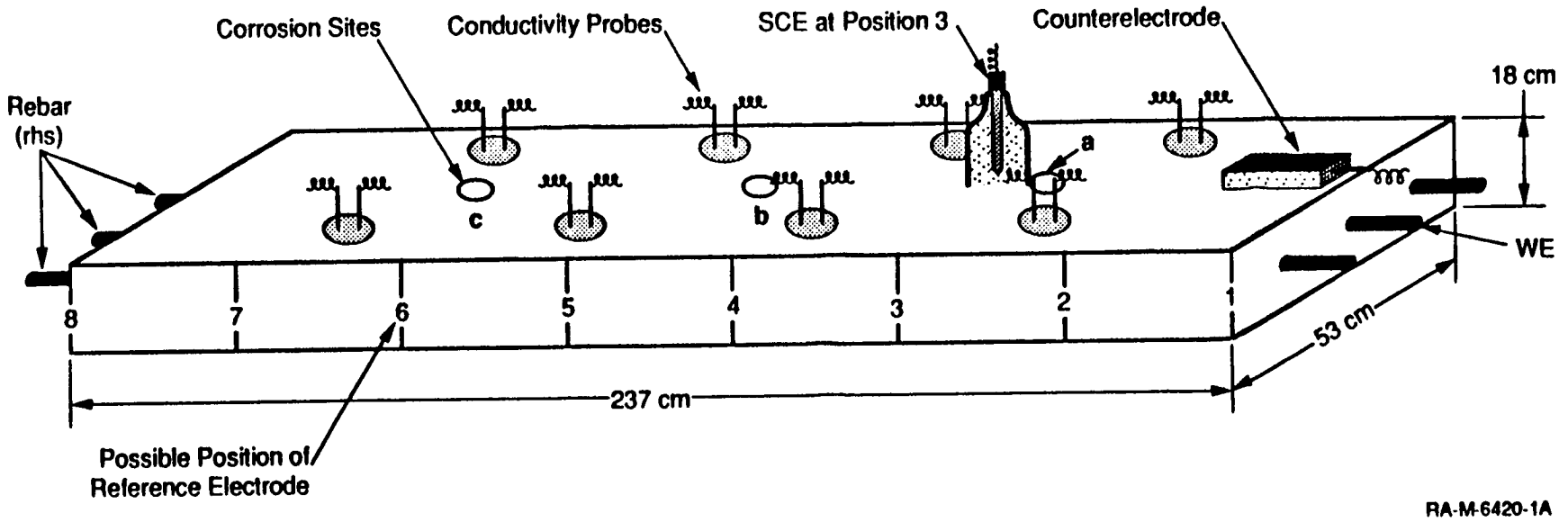

Figure 3. Schematic of concrete slab with measurement probes.

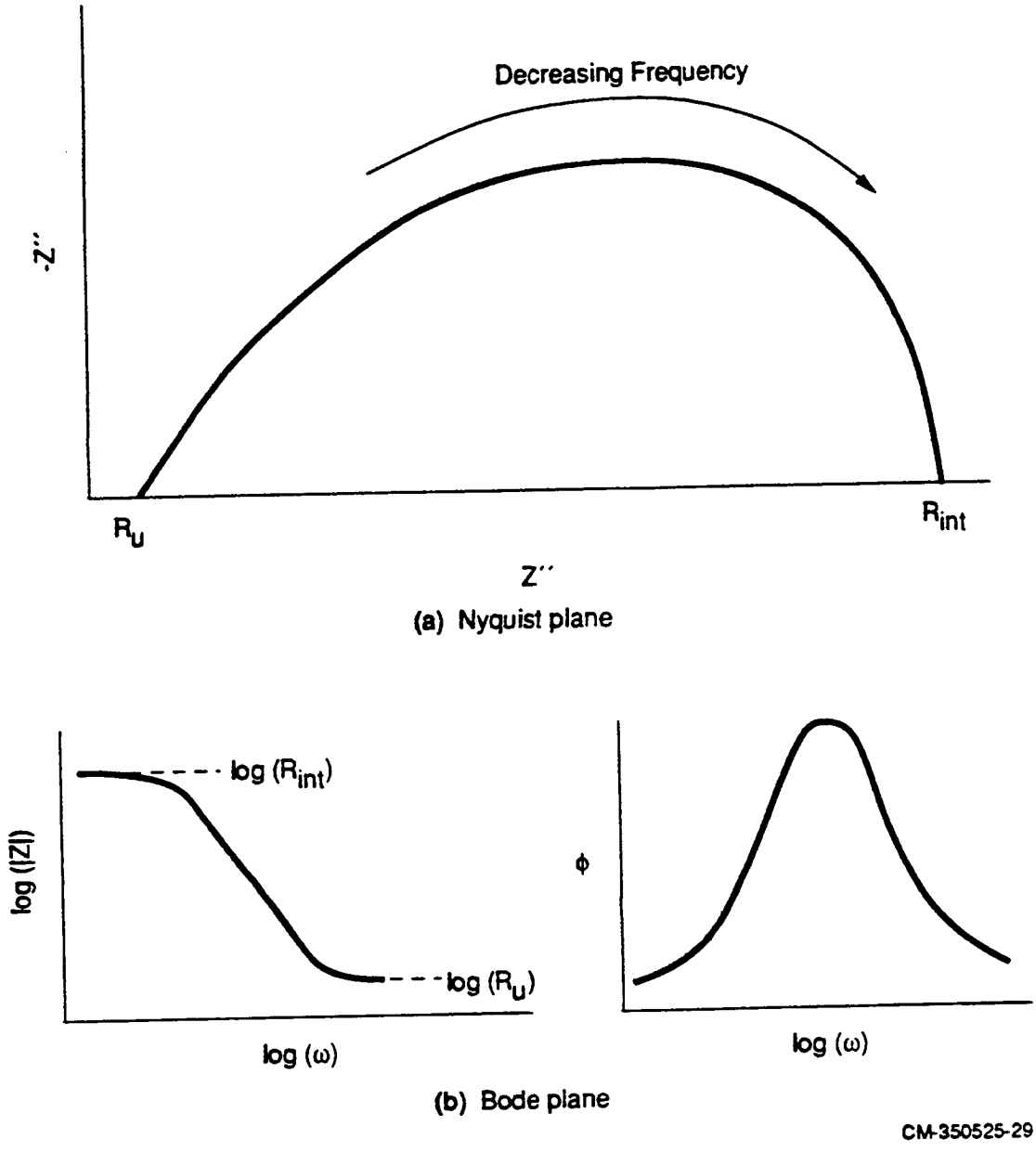

Figure 4. Schematic Nyquist and Bode plane plots of the rear/concrete impedance showing the intercepts of the impedance locus on the real (Z′) axis at limitingly high and low frequencies to yield the uncompensated resistance R_u and interfacial resistance R_{int}, respectively.

report. Once R_p has been estimated, it can be used in the Stern-Geary equation to calculate the corrosion rate.

In performing impedance measurements, it is necessary to impose an alternating current at the monitoring point between the specimen (rebar) and a counter electrode, as noted above and as indicated schematically in Figure 5. However, because we are interested in sampling the interfacial impedance only it is necessary to measure the alternating voltage at a point that is as close to the interface as possible. This measurement is made using a reference electrode, which provides a constant voltage against which the voltage at the sensing point may be compared. Noting that the measured voltage $\tilde{V}$ and the imposed current ($\tilde{I}$) are vector quantities (i.e., they contain both magnitude and phase information) the impedance of the system is defined as

$$Z = \tilde{V}/\tilde{I} \tag{5}$$

An in-depth discussion of electrochemical impedance spectroscopy is well beyond the scope of this report. However, several excellent reviews are available[5-7] in the scientific and engineering literature and the readers are referred to these sources for additional information.

It is also possible (and indeed common) to measure impedance data by imposing an alternating voltage between the specimen and the reference electrode and monitoring the resultant current between the specimen and the counter electrode. We have employed both methods in this work to measure the impedance of rebar in concrete, but we have found that the imposed alternating current method is the best for our purposes. Accordingly, all impedance measurements reported in this work were carried out using the imposed current method.

The electrochemical impedance measuring system was based on a frequency response analyzer (Solartron Model 1250), which is capable of generating sinusoidal voltages having frequencies of 10^{-5} to 6 x 10^4 Hz and amplitudes from 0.01 mV to 10 V. However, the frequency range covered in the present study was 2 x 10^{-4} to 10^4 Hz. A Model 362 EG&G (PARC) scanning potentiostat operating in the galvanostatic mode was employed to impose an alternating current between the rebar and the counterelectrode. A Macintosh Plus desktop computer coupled to a Mac 488B Iotech interface was used to control the experiment. Whenever needed, the current and voltage were checked using a Keithley 171 digital multimeter.

The impedance data obtained were displayed as complex-plane, Bode, and phase angle plots using a Macintosh II microcomputer coupled to a printer.

COUNTERELECTRODE

Because the measurement of one impedance spectrum over the frequency range 2 x 10^{-4} to 10^4 Hz requires about 12 hours, we had to develop a special counterelectrode that ensured,

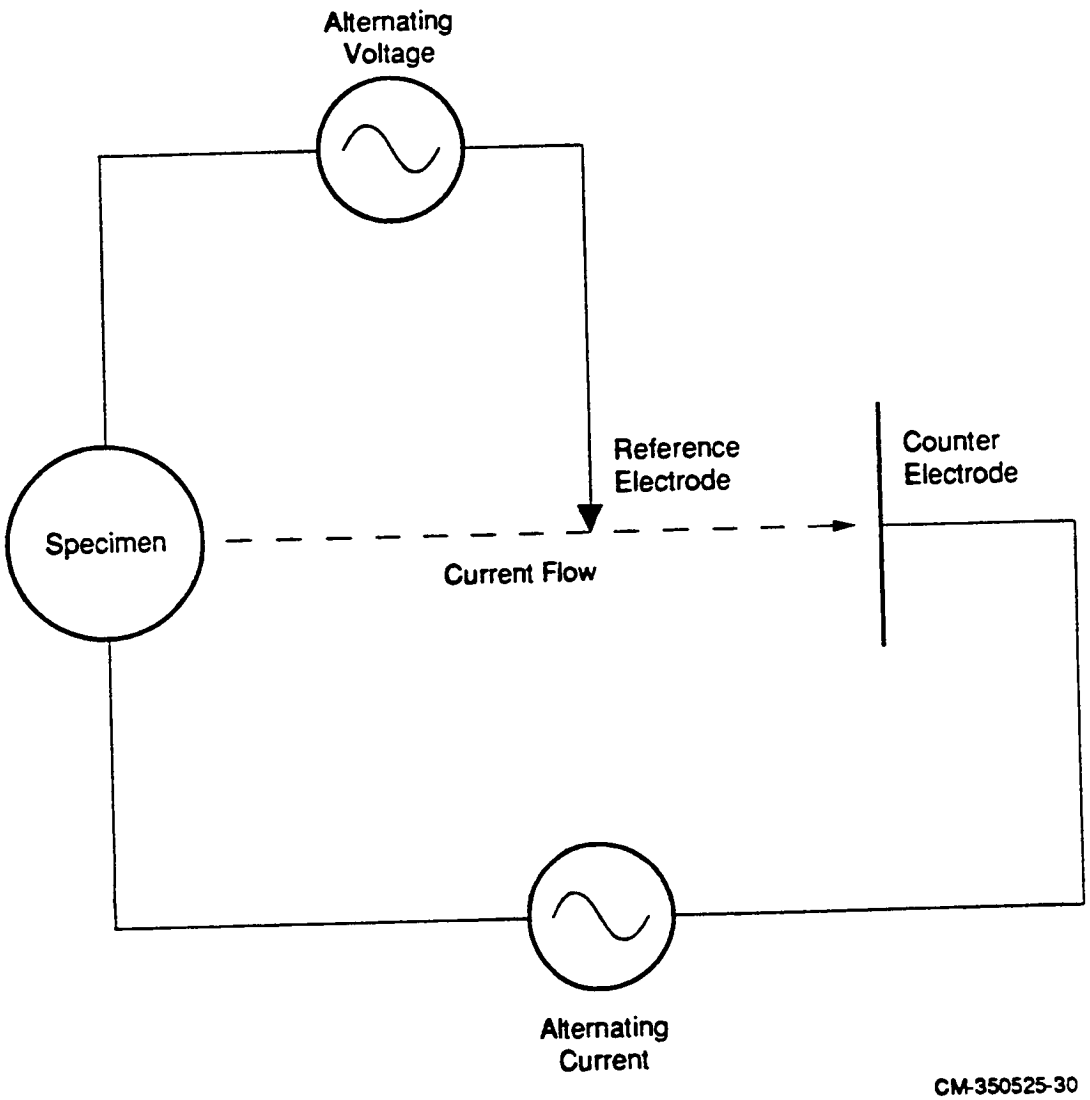

Figure 5. Schematic of experimental setup for electrochemical impedance spectroscopy.

consistently, a relatively long period of reproducible electrolytic contact with the concrete. After considerable trial and error, the required electrode evolved as a combination of a suitably cut piece of graphite fabric enveloping a piece of foam rubber (5 x 7 x 15 cm) which was moistened with saturated aqueous sodium sulfate solution. Electrical connection of this counterelectrode to the measuring device was obtained via a high density graphite rod partially inserted in the graphite fabric-foam assembly.

REFERENCE ELECTRODE

A commercially available saturated calomel reference electrode was employed throughout this study. To achieve suitable electrolytic contact with the concrete surface, the calomel electrode was tightly fitted into a specially cut piece of foam rubber that was also moistened with saturated sulfate solution. The calomel-foam reference electrode was wrapped in a thin plastic sheath to minimize evaporation of water.

CONCRETE CONDUCTIVITY PROBE

To determine the bulk resistivity of concrete from impedance spectral measurements, we prepared special conductivity probes. These probes (Figure 6) were essentially composed of two identical stainless steel plates, each of which was independently welded to a steel wire of suitable length. The two plates were kept fixed in a parallel configuration at a distance of 2.6 cm apart, using hardened Evercoat "Marine Resin". Figure 7 shows how the measured resistivity varies with changing content of $CaCl_2$ in concrete. The resistivity values given in Figure 3 were calculated from the real component of the impedance extrapolated to a sufficiently high frequency that the imaginary component is effectively zero.

MEASUREMENTS

The length of the concrete slab was divided into seven equal segments (Figure 3), and the following experiments were carried out during this research program:

(a) Duplicate impedance spectra were measured with the counterelectrode positioned over the middle rebar (which served as the working electrode, WE) and with the counter electrode and the connection to the rebar being located at the same end of the slab (counterelectrode at position 1). The position of the reference electrode was then varied, according to the segment numbers depicted in Figure 3, from position 2 to 8. A total of fourteen impedance spectra were measured for each slab.

(b) The set of measurements described in (a) were repeated but with the counter electrode moved to the opposite end of the slab (position 8), i.e., the connections to the working electrode (middle rebar) and the counterelectrode were at opposite ends.

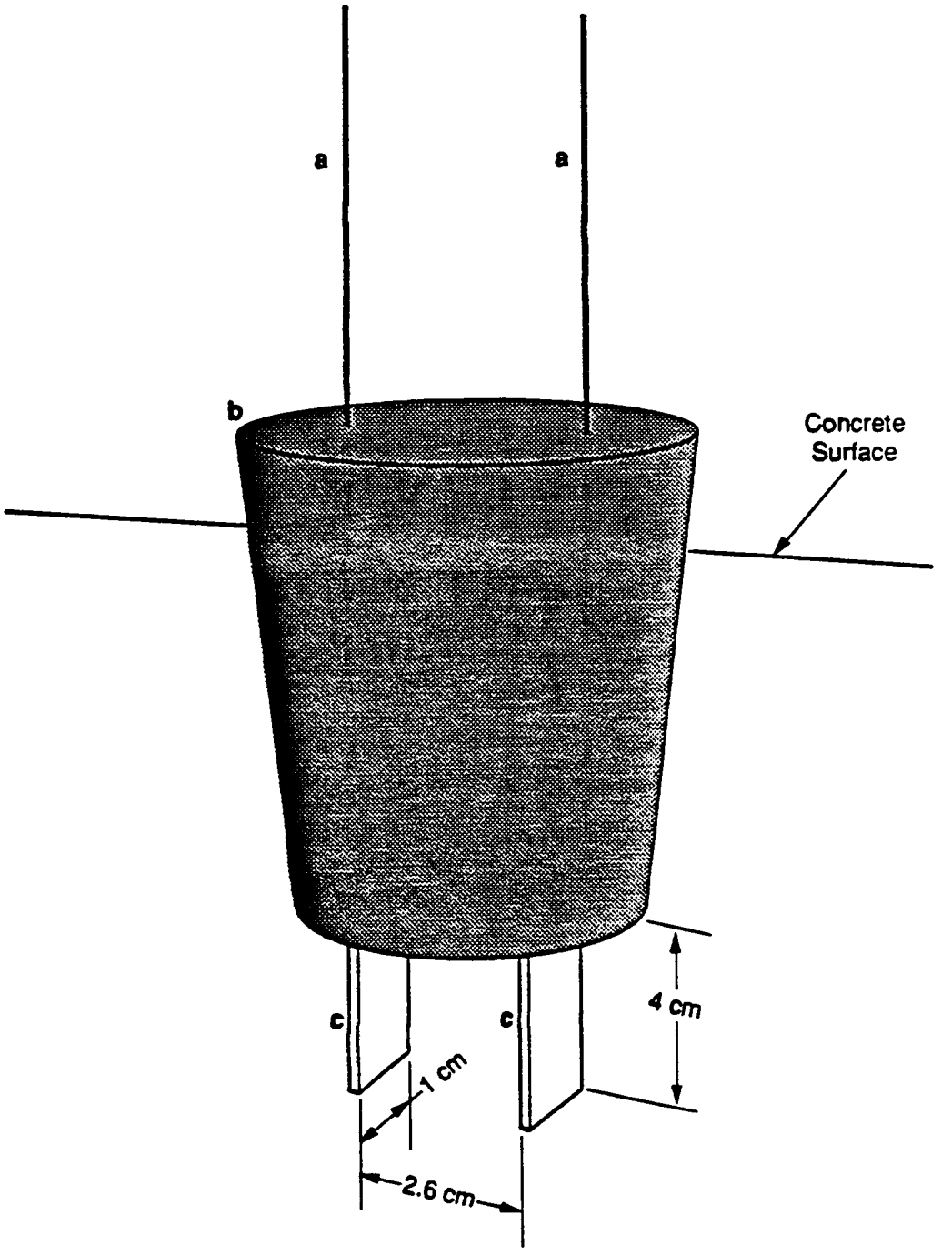

Figure 6. Conductivity probe for concrete: (a) steel wires; (b) hardened Evercoat "Marine Resin"; (c) two parallel plates of steel.

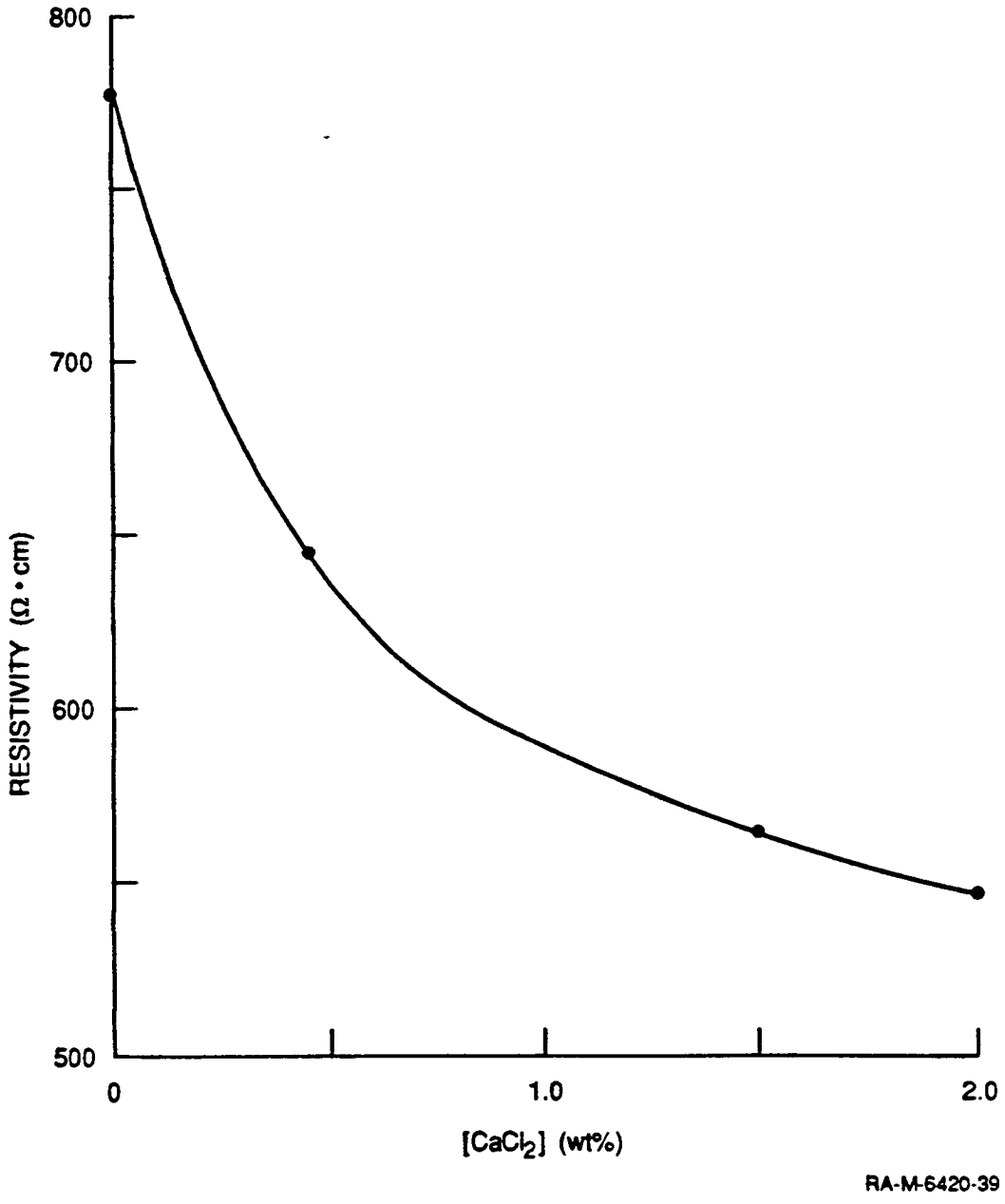

Figure 7. Variation of concrete resistivity with calcium chloride content.

(c) The measurements described in (a) and (b) were repeated while the rebar was actively corroded by hydrochloric acid (added at one of the corrosion cavities illustrated in Figure 3).

To improve the signal-to-noise ratio at low frequencies (so as to minimize scattering in the impedance data), we performed all impedance measurements galvanostatically, i.e., employing an alternating current perturbation rather than an alternating voltage.

EXPERIMENTAL RESULTS

The Impedance Function

As noted previously, the interfacial impedance is a measure of the ease with which charge passes across the corroding rebar/concrete interface and hence is related to the corrosion rate of the steel. While extraction of the polarization resistance from impedance data for rebar is far from straightforward, as explained later in this report, the impedance function (the impedance as a function of the frequency of the applied alternating current (ω)) contains a great deal of information that may be used by the highway engineer to ascertain the extent of corrosion damage to the rebar in reinforced structures.

Traditionally, two methods have been employed to present impedance information. All methods are based on the fact that the impedance is a complex number

$$Z(\omega) = \tilde{V}/\tilde{I} = Z' - jZ'' \tag{6}$$

reflecting the fact that the applied alternating current ($\tilde{I}$) and the resultant alternating voltage ($\tilde{V}$) generally are not in phase thereby leading to a finite imaginary component (Z"), where j is the complex variable ($j = \sqrt{-1}$). By noting that the phase angle between the response ($\tilde{V}$) and the perturbation ($\tilde{I}$) is given as

$$\text{Tan } \phi = -Z''/Z' \tag{7}$$

we are also able to write the impedance function as

$$Z(\omega) = |Z(\omega)|e^{j\phi} \tag{8}$$

where $|Z(\omega)|$ is the magnitude of the impedance

$$|Z(\omega)| = [(Z')^2 + (Z'')^2]^{1/2} \tag{9}$$

In many cases, impedance data are presented as a plot of the imaginary component (-Z") against the real component (Z') for each frequency resulting in a complex plane (or Nyquist plane) plot of the type shown in Figure 4(a). In the other method, plots are made of $\log(|Z(\omega)|)$ and ϕ versus $\log(\omega)$ thereby displaying the impedance data explicitely as a function of frequency (ω). This form of presentation is known as the Bode plane and is displayed in Figure 4(b). Because different aspects of the impedance function are more readily displayed in the Nyquist or Bode planes, we will use both presentations in this report.

Impedance Characteristics of Noncorroding Rebar

Figures 8(a) and 8(b) illustrate typical impedance spectra for noncorroding ($[CaCl_2] = 0$ wt%) reinforcing bar in concrete as a function of the reference electrode position (see Figure 3). It is clear from the figures that as the distance between the reference electrode and counterelectrode (in position 1) increases, the total impedance at any frequency decreases. The other impedance spectra measured for positions that are not shown (to avoid crowding of the figure) were found to follow the same trend.

Further, the high frequency limit of the impedance is unexpectedly low (~20 Ω), probably owing to the very large rebar-concrete contact surface area. Moreover, the high frequency limit is observed to decrease slightly as the reference electrode is progressively positioned farther from the counterelectrode. We also observe from Figure 8 that, at very low frequencies, the impedance loop curves upward toward higher imaginary impedance values. At best, the impedance spectra given in Figure 8 may be looked upon as arcs of very large diameter semicircles, which may indicate a passive state of the reinforcing bar.

Close examination of the impedance spectra shown in Figure 8 reveals that the angle of intersection of the locus with the real axis is well below the 90° ($\pi/2$) expected for a system that could be represented by a parallel R-C equivalent circuit having a single time constant. Indeed, the angles of intersection are typically 60° to 70° and decrease as the distance of the reference electrode from the counterelectrode increases. As discussed later in this report, we also observed that the angle of intersection at a fixed monitoring location decreased as corrosion of the rebar was initiated by hydrochloric acid additions.

Figure 9 illustrates typical Bode plots (logarithm of impedance modulus as a function of logarithm of frequency) for noncorroded reinforcing rebar in concrete. A linear region is observed at intermediate frequencies. The slope, $(\partial \log|Z|/\partial \log \omega)$, of the linear section (Table 1) consistently increases as the reference electrode is moved from position 2 to 4 but decreases as position 5 is reached; thereafter the slope stays more or less constant as the reference electrode is moved further down the concrete slab. Examination of these slope values (Table 1) shows that, in general, they fall between -0.45 and -0.75, with an average value of about -0.6. These values are higher than expected for a purely diffusional impedance (slope = -0.5), indicating that diffusion alone cannot account for the experimental data. However, the impedance function clearly is sensitive to the dimensional characteristics of the specimens.

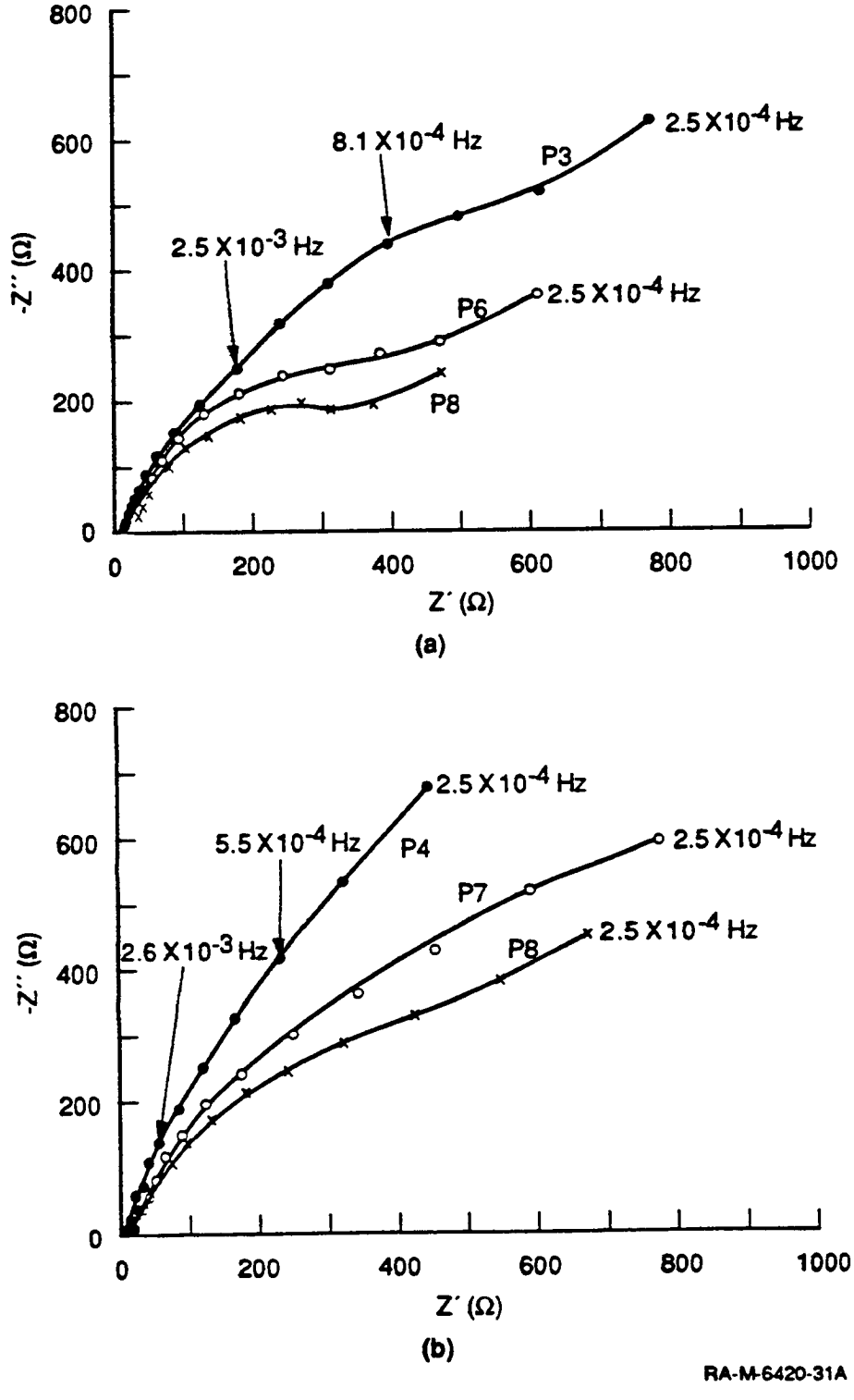

Figure 8. Sample plots of noncorroding rebar in concrete for different positions (p) of the reference electrode, as indicated on each curve.

[$CaCl_2$] = 0; counterelectrode at position 1; imposed current = 50 μA; (a) Run No. 1; (b) Run No. 2.

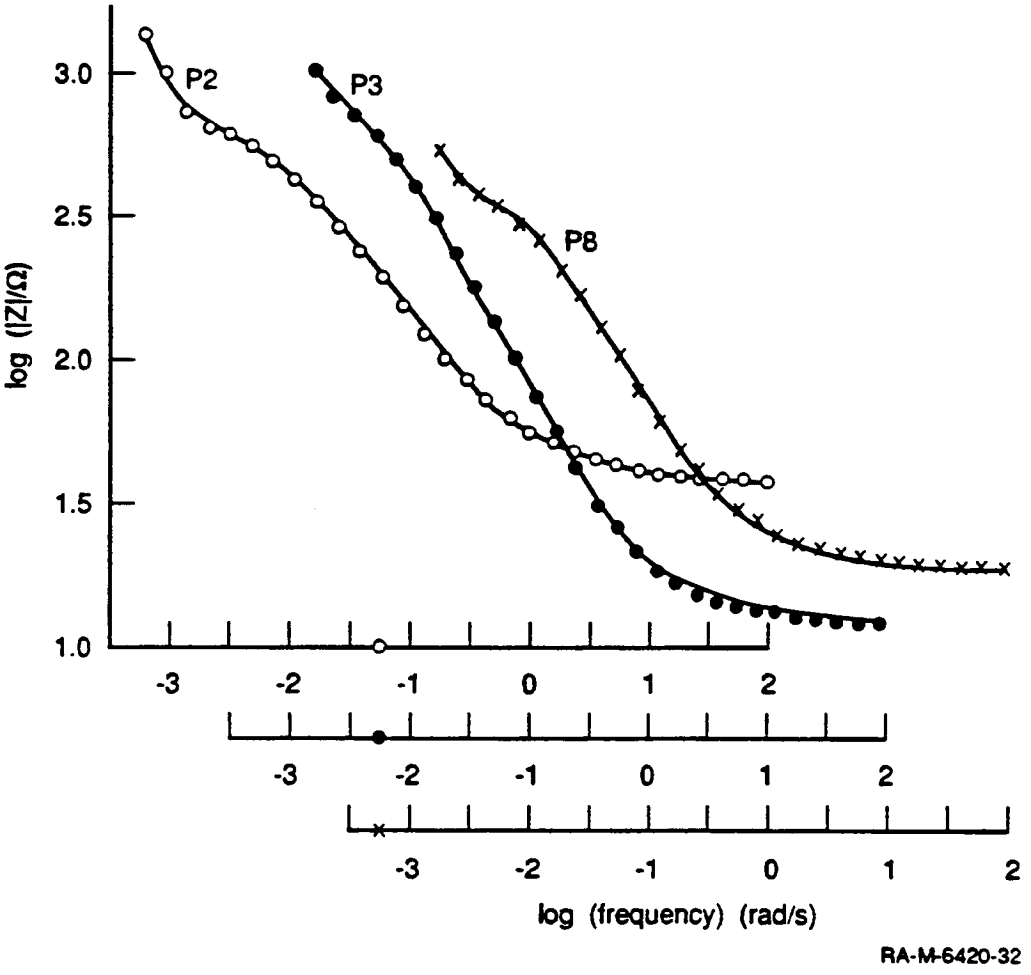

Figure 9. Sample plots of log (impedance modulus) versus log (frequency) for three different positions of reference electrode , as indicated on each curve.

[$CaCl_2$] = 0 wt%; counterelectrode at position 1; imposed current = 50 μA; Run No. 1 (noncorroding rebar).

Table 1

DEPENDENCE OF DIFFERENT PARAMETERS ON THE POSITION OF THE REFERENCE ELECTRODE FOR NONCORRODED REINFORCING BAR IN CONCRETE[a]

Reference Electrode Position	Bode slope -(∂log|Z|/∂log(f)) 1[b]	2[b]	Θ_{max}/deg 1[b]	2[b]	f_{max}/Hz 1[b]	2[b]	|Z|/Ω(0.0038 Hz) 1[b]	2[b]
2	0.48	0.45	44.4 44.1	46.7 46.3	0.0062 0.0094	0.0094 0.0062	282	272.5
3	0.71	0.74	62.7	63.7	0.0083	0.012	231.4	227.5
4	0.75	0.75	68.2	63.5	0.0083	0.012	213.6	205.7
5	0.62	0.55	51.6	52.6	0.0083	0.0083	197.2	184.3
6	0.63	0.67	57.0 57.1	58.7	0.0083 0.0057	0.0057	170.5	179.2
7	0.63	0.73	56.2	60.3	0.0057	0.0057	169.5	174.9
8	0.63	0.62	52.4	52.4	0.0083	0.0038	164.6	163.6

[a]Slope of the linear intermediate segment of the Bode plot, maximum phase-angle value (Θ_{max}), frequency at which Θ is maximum (f_{max}), and impedance modulus (|Z|) at a fixed frequency of 0.0038 Hz.

[b]Run number.

$[CaCl_2]$ = 0 wt%; counterelectrode at position 1; imposed current = 50 μA.

Figure 10 shows how the phase angle changes as the position of the reference electrode is varied from 2 to 4. The maximum value of the phase angle (Θ_{max}) increases as the distance between counter and reference electrodes is varied from position 2 to 4. However, as shown by the data in Table 1 for position 5, Θ_{max} decreases to a value that then stays more or less constant as the reference electrode is moved to the higher positions. Thus, the value of Θ_{max} passes through a maximum when the reference electrode is at position 4. The frequency (f_{max}) where Θ_{max} occurs for each position of the reference electrode (see Table 1) does not appear to follow a definite trend but falls within the range 5-9 mHz for the experiments reported here. The range of values for Θ_{max} (~40° to 70°) indicates that the impedance has a significant contribution from reactance, even though the rebar and concrete alone are purely resistive. The reactance, of course, arises from corrosion processes at the rebar/concrete interface.

The last two columns of Table 1 contain values of the impedance modulus, |Z|, at a fixed frequency (3.8 mHz), for two successive runs. The close agreement found between |Z| values for duplicate runs demonstrates the good reproducibility of the impedance spectra.

Impedance Characteristics of Corroding Rebar

Figures 11(a) and 11(b) show, for two different runs, how the impedance spectra change with the position of the reference electrode for a rebar made to corrode between positions 4 and 5 by injection of a 2.0 M HCl solution into the middle cavity of the slab. Again, none of the spectra are semicircular. However, for all positions of the reference electrode, the spectra exhibit a clear downward bending in the lower frequency range, a behavior not present in the spectra for noncorroded reinforcing bar (see Figure 8). As for the noncorroding rebar, the spectra become smaller as the position of the reference electrode increases. Again, the angle of intersection of the locus with the real axis is well below 90° (~50°), and is smaller than that for noncorroded rebar (see previous sub-section).

Figure 12 illustrates how the Bode plots vary with the position of the reference electrode. As in the case for noncorroded rebar, there is a linear region at intermediate frequencies whose slope (Table 2) increases with the position of the reference electrode up to positions 3-4 and then decreases. A comparison of these slope values (Table 2) with those for noncorroding rebar (Table 1) shows that they generally are smaller, having an average value of about -0.45.

The dependence of the phase-angle plot on the position of the reference electrode is illustrated in Figure 13; as for noncorroded rebar, each plot presents only one maximum. This maximum value of the phase angle (Θ_{max}) for the different reference electrode positions falls in the range 25° to 49° (Table 2), which is generally lower than that for noncorroded rebar (40° to 70°) (Table 1). The values of frequency where Θ_{max} occurs (f_{max}) again do not show a very clear trend, varying between 8 and 33 mHz. The highest value of Θ_{max} is observed for position 3 of the reference electrode, compared to position 4 for the case of noncorroded rebar (Table 1).

When the impedance spectra obtained for rebar corroding at a single site (Figure 11) are compared to those for noncorroding rebar (Figure 8), a marked difference in the impedance

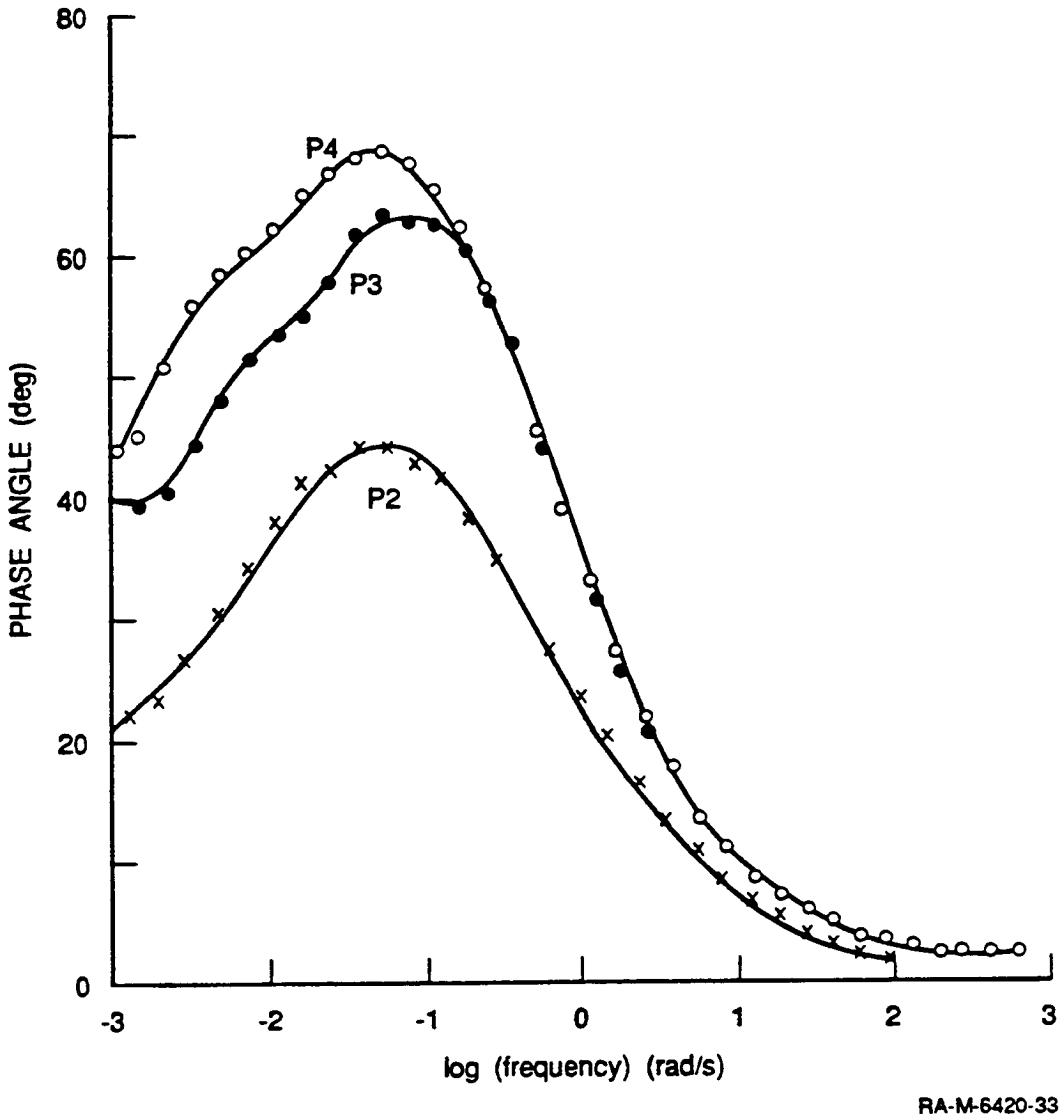

Figure 10. Change of phase angle with position of reference electrode for non-corroding rebar in concrete.

[$CaCl_2$] = 0 wt%; counterelectrode at position 1; imposed current = 50 μA; Run No. 1.

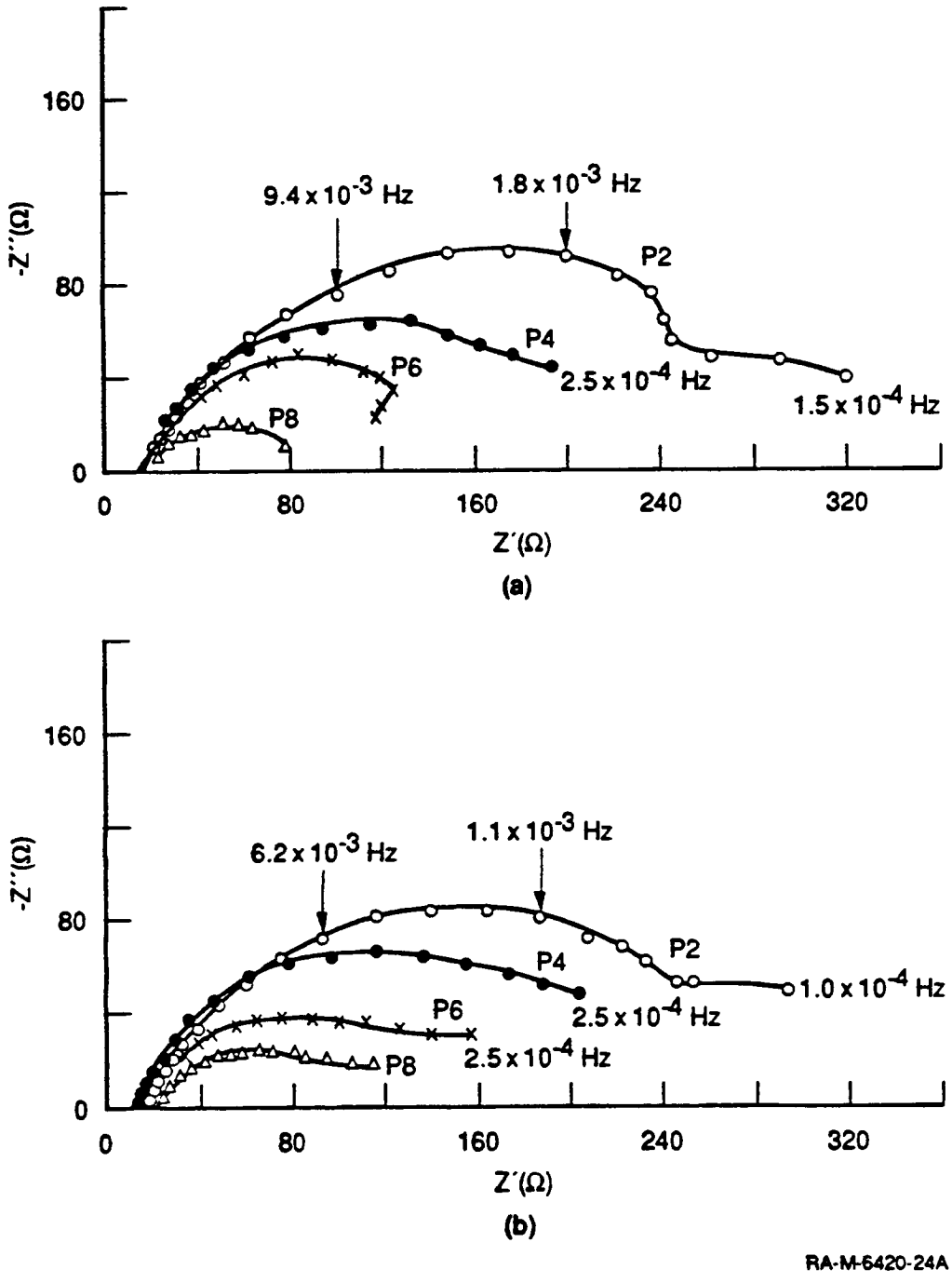

Figure 11. Representative impedance spectra for corroding rebar in concrete (see Figure 1), with the reference electrode located at the position indicated on each curve.

[$CaCl_2$] = 0 wt%; corroding site at middle cavity b (mid position 4-5); imposed current = 50 μA; (a) Run No. 1; (b) Run No. 2; counter-electrode at position 1.

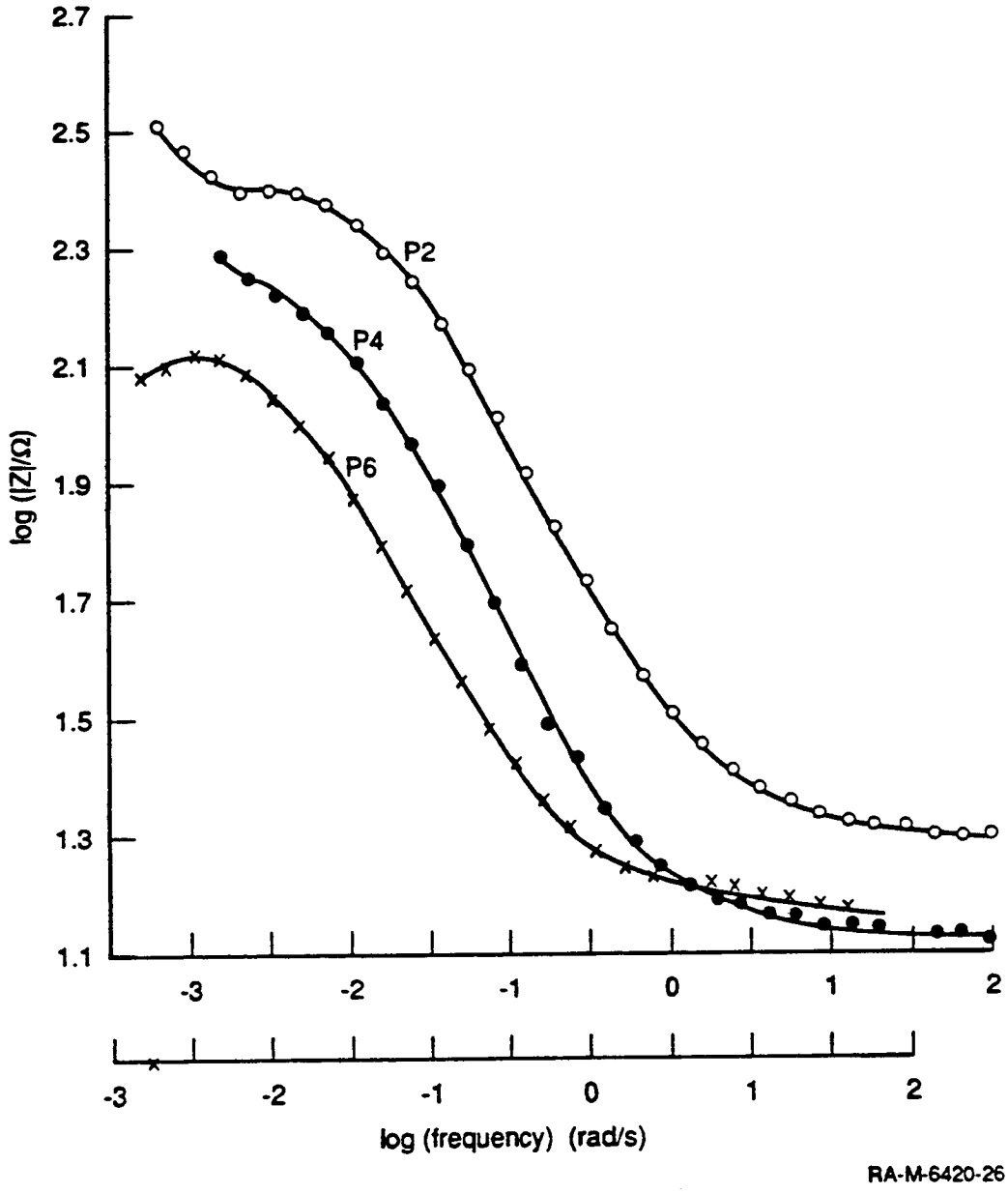

Figure 12. Representative plots of log (impedance modulus) versus log (frequency) for three different positions of the reference electrode, as indicated by the labels on the curves.

$[CaCl_2]$ = 0 wt%; counterelectrode at position 1; imposed current = 50 μA; rebar corroding at cavity b; Run No. 1.

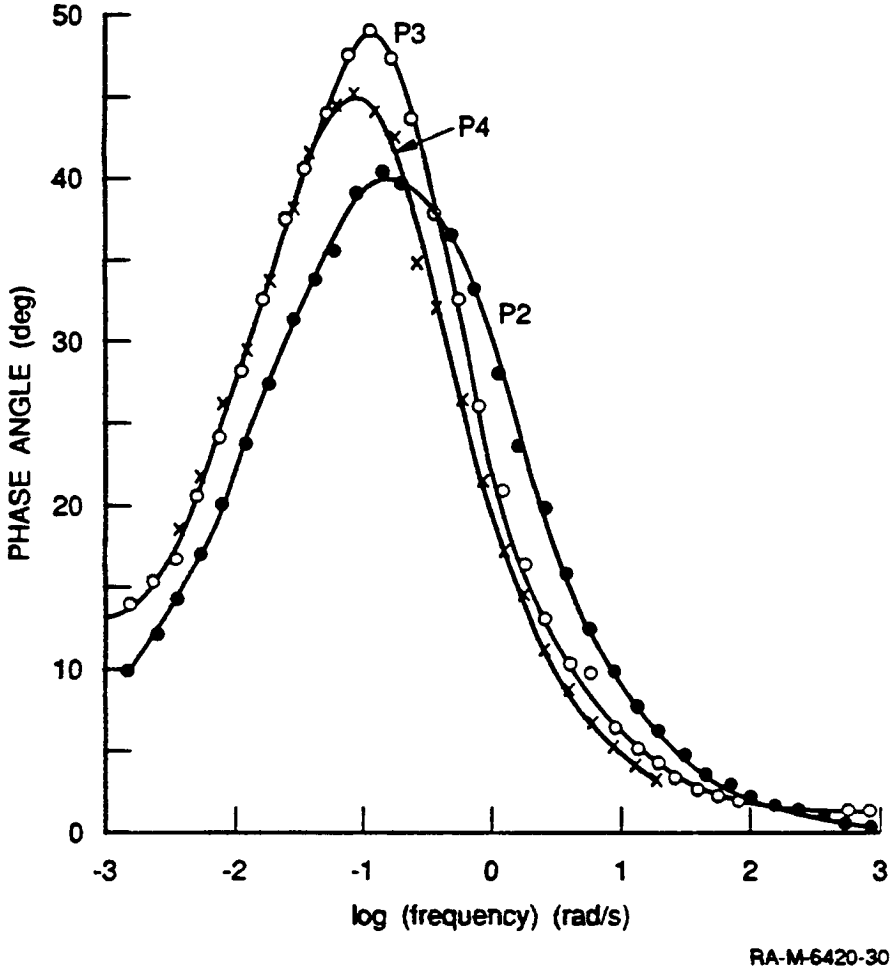

Figure 13. Dependence of phase angle on frequency for three different locations of the reference electrode.

[$CaCl_2$] = 0 wt%; counterelectrode at position 1; imposed current = 50 μA; middle rebar corroding at mid position 4-5, cavity b; Run No. 1.

Table 2

DEPENDENCE OF DIFFERENT PARAMETERS ON THE POSITION OF THE REFERENCE ELECTRODE FOR ONE-SITE CORRODED REINFORCING BAR IN CONCRETE FOR AN IMPOSED AC CURRENT OF 50 μA[a]

Reference Electrode Position	Bode slope -(∂log|Z|/∂log(f)) 1[b]	2[b]	Θ_{max}/deg 1[b]	2[b]	f_{max}/Hz 1[b]	2[b]	|Z|/Ω(0.0038 Hz) 1[b]	2[b]
2	0.48	0.49	40.7	42.3	0.022	0.033	174.6	162.5
3	0.56	0.56	48.8	49.0	0.018	0.018	119.9	110.7
4	0.50	0.59	45.4	46.6	0.012	0.012	99.4	99.0
5	0.45	0.44	40.5	39.3	0.008	0.012	83.9	80.7
6	0.43	0.41	38.0	35.8 35.1	0.018	0.018 0.027	86.3	74.0
7	0.36	0.38	31.2	31.3 31.0	0.012	0.012 0.018	65.4	69.2
8	0.32	0.30	24.7	23.7 23.1	0.018	0.008 0.012	60.9	61.9

[a]Slope of the linear intermediate segment of the Bode plot, maximum phase-angle value (Θ_{max}), frequency at which Θ is maximum (f_{max}), and impedance modulus (|Z|) at a fixed frequency of 0.0038 Hz.

[b]Run number.

$[CaCl_2]$ = 0 wt%, counterelectrode at position 1; imposed current = 50 μA; reinforcing bar corroded at cavity b (see Figure 3).

values is noted, with those for the corroding rebar being much smaller at equivalent frequencies. This difference can be seen by comparing the values of |Z| at f = 3.8 mHz for the two cases for different positions of the reference electrode (see Tables 1 and 2).

To check the linearity of the system when probed using an ac current of 50 μA, we obtained two other sets of data using higher ac currents: 330 μA and 500 μA. The results of these two last cases are now described.

Figures 14(a) and 14(b) show, for two different runs, the impedance spectra obtained for different positions of the reference electrode when an ac current of 330 μA is imposed. Comparison of these spectra [(Figures 14(a) and 14(b)] with those for an imposed ac current of 50 μA [(Figure 11(a) and 11(b)] shows that the results for position 2 of the reference electrode (only slightly higher for the 50 μA case). However, the results for positions of the reference electrode farther from the counterelectrode are quite different, the spectra presenting higher values of the imaginary impedance for the 330 μA case (e.g., compare spectra for position 8 in Figures 11and 14). At the same time, the comparison shows that a lower imposed ac current led to better differentiation (discrimination) between results for the different positions of the reference electrode. The spectra for the higher ac imposed current also are less curved downward at the low frequencies, presenting an almost invariable imaginary impedance as the frequency is lowered.

The Bode plots obtained for the ac imposed current of 330 μA, illustrated in Figure 15, are somewhat similar to those for the lower ac imposed current (see Figure 12), with comparable slopes for the intermediate-frequency linear region at intermediate frequencies (see Tables 2 and 3). The highest slope value occurs for positions 3-4, as was found for the data obtained using an ac current of 50 μA.

Figure 16 illustrates the phase-angle plots for three different positions of the reference electrode when the imposed ac current is 330 μA. The trends presented are similar to those for the lower current (see Figure 13). The maximum value of the phase angle (Θ_{max}) falls in the range 33° to 44° (see Table 3). This range lies within the range obtained for the lower current (25° to 49°; see Table 2); thus, the rate of decrease of Θ_{max} as the distance between counter and reference electrodes is increased is higher for the ac imposed current of 50 μA. The frequency (f_{max}) at which Θ is maximum is independent of the position of the reference electrode (see Table 3).

The variation of the impedance modulus at a fixed frequency of 0.0037 Hz (0.1 mHz lower than for previous cases; see Tables 1 and 2) with reference electrode position, as summarized in Table 3, is similar to that discussed previously for noncorroded rebar (Table 1) and for the measurements carried out at a lower ac current (Table 2).

The other set of impedance spectra that will be discussed now were obtained for an even higher value of the ac imposed current, i.e., 500 μA. Furthermore, in this case, the position of the counter electrode was changed from 1 to 8; thus, the connections for the counter and working electrodes were at opposite ends of the concrete slab. Figures 17(a) and 17(b) show the impedance spectra obtained for two different runs for different positions of the reference electrode. Contrary to the prior case (see Figure 14), the spectra for different reference electrode positions are well differentiated, exhibiting the type of

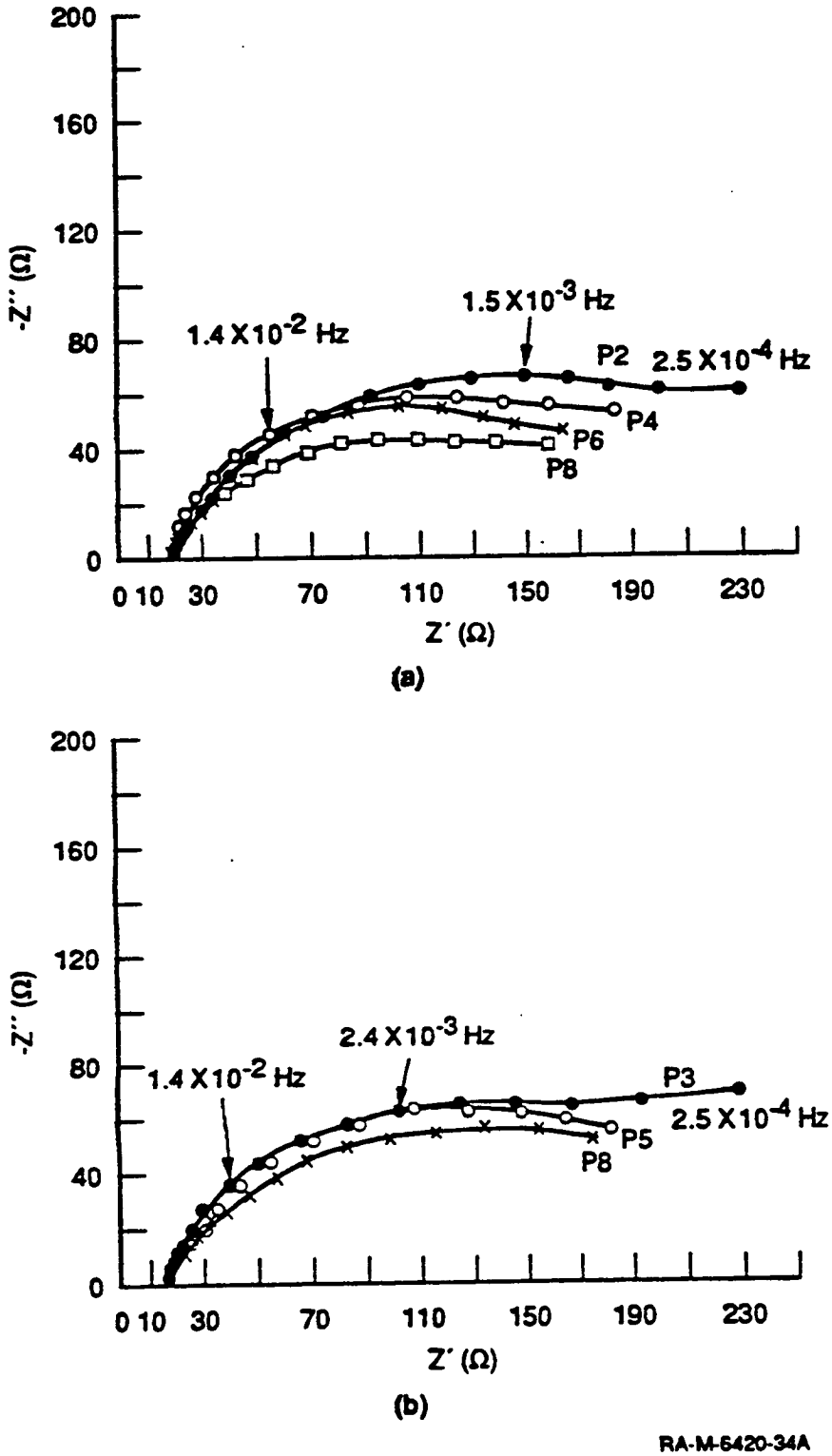

Figure 14. Representative impedance spectra of corroding rebar in concrete. Each spectrum represents a different location of reference electrode as labeled on each curve.

[$CaCl_2$] = 0 wt%; counterelectrode at position 2; imposed current = 330 μA; corroding site at mid position 4-5, cavity b; (a) Run No. 1; (b) Run No. 2.

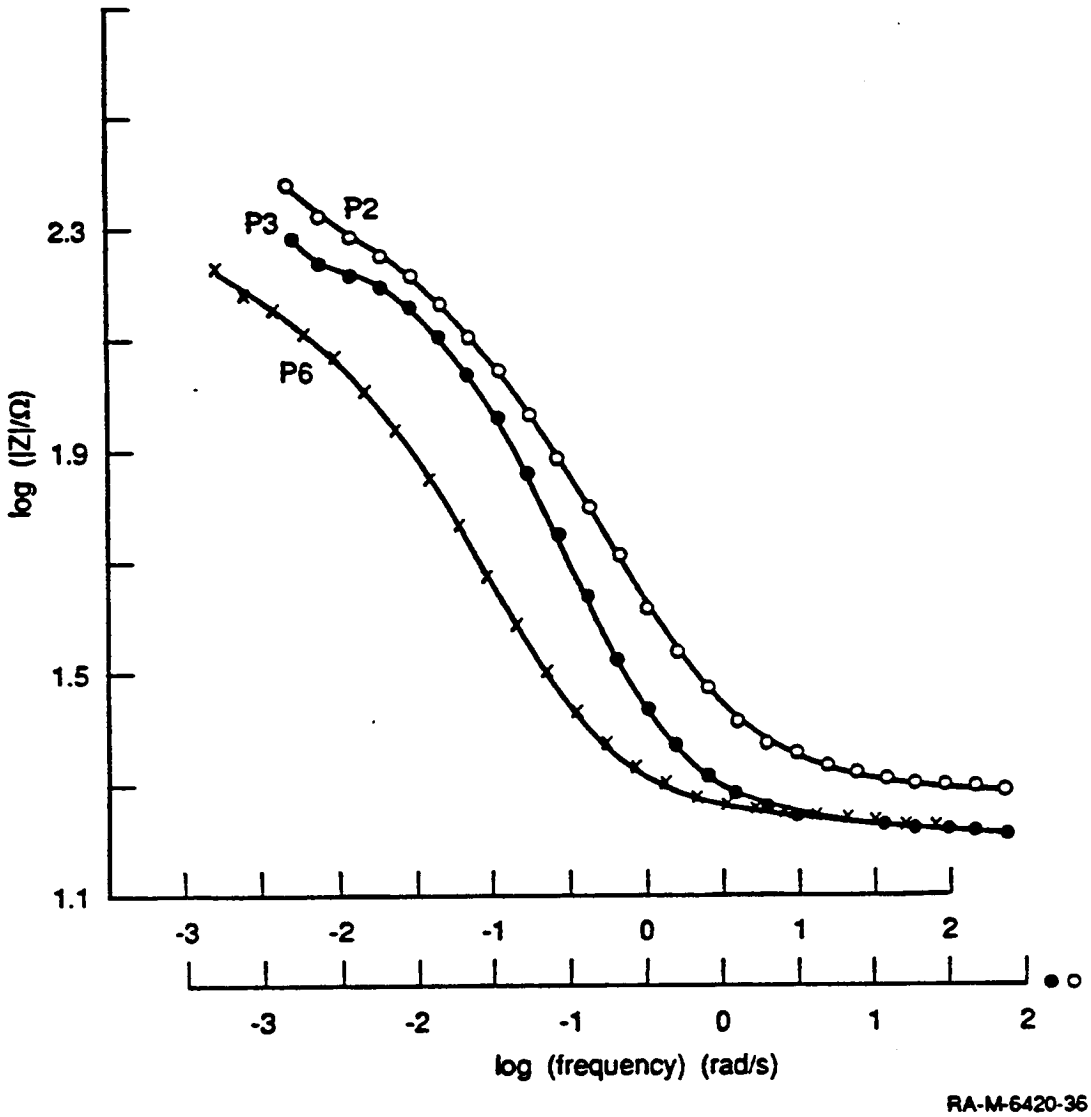

Figure 15. Plots of log (impedance modulus) versus log (frequency). Reference electrode position is given on each curve.

[$CaCl_2$] = 0 wt%; counterelectrode at position 1; imposed current = 330 μA, rebar corroding at cavity b.

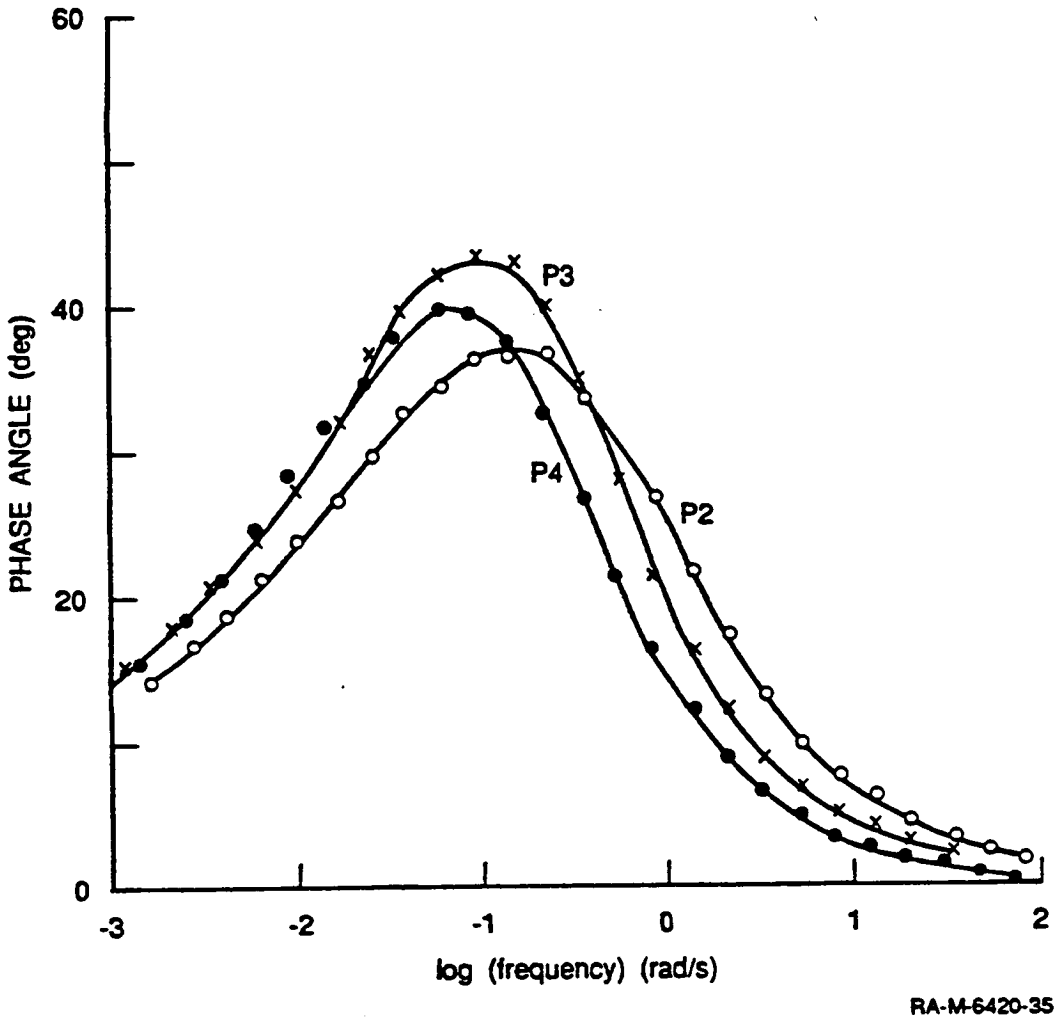

Figure 16. Dependance of phase angle on log of frequency. For each curve, the reference electrode is at the position indicated.

[$CaCl_2$] = 0 wt%; counterelectrode at position 1; imposed current = 330 μA; middle rebar corroding site at mid position 4-5, cavity b;Run No. 1.

Table 3

DEPENDENCE OF DIFFERENT PARAMETERS ON THE POSITION OF THE REFERENCE ELECTRODE FOR ONE-SITE CORRODED REINFORCING BAR IN CONCRETE FOR AN IMPOSED AC CURRENT OF 330 μA[a]

Reference Electrode Position	Bode slope -(∂log|Z|/∂log(f)) 1[b]	2[b]	Θ_{max}/deg 1[b]	2[b]	f_{max}/Hz 1[b]	2[b]	-|Z|/Ω(0.0037 Hz) 1[b]	2[b]
2	0.43	0.45	37.3	37.9	0.022	0.022	127.0	137.3
3	0.53	0.51	43.5	42.0	0.014	0.014	106.8	101.4
4	0.48	0.51	40.4	41.8	0.009	0.009	89.3	94.5
5	0.45	0.47	35.2	38.7	0.014	0.009	76.5	86.8
6	0.46	0.43	37.9	36.7	0.009	0.009	87.1	86.5
7	0.42	0.42	36.5	34.4	0.009	0.009	87.2	79.5
8	0.39	0.40	33.8 33.8	33.7 33.2	0.009	0.014 0.009	76.6	81.1

[a]Slope of the linear intermediate segment of the Bode plot, maximum phase-angle value (Θ_{max}), frequency at which Θ is maximum (f_{max}), and impedance modulus (|Z|) at a fixed frequency of 0.0037 Hz.

[b]Run number.

[$CaCl_2$] = 0 wt%, counterelectrode at position 1; imposed current = 330 μA; forcing bar corroded at cavity b (see Figure 3)

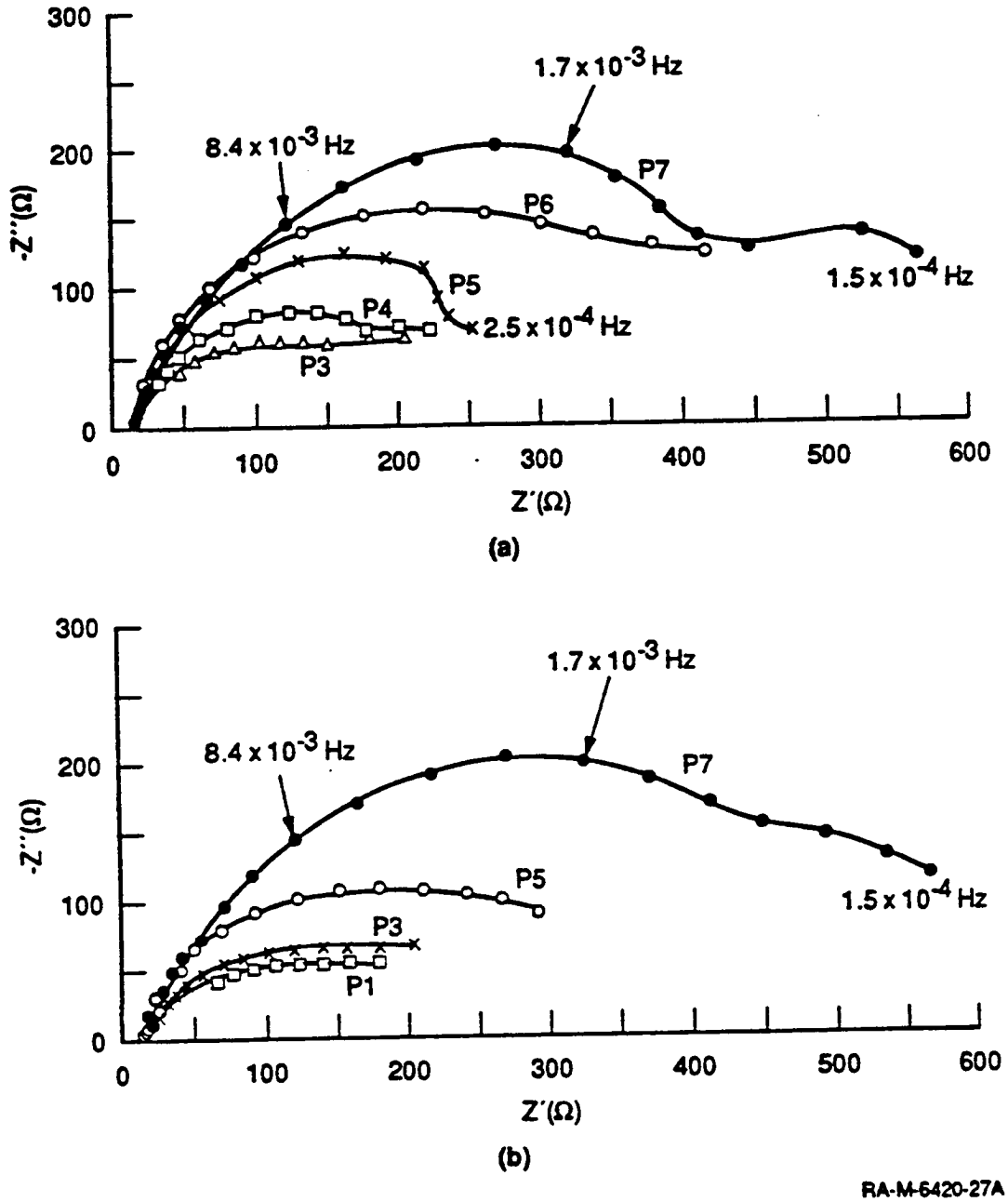

Figure 17. Impedance spectra of corroding rebar for reference electrode at the positions indicated on each curve.

[$CaCl_2$] = 0 wt%; counterelectrode at position 8; imposed current = 500 μA; corroding site at mid position 4-5, cavity b; (a) Run No. 1; (b) Run No. 2.

downward curvature at low frequencies seen above for an imposed ac current of 50 μA (see Figure 11). However, the range of values of the impedance is somewhat greater than for the previous cases (compare Figure 17 with Figures 11 and 14); nevertheless, the values are still smaller than those for noncorroded reinforcing bar (compare Figures 17 and 8). Again, the impedance spectra become smaller as the reference electrode is moved away from the counterelectrode.

Figure 18 illustrates the Bode plots obtained when the imposed ac current is 500 μA and the counterelectrode is at position 8. These plots are similar to those previously analyzed (see Figures 9, 12, and 15), in that they also display a linear segment at intermediate frequencies. The slopes for these linear segments for the different reference electrode positions are listed in Table 4. The highest value for the slope occurs for position 6 of the reference electrode; since this position is analogous to position 3 when the counterelectrode is at position 1, this result falls within the trend previously noted, i.e., an increase in $(\partial|Z|/\partial \log f)$ for first positions of reference electrode near the counterelectrode, followed by a decrease for farther positions.

Figure 19 illustrates the phase-angle plots for three positions of the reference electrode when the imposed ac current is 500 μA. The trends presented are similar to those for the cases previously analyzed, although the range of values for Θ_{max} is greater than those reported in Tables 2 and 3 but is still smaller than that reported in Table 1. The value of f_{max}, except for positions of the reference electrode close to the counterelectrode, is almost constant; this trend is similar to that previously observed (compare Tables 3 and 4).

The variation of the impedance modulus at a fixed frequency of 0.0038 Hz shown in Table 4 is analogous to those previously analyzed, i.e., |Z| becomes smaller as the distance between counter and reference electrodes increases.

Since the concrete slabs that were prepared for this study had three cavities for inducing corrosion on the rebar with acid, we also recorded impedance spectra while the rebar was being corroded at two or at three well-defined and well-separated sites at the same time.

The studies of two-site corroding reinforcing bar in concrete were carried out while corrosion was made to occur simultaneously in cavity b (located between positions 4 and 5) and in cavity a (located between positions 2 and 3) by injection of a 2.0 M HCl solution. The counterelectrode was kept at position 1, while the ac imposed current was 50 μA.

Figure 20 shows the impedance plots obtained for the reference electrode at positions 2, 3, 7, and 8. A comparison of these plots with those for similar conditions but only one corroding site (see Figure 7) shows that their shapes are similar; however, they are smaller for the two-site case. Furthermore, for the two-site case, the impedance decreases greatly when the reference electrode is changed from position 2 to 3, i.e., from a position where no corroding site lies between the counter and reference electrode to a position where there is a corroding site between them. Additionally, the impedance plots for the cases where the two corroding sites were between the counter and reference electrode (e.g., positions 7 and 8;- see Figure 20) exhibit a semicircular shape, almost intersecting the real-impedance axis at two points.

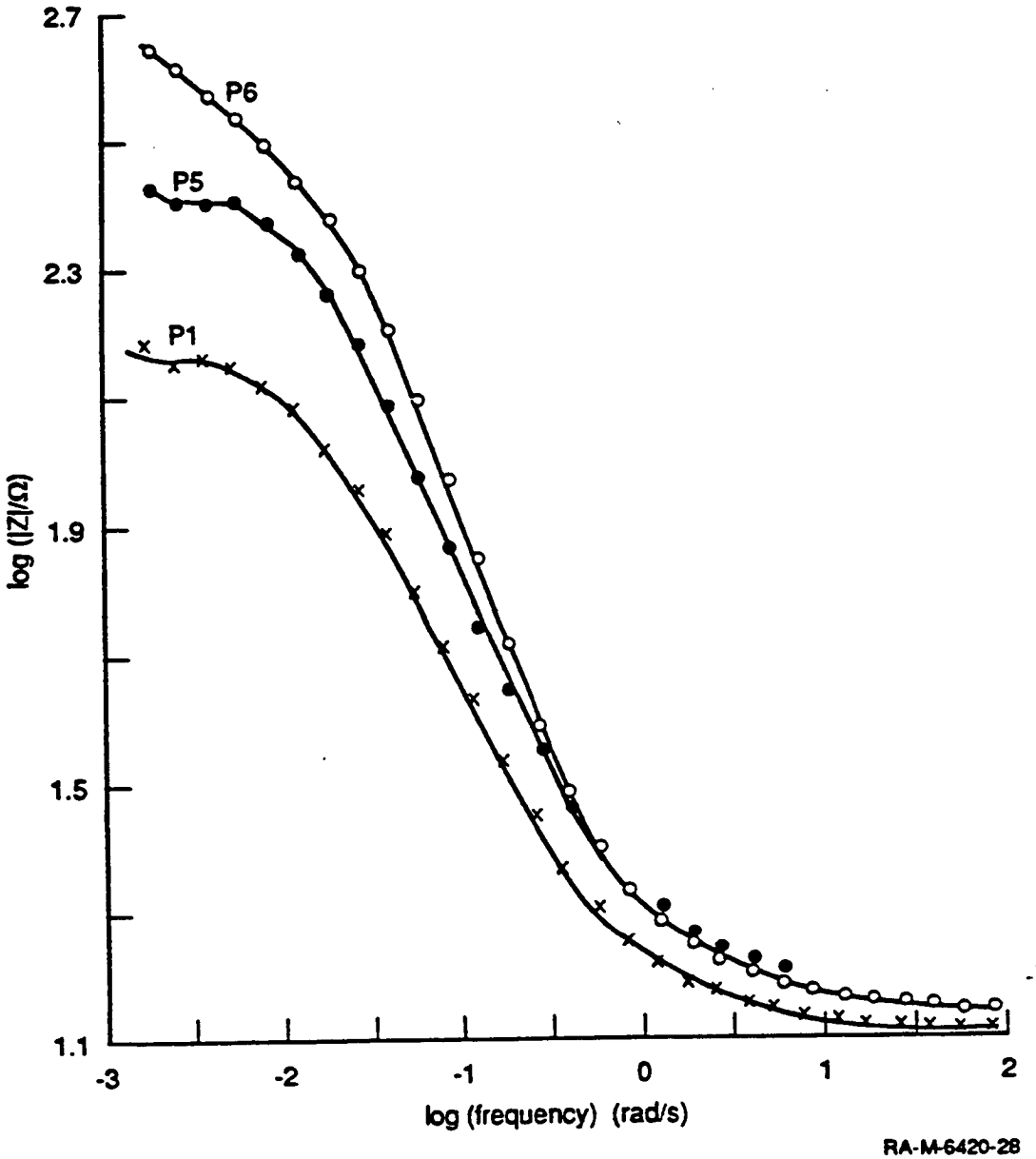

Figure 18. Plots of log (impedance modulus) versus log (frequency). Reference electrode positions shown on the curves.

[$CaCl_2$] = 0 wt%; counterelectrode at position 8; imposed current = 500 μA; corroding site at mid position 4-5, cavity b; Run No. 1.

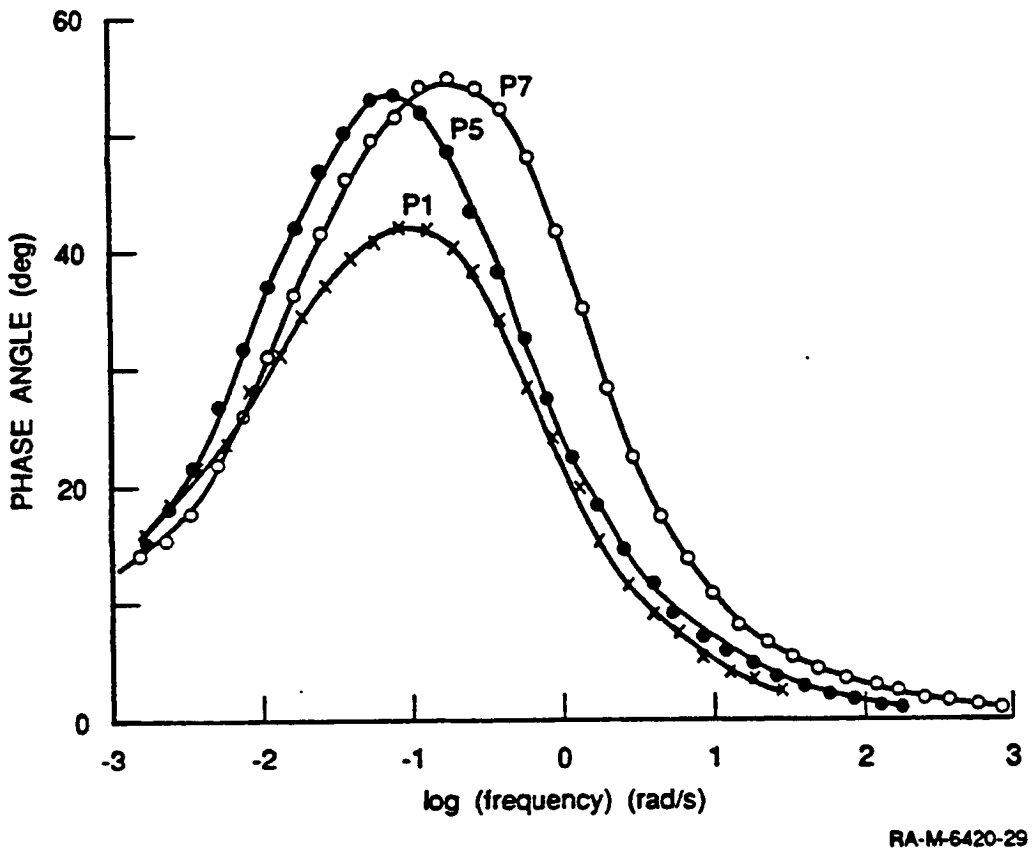

Figure 19. Phase angle dependence on log (frequency). For each curve, the reference electrode is at the position indicated.

$[CaCl_2]$ = 0 wt%; counterelectrode at position 8; imposed current = 500 μA; corroding site at mid position 4-5, cavity b; Run No. 1.

Table 4

DEPENDENCE OF DIFFERENT PARAMETERS ON THE POSITION OF THE REFERENCE ELECTRODE FOR ONE-SITE CORRODED REINFORCING BAR IN CONCRETE FOR AN IMPOSED AC CURRENT OF 500 μA[a]

Reference Electrode Position	Bode slope -(∂log|Z|/∂log(f)) 1[b]	2[b]	Θ_{max}/deg 1[b]	2[b]	f_{max}/Hz 1[b]	2[b]	|Z|/Ω(0.0038 Hz)** 1[b]	2[b]
1	0.50	0.50	42.3	39.2 39.1	0.012	0.008 0.012	87.7	76.9
2	0.41	0.44	41.8	39.0	0.012	0.012	103.0	83.9
3	0.45	0.56	40.6 40.6	43.3 43.3	0.012 0.008	0.012 0.008	89.7	105.0
4	0.52	0.58	47.1	47.5	0.008	0.008	107.6	114.7
5	0.58	0.61	53.7	52.0 51.9	0.012	0.012 0.008	149.3	130.7
6	0.71	--	58.6	--	0.018	--	195.6	--
7	0.65	0.58	54.9	56.1	0.028	0.042	288.3	299.3

[a]Slope of the linear intermediate segment of the Bode plot, maximum phase-angle value (Θ_{max}), frequency at which Θ is maximum (f_{max}), and impedance modulus (|Z|) at a fixed frequency of 0.0038 Hz.

[b]Run number

[$CaCl_2$] = 0 wt%, counterelectrode at position 8; imposed current = 500 μA; reinforcing bar corroded at cavity b (see Figure 3).

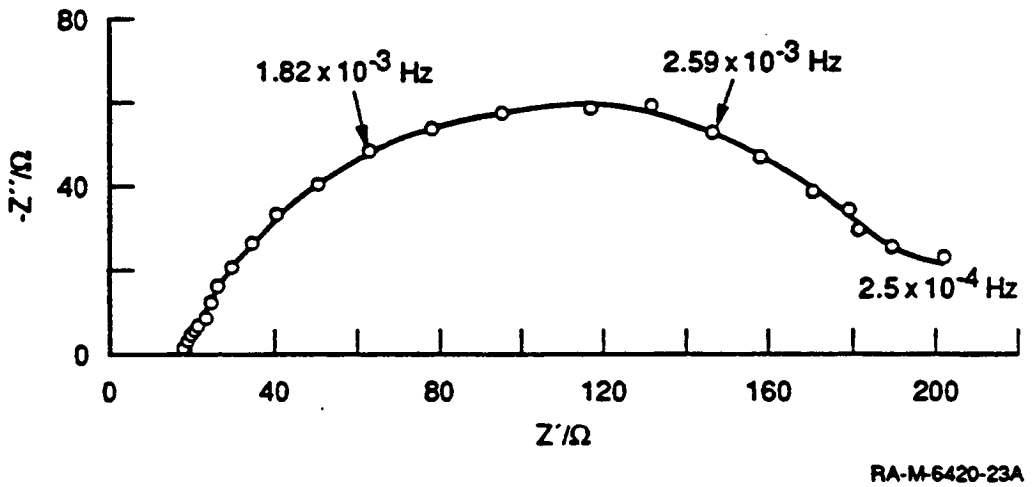

Figure 20. Typical impedance spectrum of corroding rebar in concrete. [$CaCl_2$] = 0 wt%; imposed current = 50 μA (peak-to-peak).

Figure 21 shows three representative Bode plots, which exhibit the same general characteristics of those already analyzed (Figures 12, 15, and 18). The values of the slopes of the linear segments of these plots at intermediate frequencies are listed in Table 5. The comparison of these slope values with those for one-site corrosion (see Table 2) shows clearly that they become smaller after one (or two) corrosion sites are located between the counter and reference electrodes. These cases occur for the reference electrode at position 5 for one-site corrosion (see Table 2) and at position 3 for two-site corrosion (see Table 5). In conclusion, corrosion at localized regions between the counter and reference electrodes seems to especially modify the impedance spectra.

Phase-angle plots are illustrated in Figure 22; the plots become smaller as the reference electrode is moved away from the counterelectrode (plots for reference electrode positions not shown follow the same trend). Accordingly, the values for Θ_{max} (see Table 5) decrease steadily as the reference electrode is moved away from the counterelectrode. The range of Θ_{max} values is now 19° to 39° compared with 24 to 49° for one-site corroding rebar (see Table 2). The values of f_{max} are almost constant for all reference electrode positions which correspond to having one or two corrosion sites between counter and reference electrodes (positions 3-8). However, the f_{max} values are slightly higher for position 2.

Values of the impedance modulus at a frequency of 3.8 mHz (Table 5) clearly illustrate once again the influence of a corrosion site between the counter and reference electrodes on the impedance response of the system, since they fall sharply when the reference electrode position is changed from 2 to 3.

The impedance spectra for three-site corroding rebar (cavities a, b, and c shown in Figure 3) for different positions of the reference electrode are illustrated in Figures 23(a) and 23(b). The spectra are smaller, at any given frequency, than those obtained for two-site corroding rebar (see Figure20); significantly, the spectrum for the reference electrode at position 2 (no corroding site between counter and reference electrodes) is the one that displays the smallest decrease. As the number of corroding sites between counter and reference electrodes increases, the impedance spectrum becomes smaller with a maximum at relatively higher frequencies, presenting in some instances a psuedo-inductive loop at low frequency [see Figure 23(b)].

The Bode plots (Figure 24) retain the general characteristics of those previously analyzed. However, the values of the slopes of the linear segment at intermediate frequencies are significantly lower (Table 6) than the approximately -0.5 value that had been found for previous cases (see Tables 2 through 5). The impedance modulus does not seem to depend as strongly on frequency as in the cases of two- and one-site corroding rebars and is much less dependent when compared with the noncorroded rebar.

The phase-angle plots (Figure 25) are similar to the previous ones analyzed but display much lower values of Θ_{max}, which decrease as the distance between counter and reference electrodes is increased (range of 10° to 36°; see Table 6). The values of f_{max} (Table 6) first decrease as the distance between counter and reference electrodes is increased, but then increase for the two largest distances (positions 6 and 7) to a value even higher than that when the reference electrode is at position 2.

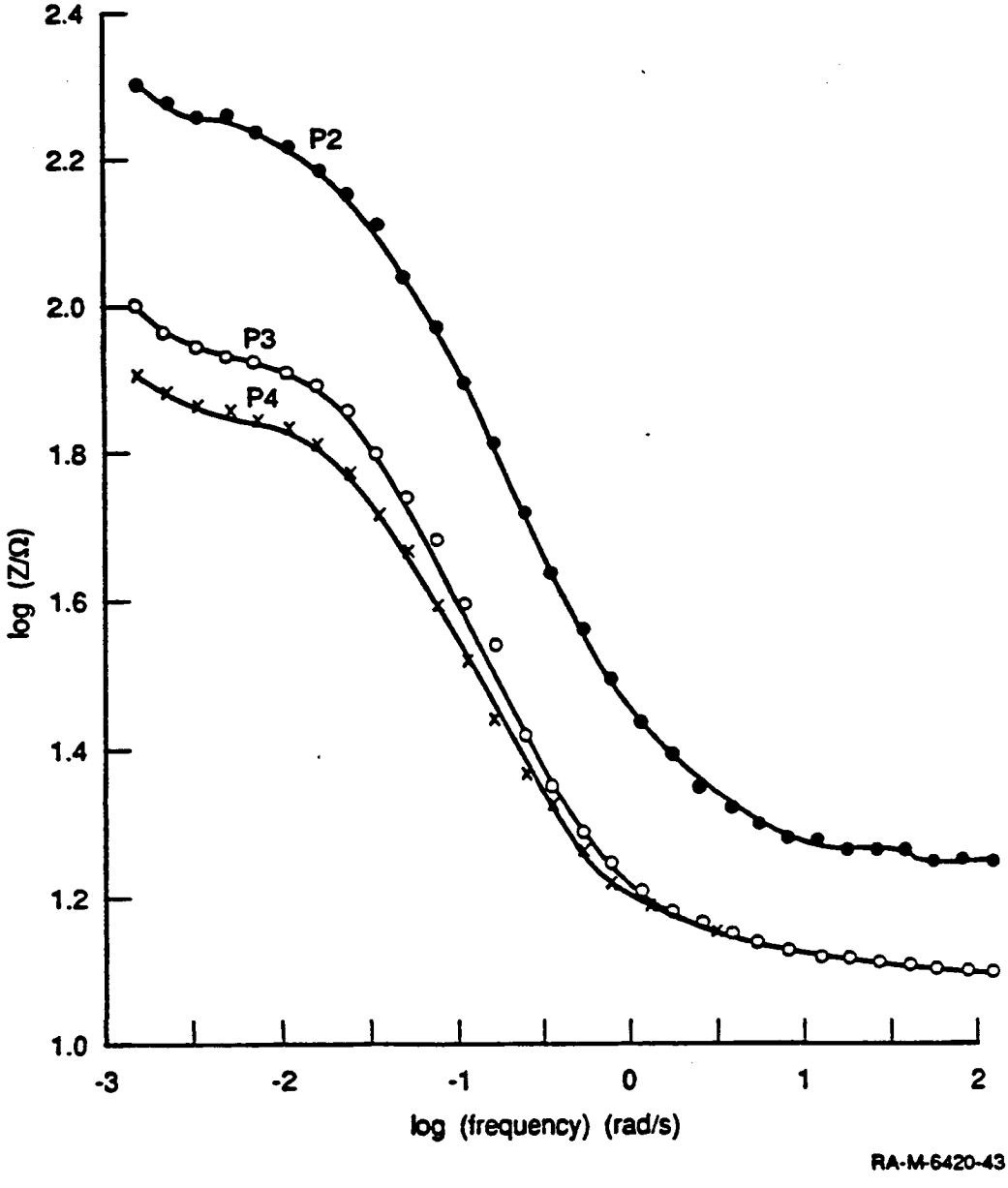

Figure 21. Sample plots of log (impedance modulus) versus log (frequency) for three different positions of reference electrode as shown.

[$CaCl_2$] = 0 wt%; counterelectrode at position 1; imposed current = 50 μA; concrete rebar corroding at middle and right-hand-side (cavities a and b in Figure 3); Run No. 1.

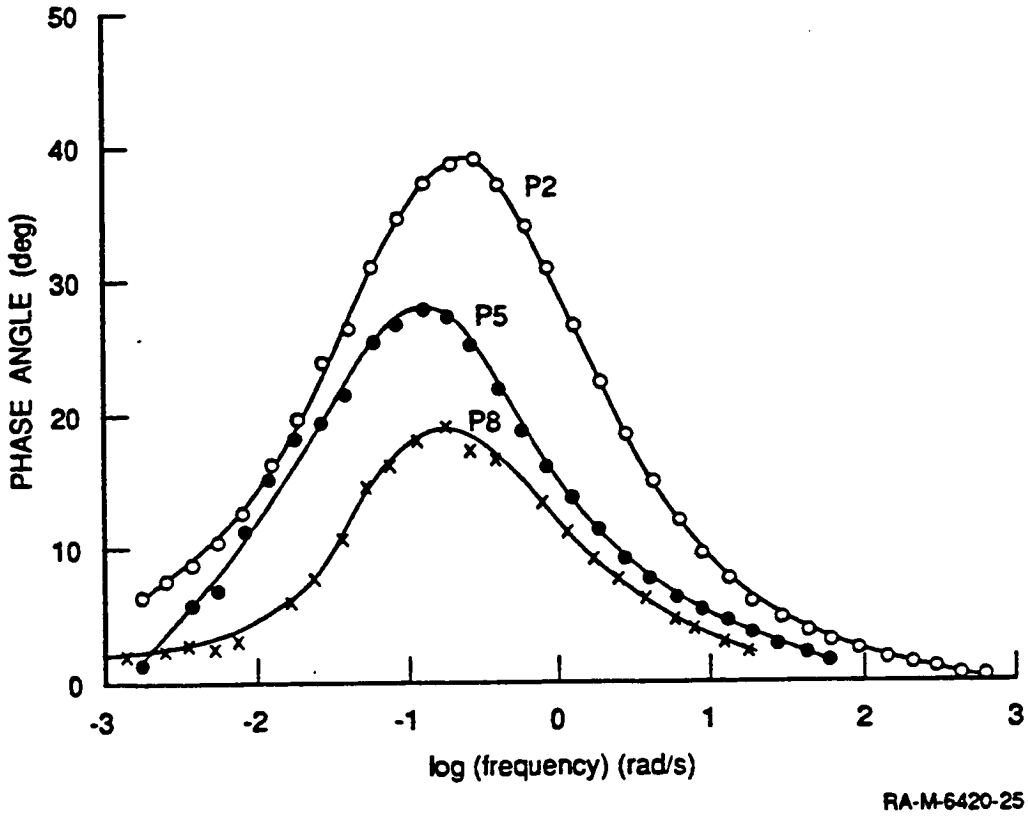

Figure 22. Dependence of phase angle on log (frequency). For each curve, the reference electrode is at the position indicated.

[$CaCl_2$] = 0 wt%; counterelectrode at position 1, imposed current = 50 μA; corroding sites at mid positions 4-5 and 2-3, cavities b and a.

Table 5

DEPENDENCE OF DIFFERENT PARAMETERS ON THE POSITION OF THE REFERENCE ELECTRODE FOR TWO-SITE CORRODED REINFORCING BAR IN CONCRETE[a]

Reference Electrode Position	Bode slope $-(\partial \log\|Z\|/\partial \log(f))$	Θ_{max}/deg	f_{max}/Hz	$\|Z\|/\Omega$(0.0038 Hz)
2	0.46	39.1	0.040	111.6
3	0.45	36.5	0.018	72.6
4	0.37	33.3	0.027	60.2
5	0.30	27.6	0.018	54.7
6	0.40	22.1	0.027	59.2
7	0.33	26.5	0.027	53.1
8	0.23	18.9	0.027	35.8

[a]Slope of the linear intermediate segment of the Bode plot, maximum phase-angle value (Θ_{max}), frequency at which Θ is maximum (f_{max}), and impedance modulus ($|Z|$) at a fixed frequency of 0.0038 Hz.
Counterelectrode at position 1, imposed current = 50 μA; reinforcing bar corroded at cavities a and b see Figure 3.

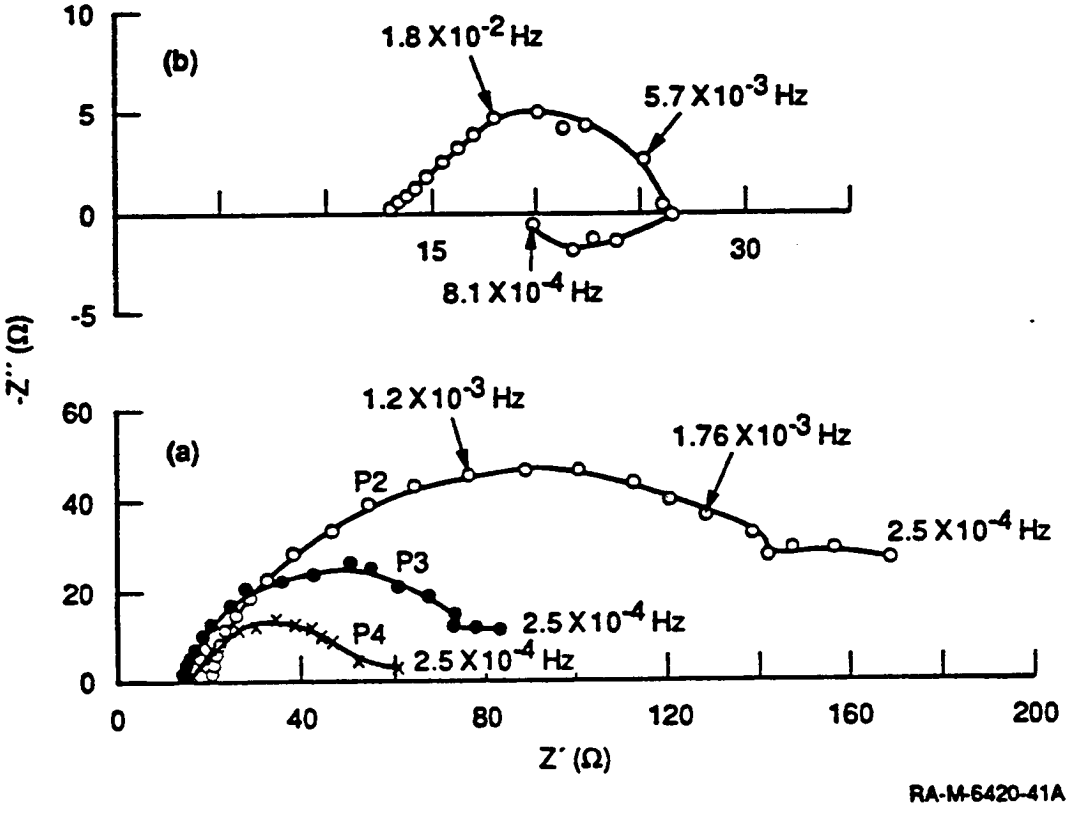

Figure 23. Impedance spectra of rebar in concrete corroding at 3 sites (the three cavities shown in Figure 3).

(a) Reference electrode positions 2 to 4. (b) Impedance spectrum for reference electrode at position 7. [$CaCl_2$] = 0 wt%; imposed current = 50 μA; counterelectrode at position 1; Run No. 1.

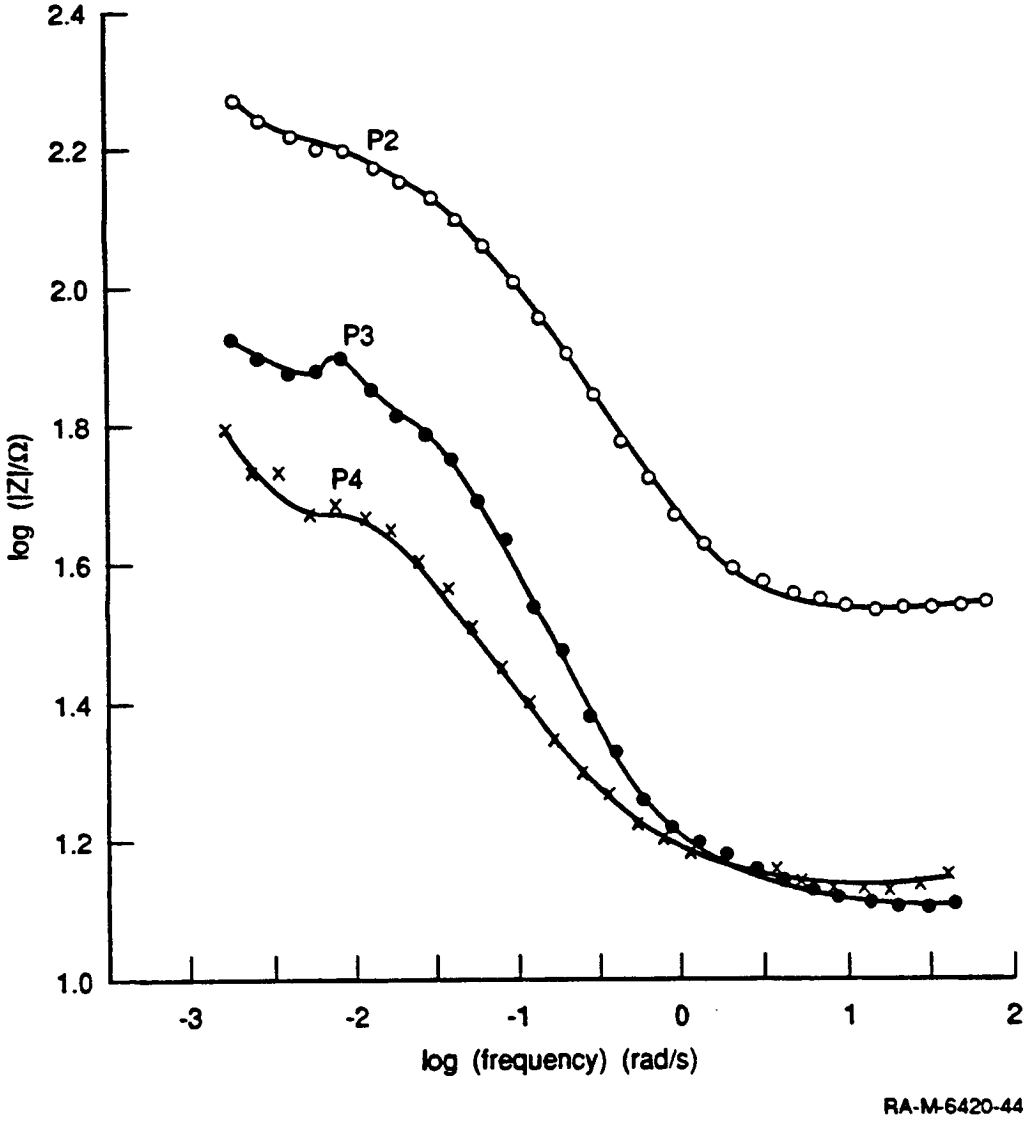

Figure 24. Sample plots of log (impedance modulus) versus log (frequency) , for three different positions of reference electrode as shown.

$[CaCl_2] = 0$; counterelectrode at position 1; imposed current = 50 μA; concrete rebar corroding at cavities a, b, and c (see Figure 3).

Table 6

DEPENDENCE OF DIFFERENT PARAMETERS ON THE POSITION OF THE REFERENCE ELECTRODE FOR THREE-SITE CORRODED REINFORCING BAR IN CONCRETE[a]

Reference Electrode Position	Bode slope $-(\partial \log\|Z\|/\partial \log(f))$	Θ_{max}/deg	f_{max}/Hz	Z/Ω(0.0038 Hz)*
2	0.32	29.9	0.027	134.4
3	0.41	36.3	0.018	60.3
4	0.29	24.8	0.012	39.7
5	0.17	14.0 14.2	0.012 0.059	29.5
6	0.13	11.9	0.059	23.7
7	0.16	14.5	0.059	26.5

[a]Slope of the linear intermediate segment of the Bode plot, maximum phase-angle value (Θ_{max}), frequency at which Θ is maximum (f_{max}), and impedance modulus (|Z|) at a fixed frequency of 0.0038 Hz. [$CaCl_2$] = 0 wt%; imposed current = 50 μA; counterelectrode at position 1; rebar corroded at cavities a, b, and c (see Figure 3).

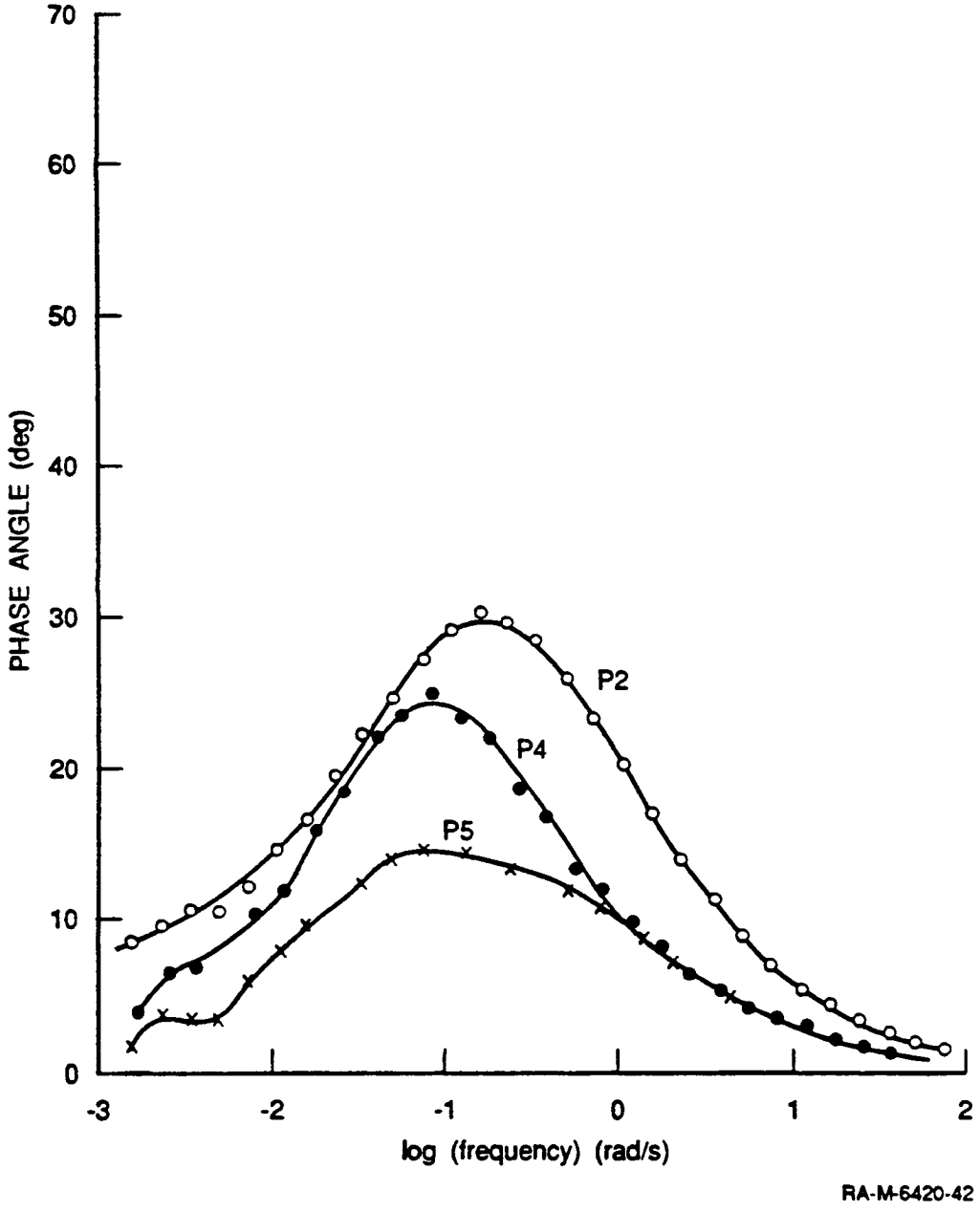

Figure 25. Dependence of phase angle on log (frequency). For each curve, the reference electrode is at the position indicated.

[$CaCl_2$] = 0 wt%; counterelectrode at position 1; imposed current = 50μA; Run No. 1; corroding sites at cavities a, b, and c (see Figure 3).

The values of the impedance magnitude (see Table 6) again confirm that there is a decrease in the impedance response when corrosion occurs at three sites instead of two sites (see Table 5).

DISCUSSION

The impedance characteristics of reinforcing bar in concrete have been experimentally investigated in detail for concrete slabs ~240 cm long, employing an ac signal of frequency as low as 0.1 mHz. Impedance spectra were obtained for different distances between counter and reference electrodes (by moving the latter) for different fixed positions of the counterelectrode and for the presence or absence of regions of high corrosion activity on the rebar as induced by hydrochloric acid. The impedance response was analyzed for trends in the complex-plane, Bode, and phase-angle plots, and with respect to changes in the maximum phase-angle (Θ_{max}), the frequency at which Θ is maximum, the values of the slopes of the linear segment (at intermediate frequencies) of the Bode plots, and the values of the impedance modulus at a fixed (low) frequency.

Figure 26 compares impedance spectra for noncorroding and corroding (cavity 6) rebar, for the same position of the reference electrode (position 2), which is 17 cm away from position 1 (the location of the counterelectrode). Figure 27 shows the same comparison for the reference electrode at position 8 (220 cm away from the position of the counterelectrode). It is clear from these figures that, irrespective of the reference electrode position, the impedance values are significantly lower for corroding rebars than for noncorroding rebars. Thus, we conclude that the impedance of the system is reduced by the occurrence of corrosion at a site that is remote from the point of sensing (the position of the reference electrode).

The variation of the impedance modulus |Z| at a fixed frequency (3.8 mHz) with the position of the reference electrode for the different sets of data experimentally obtained in this study is shown in Figure 28. This figure clearly shows that inducing corrosion (one site) on the rebar causes a sharp decrease in |Z|, which further decreases as more corrosion sites are added. Thus, it seems to be possible to differentiate between noncorroded and corroding reinforcing bar in concrete structures by careful analysis of impedance spectral measurements.

Variation of the slope of the linear segment (for intermediate frequencies) of the Bode plot with the position of the reference electrode is shown in Figure 29. When the counter electrode is kept at position 1, in general the slope reaches a maximum when the reference electrode is in position 3, irrespective of the presence or absence of corroding activity on the reinforcing bar. It is also clear from this figure that, after the maximum, the values of the Bode slope tend to become approximately constant; this trend is shared by corroding and noncorroding rebars. Furthermore, the value of the Bode slope for a given reference electrode position also decreases as the number of corroding sites is increased, becoming as low as -0.16 for three-site corroding rebars. The same trends are shown by the slopes of Bode plots for data obtained for the counterelectrode at position 8 (Figure 29).

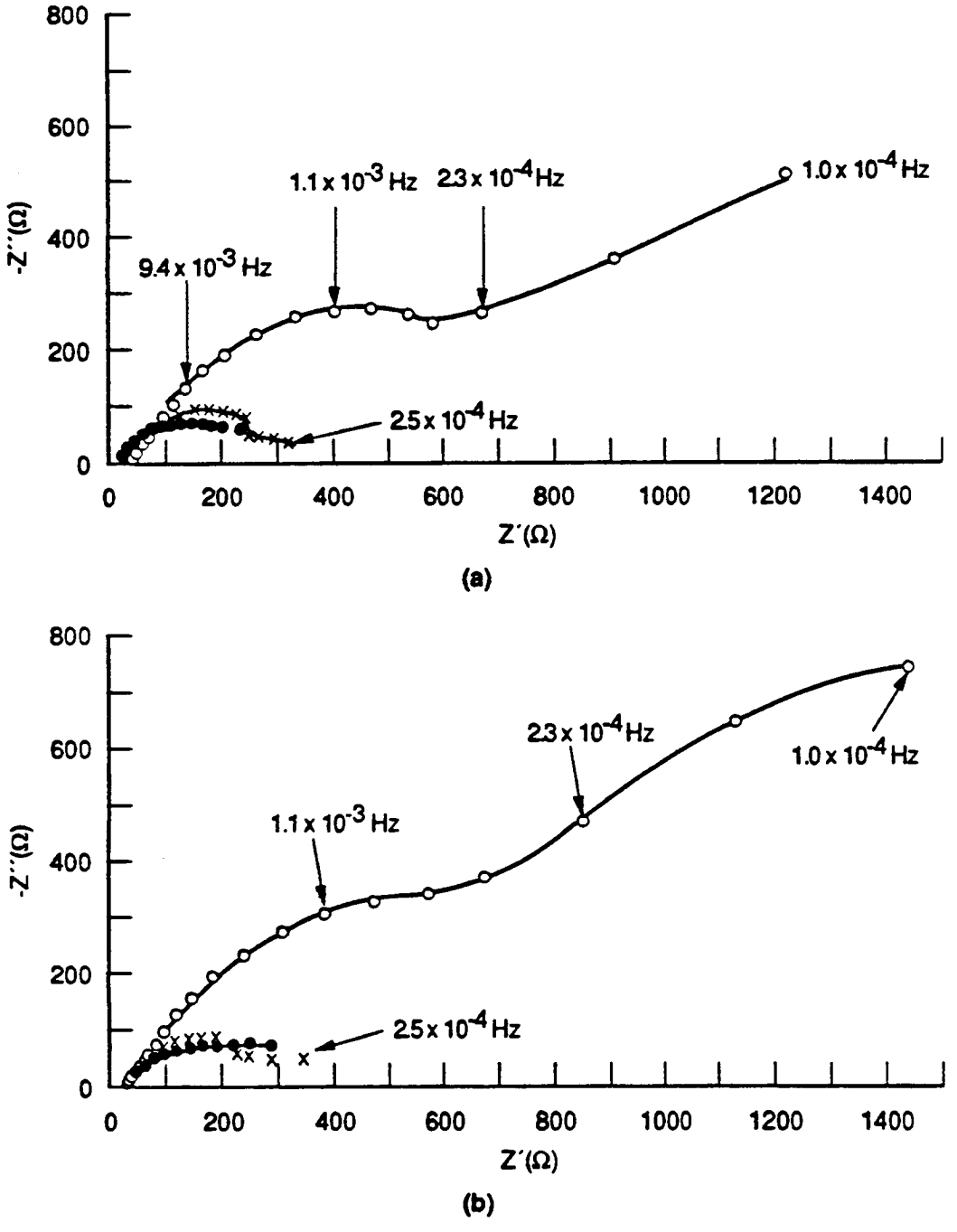

Figure 26. Comparison of impedance spectra of corroded and noncorroded rebar in concrete, where reference electrode is at position 2, counterelectrode is at position 1, and [$CaCl_2$] = 0 wt%.

o: Right-hand-side noncorroding rebar
x,•: Middle rebar corroded at mid position 4-5, cavity b (see Figure 3)
Imposed current = (x) 50μA and (•) 330μA ; (a) Run No. 1; (b) Run No. 2.

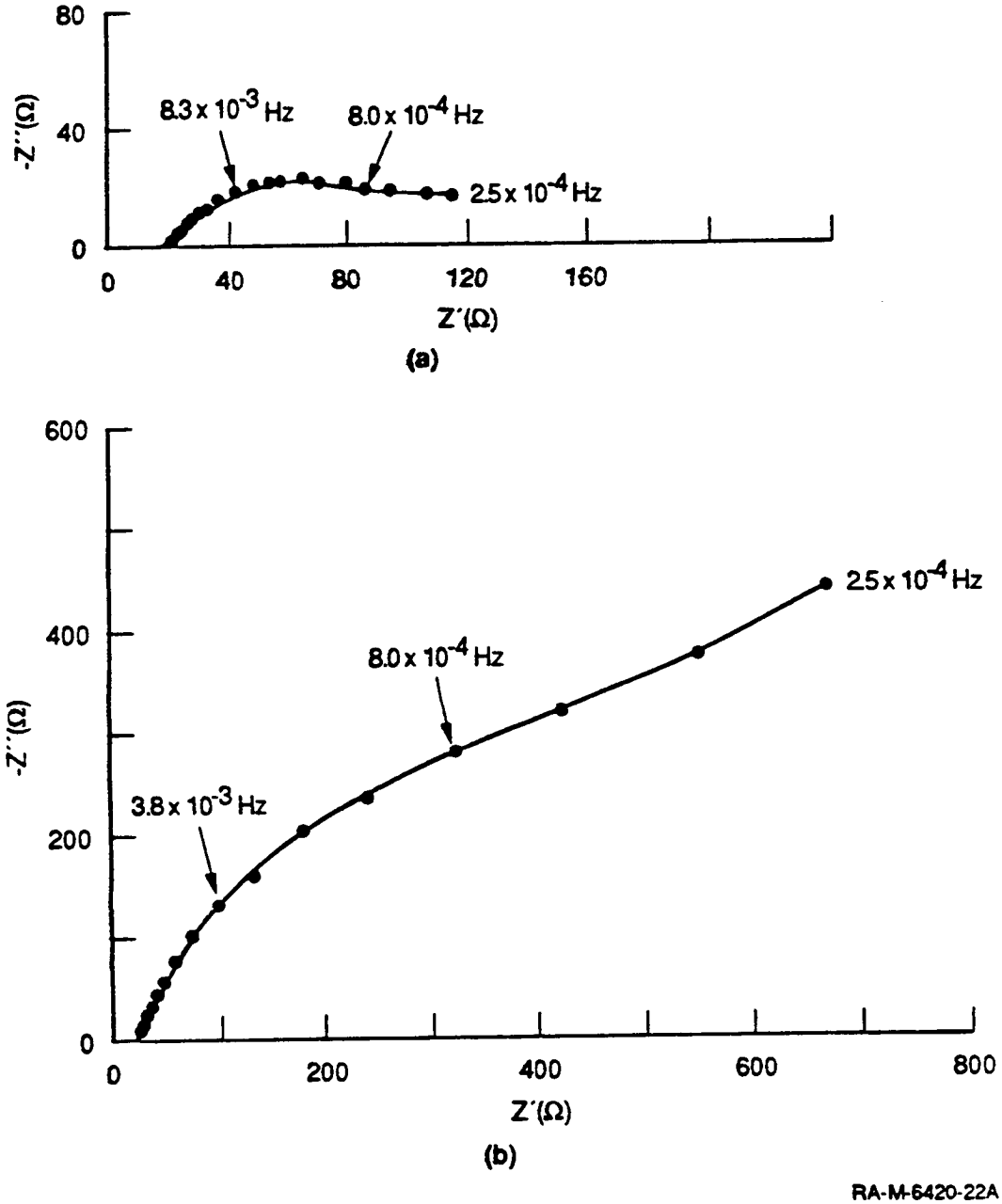

Figure 27. Impedance spectra for (a) corroding rebar at mid position 4-5, cavity b, and for (b), noncorroding rebar, for reference electrode at position 8.

[$CaCl_2$] = 0 wt%; imposed current = 50 μA; counterelectrode at position 1.

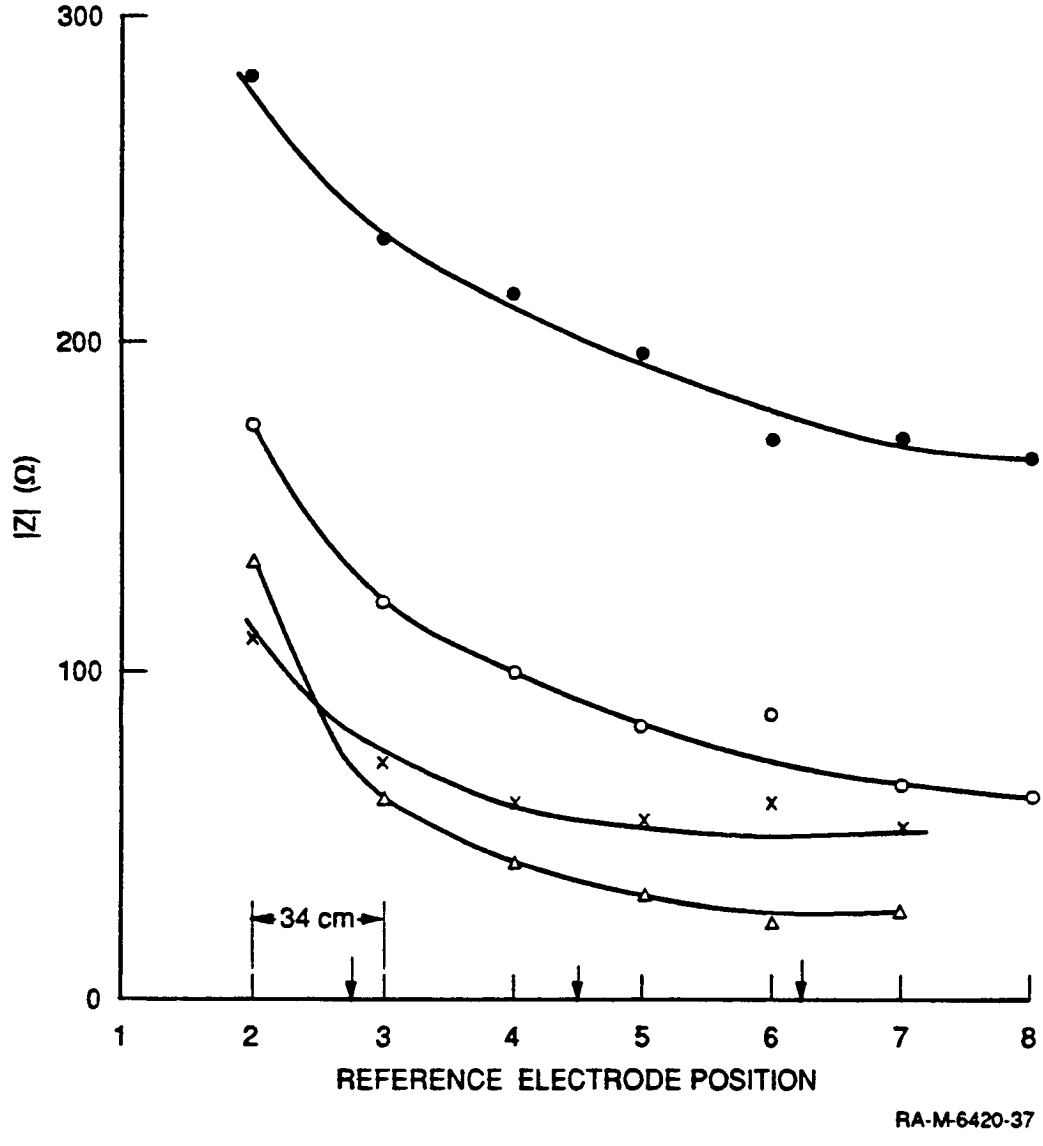

Figure 28. Impedance modulus at 0.0038 Hz as a function of the distance between the counterelectrode and reference electrode (counterelectrode at position 1).

[$CaCl_2$] = 0 wt%; imposed current = 50 μA; arrows indicate position of corrosion sites.
●: No corrosion, o: 1-site corrosion, x: 2-site corrosion,
△: 3-site corrosion.

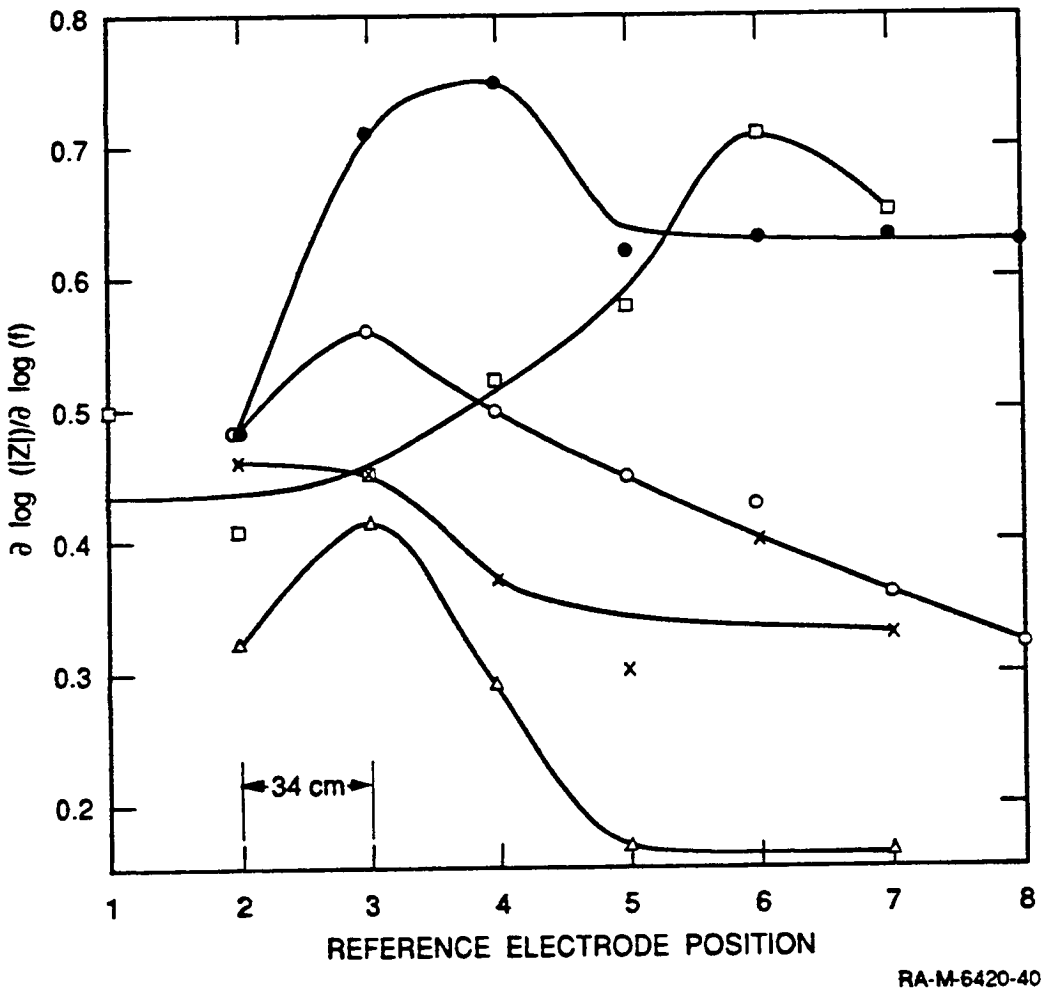

Figure 29. Value of Bode slope as a function of reference electrode location of 0-, 1-, 2-, and 3-site corroding rebar.

● : no corrosion, o: 1-site corrosion, x: 2-site corrosion and △ : 3-site corrosion; counterelectrode at position 1; imposed current = 50 μA.
□: 1-site corrosion counterelectrode at position 8; imposed current = 500 μA.

Our study has shown that the most sensitive parameter for detecting and locating corrosion on reinforcing bars in concrete structures is the maximum value of the phase angle, Θ_{max}, as well as the frequency, f_{max}, at which Θ_{max} occurs. Figure 30 shows the influence of the number of initiated corrosion sites has on the phase-angle plots. The figure clearly shows that Θ_{max} decreases as the number of corroding sites is increased; however as the plots for positions 4 and 7 of the reference electrode show, this decrease becomes more pronounced as the reference electrode is moved away from the counterelectrode. The high sensitivity of the phase angle to the presence of corrosion on rebar in reinforced concrete was predicted theoretically by Macdonald, McKubre, and Urquidi-Macdonald[4] in a study that formed the basis for the present work.

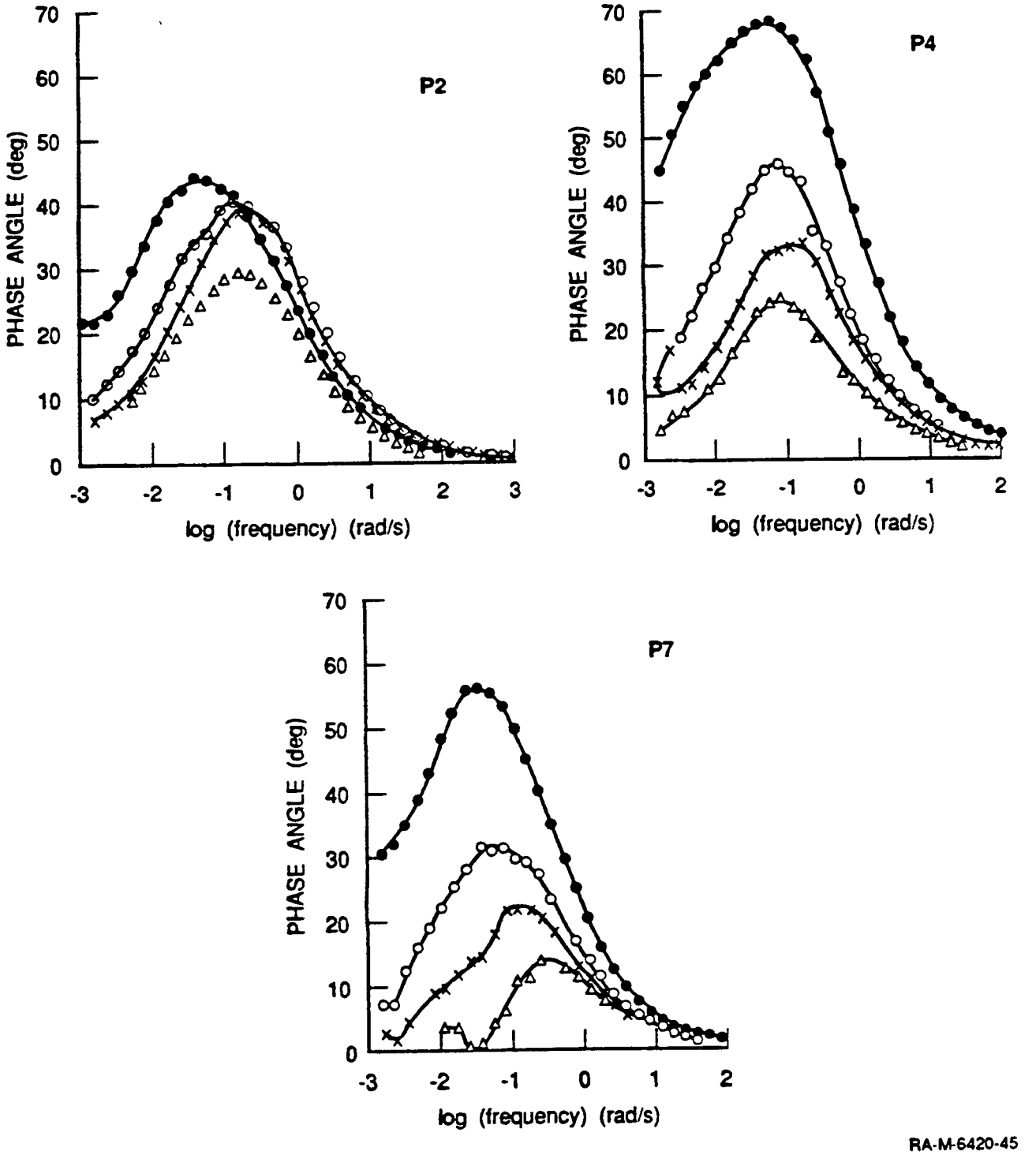

Figure 30. Effect of increasing number of corrosion sites of rebar on the phase angle plots.

Data for reference electrode at positions 2, 4, and 7 are shown.
[$CaCl_2$] = 0 wt%; counterelectrode at position 1; imposed current = 50 μA;
●: No corrosion, o: 1-site corrosion, x: 2-site corrosion,
Δ: 3-site corrosion.

3

TRANSMISSION LINE MODELING

Electrochemical methods are currently being used extensively to investigate the corrosion of rebar in concrete.[1-13] Recently, the problems associated with interpreting data from electrochemical and corrosion studies on highly asymmetric conductors (as may be the case for rebar) in a resistive, nonhomogeneous medium (as is the case for concrete) have been pointed out.[4-12,13] Until recently, impedance or polarization data usually have been interpreted in terms of simple electrical equivalent circuits. However, the reported impedance spectra typically are characteristic of distributed systems, in which the low-frequency imaginary component is depressed relative to the real component (see Experimental Studies, above). Thus, the impedance response of such systems cannot be described in terms of a simple electrical circuit but instead should be interpreted in terms of electrical transmission lines.[4,12,13]

Mathematical techniques for analyzing one-dimensional, uniform, finite, or infinite transmission lines are well developed, and these electrical models have been extensively used to describe corrosion and electrochemical processes.[4,12-21] In this project, we used electrical transmission line models to describe the impedance response of rebar in reinforced concrete slabs for several different experimental situations.

Our purpose in exploring transmission line models was to determine whether the experimental observations reported in the previous section could be understood in terms of relatively simple electrical equivalent circuits that incorporate the distributed characteristics of a one-dimensional rebar and the nonuniform nature of corrosion on localized regions of the bar. While a model of high fidelity would be of considerable theoretical value, it is not necessary for the purpose of using ULFACIS to survey corrosion damage as indicated in the previous section. However,, readers who wish to delve into the mathematical aspects of our work are directed to the full report on this project, in which we develop a method for measuring the polarization resistance of corroding rebar in concrete.

DESCRIPTION OF THE MODEL USED

On the basis of on a previous one-dimensional uniform transmission line model[4] and assuming that the electrical properties of rebar and concrete are purely resistive in nature, the reinforced concrete slabs studied in this project can be viewed as one-dimensional transmission lines (Figure 31).

The ac impedance measurements were carried out for two different arrangements of the electrodes: (1) working electrode (rebar) and counterelectrode connections at the same end of the slab (hereinafter referred to as case 1) and (2) working electrode and counterelectrode connections at opposite ends of the slab (hereinafter referred as case 2). In both arrangements, the position of the reference electrode was varied from one end to the other end of the slab. Figure 32 shows the discretized transmission line models for the reinforced concrete slabs corresponding to these two different experimental setups. In developing these models, we assumed that the resistivity of both concrete (R_C) and rebar (R_M) is independent of position. On the other hand, as a first approach, the concrete-rebar interfacial impedance (Z_i) was assumed to be position independent.

Application of Kirchhoff's voltage law for each segment of the transmission line allows the calculation of the value of I_k, i.e., the alternating current in each segment. Hence, for case 1, the impedance (Z) of the system (as a function of the angular frequency of the applied alternating current) can be calculated as

$$Z(\omega) = -\left(R_s \sum_{k=o}^{Nref} I_k(\omega) + I_1(\omega) Z_o(\omega) \right) \Big/ \; I + Z_o(\omega) \qquad (6)$$

where R_S is the resistance of concrete per segment, Nref is the position of the reference electrode along the line, $I_k(\omega)$ is the (frequency dependent) alternating current in segment k, $Z_o(\omega)$ is the rebar-concrete interfacial impedance at position 1 (see Figure 28), and I the imposed alternating current. The analogous expression for case 2 is

$$Z(\omega) = -\left(R_s \sum_{k=o}^{Nref} I_k(\omega) + I_1(\omega) Z_o(\omega) \right) \Big/ \; I \qquad (7)$$

Considering that the rebar is corroding, the rebar-concrete interfacial impedance may be modeled by the equivalent circuit shown in Figure 33(a), where Z^{NC} is the interfacial impedance attributed to the noncorroded areas and Z^C is the interfacial impedance associated with corroding areas. Thus, the interfacial impedance, Z_k, of each segment k can be viewed as having a contribution from both of these components. If we define θ as the fraction of the area of the k^{th} segment that is corroding then

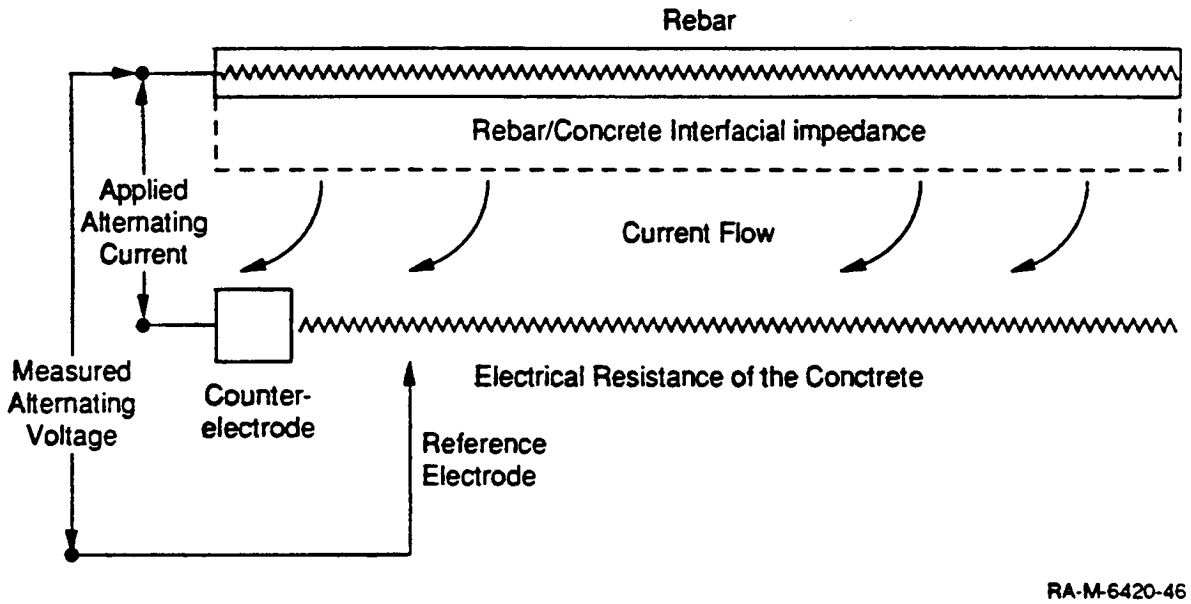

Figure 31. Schematic transmission line model for the reinforced concrete slabs.

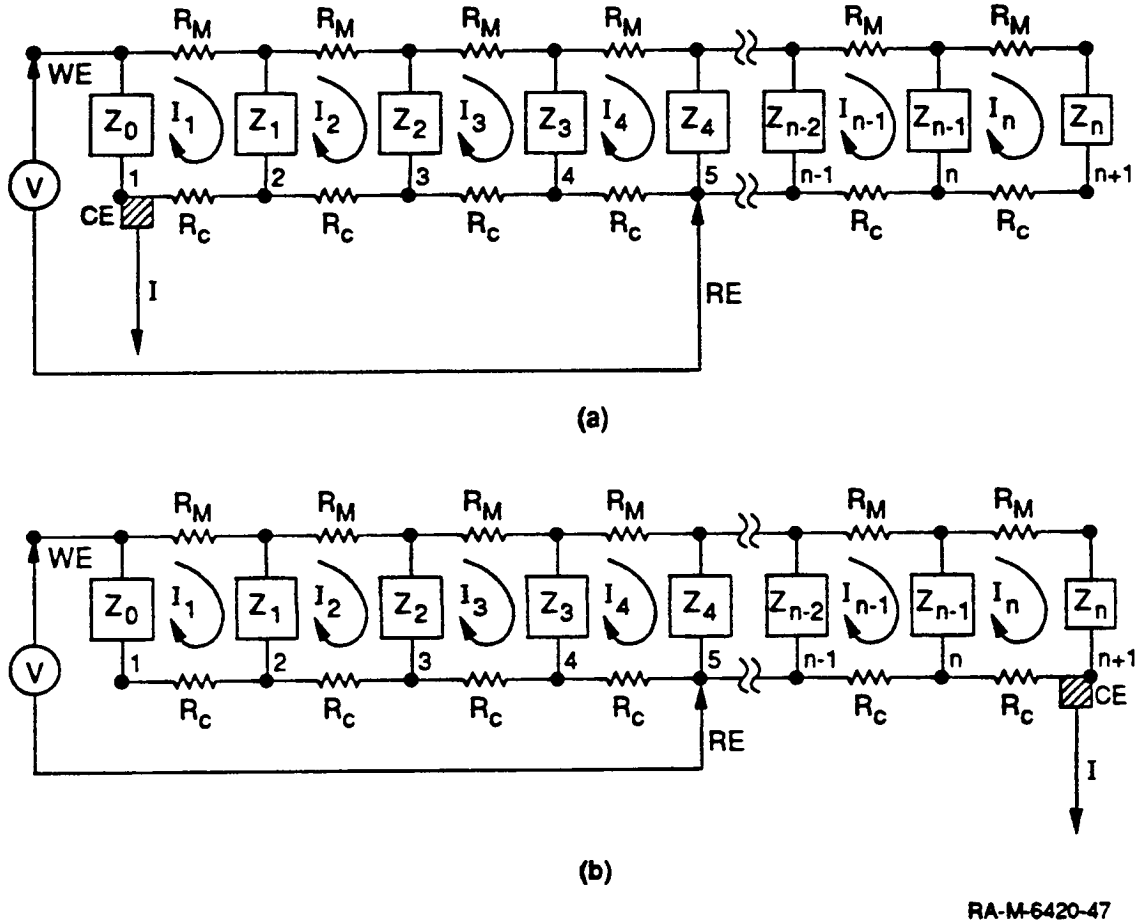

Figure 32. Discriticized transmission line models used for the reinforced concrete slabs.

WE = working electrode; CE = counterelectrode; RE = reference electrode; R_M = resistance of metal per segment; R_C = resistance of concrete per segment; Z_i = rebar/concrete interfacial impedance per segment. [I_i = alternating current in segment i; I = applied alternating current.]

(a) Case 1: counterelectrode at position 1 and reference electrode at any position between 2 and n (here illustrated at position 5); (b) Case 2: counterelectrode at position n + 1 and reference electrode at any position between 1 and n (here illustrated at position 5).

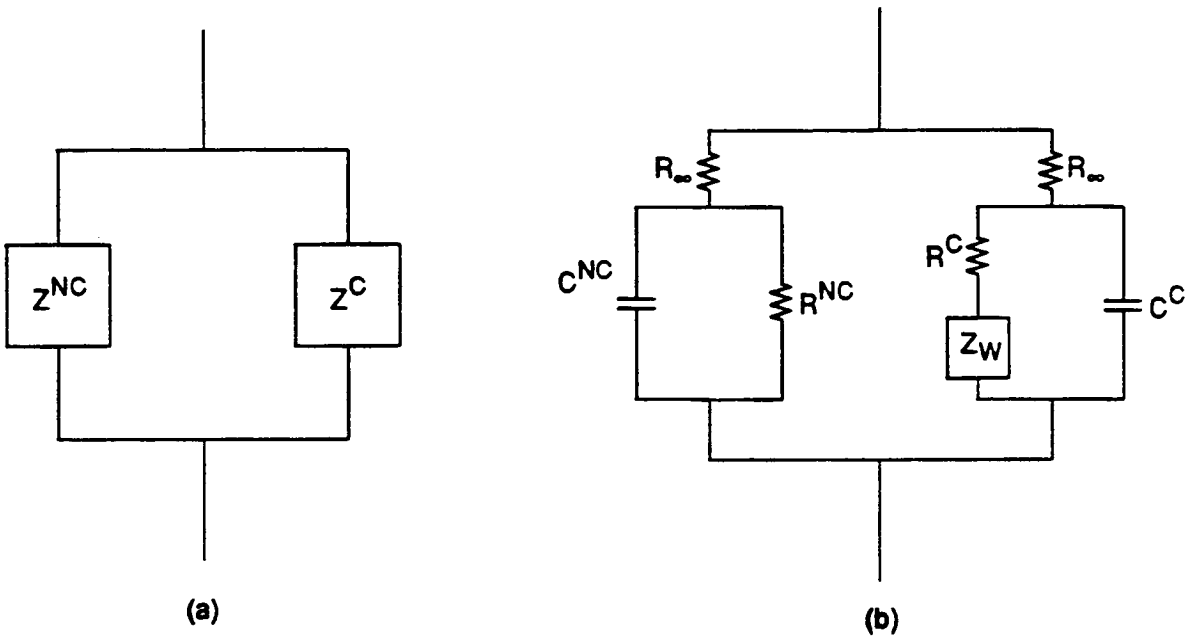

Figure 33. (a) General equivalent circuit for the rebar/concrete interfacial impedance of each segment, where Z^{NC} and Z^{C} correspond to the impedance of noncorroded and corroded areas, respectively. (b) Detailed equivalent circuits for Z^{NC} and Z^{C} (see text).

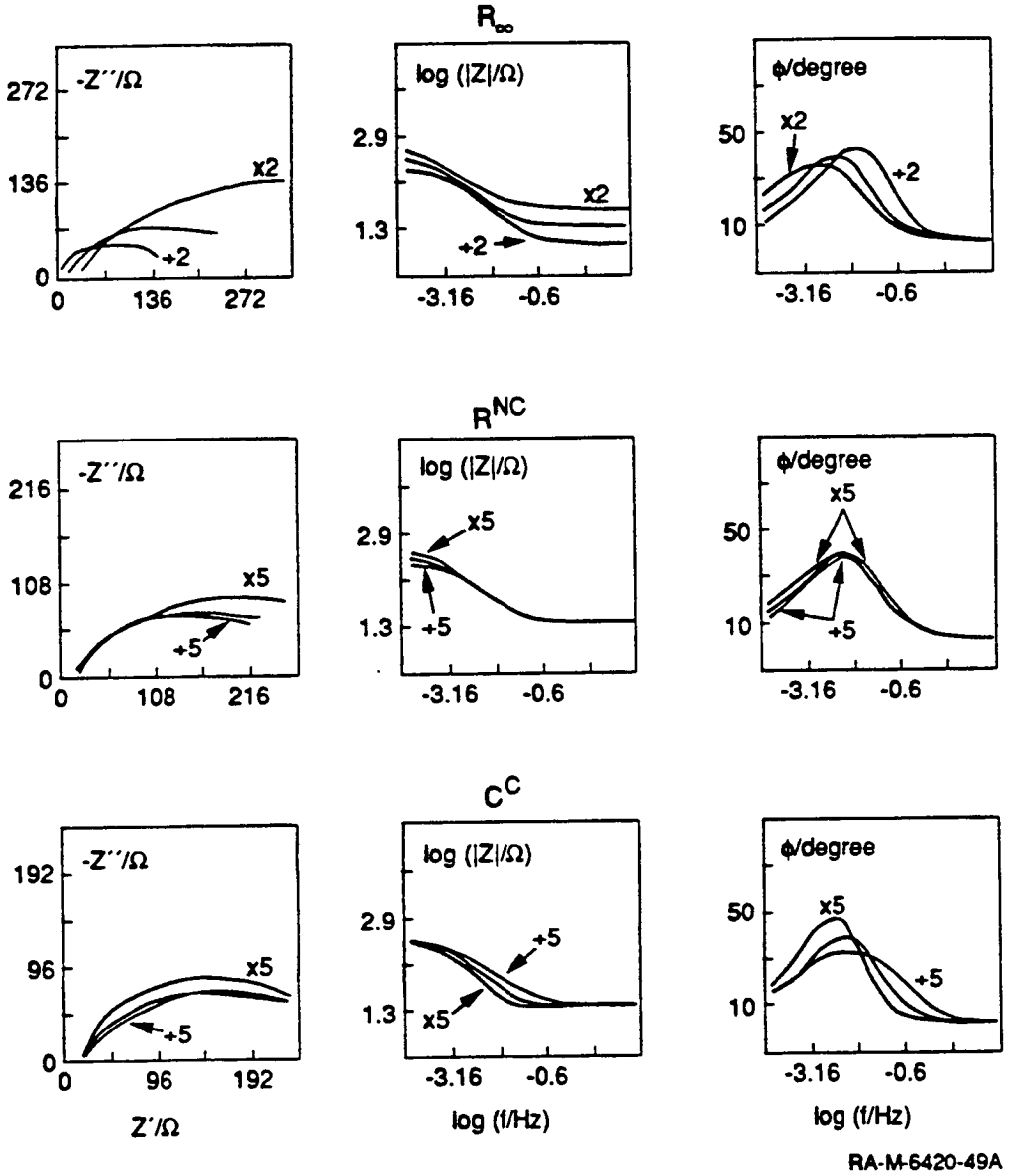

Figure 34. Changes in the complex-plane, Bode, and phase-angle plots due to variations in the values of R_{∞}, R^{NC}, and C^{C}.

Data for slab with 0% content of $CaCl_2$, Case 1, reference electrode at position 2, corrosion at middle site, Run No. 1, imposed AC current of 330 μA.

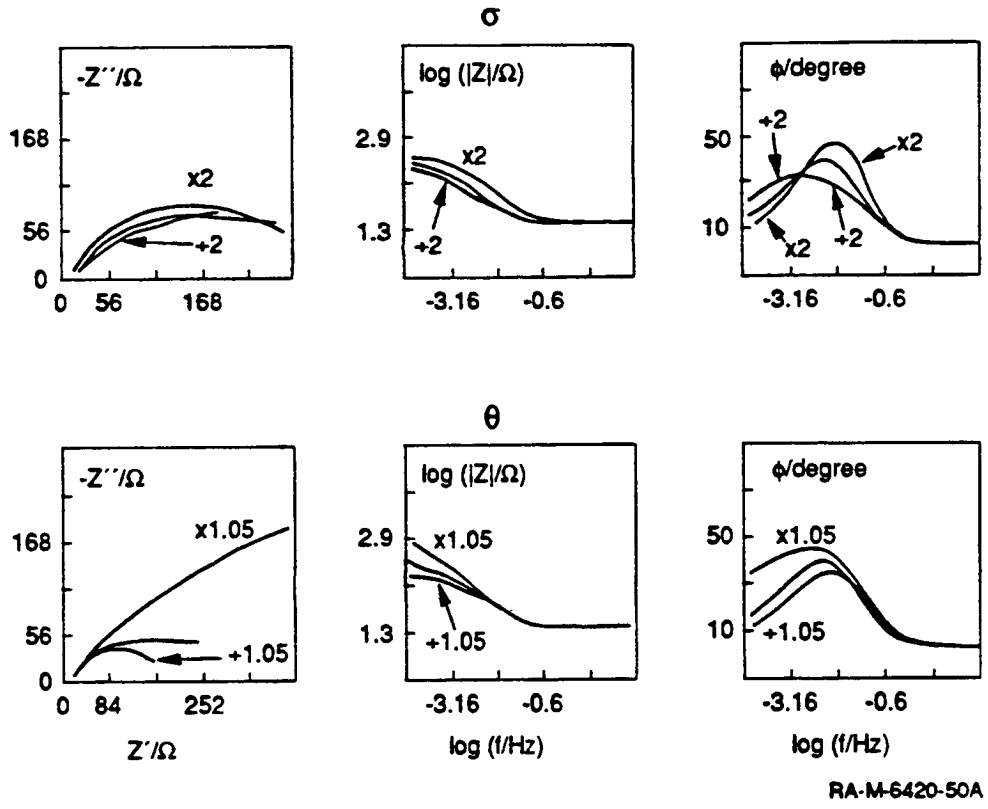

Figure 35. Changes in the complex-plane, Bode and phase-angle plots due to variations in the values of σ and θ.

Data for slab with 0% content of $CaCl_2$, Case 1, reference electrode at position 2, corrosion at middle site, Run No. 1, imposed AC current of 330 μA.

$$Z_k = \frac{Z^C \cdot Z^{NC}}{(1 - \theta)Z^C + \theta Z^{NC}} \qquad (8)$$

As shown in Figure 33(b), Z^{NC} can be viewed as an RC circuit in series with a high-frequency resistance (R_∞), while Z^C can be viewed as a Randles-type circuit in series with a high-frequency resistance (R_∞) and including a semi-infinite Warburg impedance due to oxygen diffusion. The Warburg term is given as

$$Z_W = \sigma(1 - j)\omega^{-1/2} \qquad (9)$$

where σ is the Warburg coefficient.

The complete set of equations for the transmission line models used here is given in the full technical report of this project. In all the numerical analyses carried out in this work, the number of segments in the transmission line has been kept constant and equal to seven.

MODEL FITTING AND RESULTS OBTAINED

The use of transmission line models to simulate impedance data for corroding rebar required the development of suitable computer algorithms. Initially, we thought that this could be simply accomplished by using a commercially available computer program, OPTDES, which was written especially to aid interactively in the optimization of models to describe experimental data. However, the efficient use of OPTDES depended on having reasonable initial values for the several parameters being optimized. In order to generate the initial values, we developed a computer program in BASIC 5.0 for HP 9816S computer that enabled us to vary the parameters employed in the transmission line model in an interactive manner to simulate the experimental impedance data (this simulation was quite stringent, since the complex-plane, Bode, and phase-angle plots for a specific data set were all required to be simulated by the model at the same time). A copy of this program is given in the final technical report.

Using the HP 9816S computer, we searched for appropriate values for the different parameters in the equations; we refer to the process as **fitting**. Fitting became possible after a sensitivity study, i.e., a study of how variations in the values of the different parameters (R_c, R_∞, R^{NC}, C^{NC}, R^C, C^C, σ, and θ) affect the theoretical data obtained and hence the theoretical complex-plane, Bode, and phase-angle plots. Results of the sensitivity study showed that variations in three (R_c, C^{NC}, and R^C) of the eight parameters did not greatly affect the results; thus, these parameters were kept constant thereafter. Figures 34 and 35 show how variations in R_∞, R^{NC}, C^C, σ, and θ affect the complex-plane, Bode, and phase-angle plots. Taking these variations into account, we find sets of values for the parameters resulted in good fits for each of the different experimental data sets. This fitting was carried out by fixing values for the different parameters and seeing (with the help of the HP 9816S computer) the resulting complex-plane, Bode, and phase-angle plots; then, depending on the resulting plots, the values of the parameters were

modified until satisfactory results were obtained. Thus, the values of the parameters were fixed by the computer operator using the previous sensitivity study as a guide.

Examples of the fittings obtained are shown in Figures 36 through 38 for the experimental configurations cited. By inspecting these figures, we infer that the theoretical fitting is good for all three plots; this is also the case for the majority of the experimental data obtained. Table 7 contains the fitted values for the different parameters of the transmission line model used. As can be seen from this table, the fitting of the data for each position of the reference electrode requires a different set of values for the model parameters. The use of the average value of these parameters was tested to describe the three different cases without success, confirming that each position of the reference electrode requires its own set of parameter values.

This finding is surprising because a single set of model parameters might be expected to describe the impedance function measured at all reference electrode positions. However, our experimental studies indicated that when the ac amplitude is large, the system response is not strictly linear, so that an equivalent circuit composed of passive elements, such as resistors and capacitors, cannot be used. In addition, the measurements were performed over several weeks, so that the system parameters (e.g., concrete/rebar impedance and concrete resistivity) may have changed with time.

We further explored the effect of reference electrode position by fabricating an electrical equivalent circuit (transmission line) using standard resistors and capacitors. By measuring the impedance with the reference electrode positioned at various distances down the line from the counterelectrode, we found the same trend in impedance with reference position as for the concrete slab. Furthermore, on fitting the transmission line model to the experimental data from the electrical equivalent circuit, we did indeed obtain different sets of parameters. The most likely explanation is that when the potential is sensed at any point other than that at which the current is sensed, the system is no longer of "minimum phase" as demanded by linear system theory.[22]

After the first fitting using the BASIC 5.0 program, if further refinements were necessary, then the OPTDES program can be used. For instance, if we want the theoretical and experimental complex-plane data to not differ much for the low-frequency range, we can achieve this by setting OPTDES to minimize the following function:

$$A = \sum_{i=1}^{n} \left(\frac{\log|Z^i_{exp}| - \log|Z^i_{calc}|}{\log|Z^{max}_{exp}|} \right)^2 \qquad (10)$$

where the summation is carried out over all (n) frequencies, $|Z^i_{exp}|$ is the experimental impedance modulus for frequency i, $|Z^i_{calc}|$ is the calculated (from the model) impedance modulus for the same frequency i, and $|Z^{max}_{exp}|$ is the highest value for the experimental impedance modulus in the frequency range of the specific data set being fitted. At the same time OPTDES can be set to keep the value of the following functions below specified values:

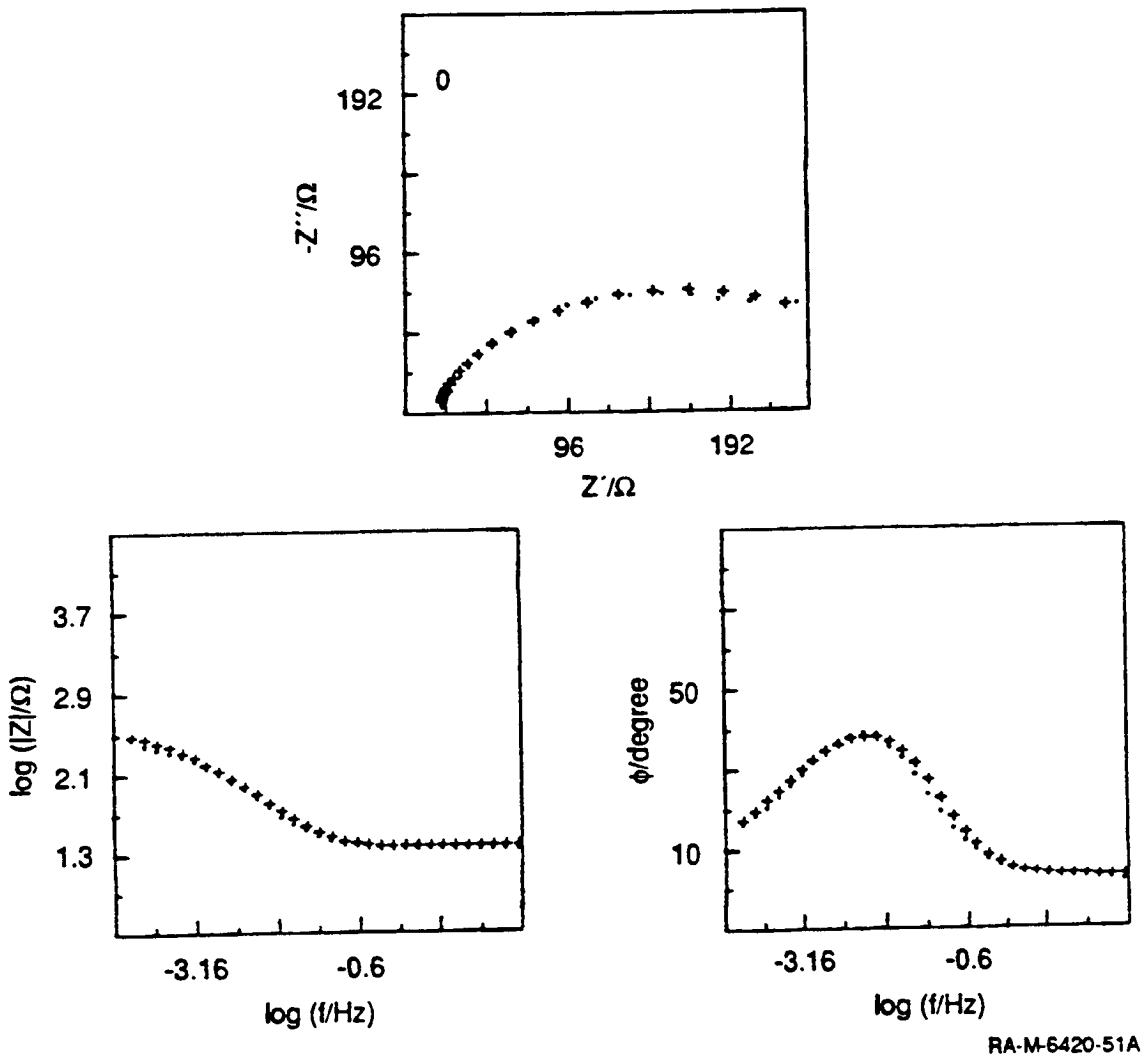

Figure 36. Experimental (•) and theoretical (+) complex-plane, Bode, and phase-angle plots for experimental configuration, Case 1: slab with 0% content of $CaCl_2$, corrosion at middle site, Run No. 1, imposed AC current of 330 μA, reference electrode at position 2 (see text).

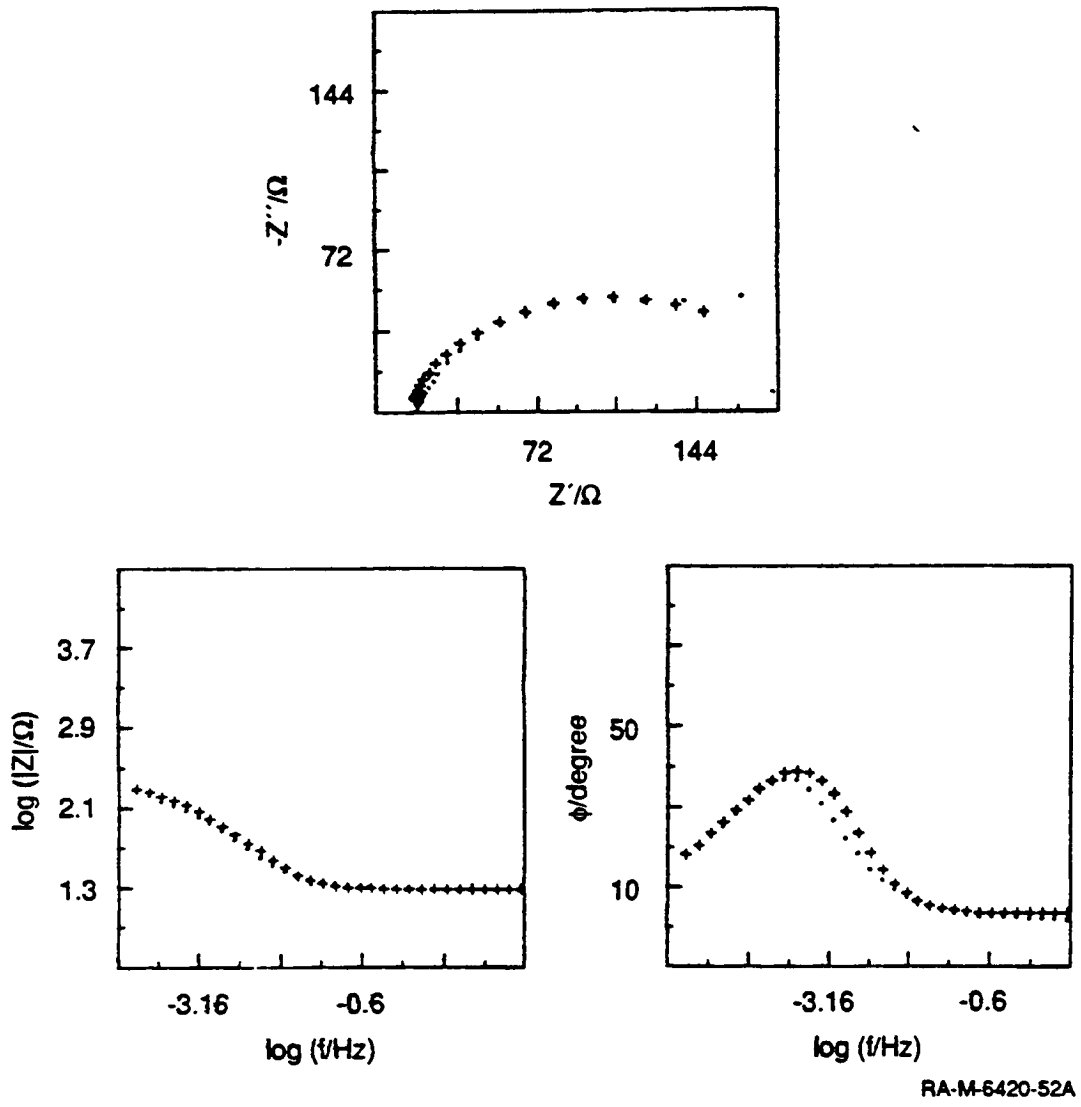

Figure 37. Experimental (•) and theoretical (+) complex-plane, Bode, and phase-angle plots for same experimental configuration as that for Figure 32, except reference electrode is at position 5 (see text).

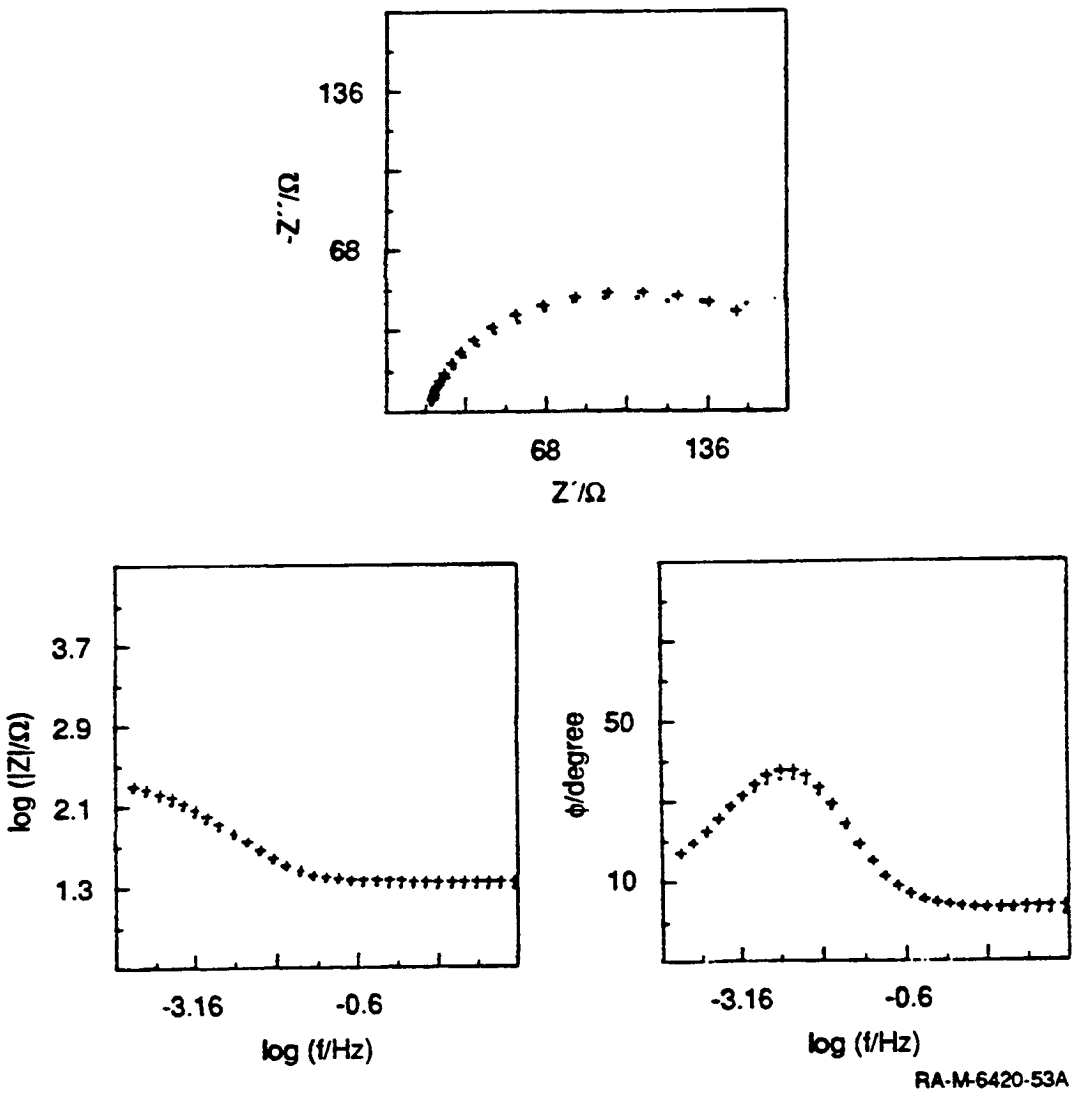

Figure 38. Experimental (•) and theoretical (+) complex-plane, Bode, and phase-angle plots for same experimental configuration as that for Figure 32, except reference electrode is at position 8 (see text).

Table 7

FITTED VALUES FOR THE DIFFERENT PARAMETERS OF THE TRANSMISSION LINE MODEL USED TO SIMLUATE THE RESULTS FOR EXPERIMENTAL CONFIGURATIONS[a]

	Reference Electrode Position		
Parameters	2	5	8
$R_s/(\Omega.cm)$	945.0	945.0	945.0
$R_\infty/(\Omega.cm^2)$	12000.0	55000.0	95000.0
$R^{NC}/(\Omega.cm^2)$	300.0	300.0	300.0
$C^{NC}/(\mu F.cm^{-2})$	10.0	10.0	10.0
$R^C/(\Omega.cm^2)$	0.5	0.5	0.5
$C^C(\mu F.cm^{-2})$	75.0	50.0	25.0
$\sigma/(\Omega.cm^2.s^{-1/2})$	9000.0	18000.0	25000.0
Θ	0.942	0.820	0.750

[a]Slab with 0% content of $CaCl_2$, case 1, corrosion at middle site, imposed ac current of 330 μA, run no. 1, and reference electrode position as shown.

$$B = \sum_{i=1}^{n} \left(\frac{\phi^{i}_{exp} - \phi^{i}_{calc}}{\phi^{max}_{exp}} \right)^2 \quad (11)$$

$$C = \sum_{i=1}^{m} \left| Z'^{i}_{exp} - Z'^{i}_{calc} \right| \quad (12)$$

and

$$D = \sum_{i=1}^{m} \left| Z''^{i}_{exp} - Z''^{i}_{calc} \right| \quad (13)$$

where ϕ is the phase angle, Z' is the real component of the impedance, Z" is its imaginary component, and m is the number of low-frequency data points for which the fitting should be optimized. The final technical report contains a copy of the computer subroutine for OPTDES that carries out such a fitting for m = 7.

In summary, we were able to successfully model experimental impedance data for rebar in concrete in terms of an electrical transmission line. Consequently,we can derive the value for the polarization resistance for the rebar/concrete interface (see below) and also map the distribution of corrosion, provided a reasonable understanding of the model parameters is gained. While our work has demonstrated the sensitivity of the impedance function to corrosion of rebar, we have not developed ULFACIS as a practical tool; doing so would require additional theoretical and experimental work to derive suitable data analysis algorithms and to explore the ultimate sensitivity of the method.

The importance of the work described above lies in our demonstration that the electrical properties of reinforcing bar in concrete may be modeled using an electrical transmission line. Thus, we are now in the position of possessing the necessary techniques for extracting the polarization resistance from measured impedance data and to use this quantity to estimate the corrosion rate of the rebar. It is important to note that, because the length of the rebar sampled by the electrical perturbation increases as the frequency decreases, it is not possible to determine the true polarization resistance (R_p) directly from the impedance locus of the type illustrated in Figure 4(a) even though in the past many authors have erroneously assumed that R_p is equal to $R_{int} - R_u$.

4

MEASUREMENT OF CORROSION RATE

In the previous sections, we explored the viability of ULFACIS for surveying corroding rebar to determine the position(s) at which corrosion occurs in nonuniform, one-dimensional extended structures. However, Feliu et al.[11] have argued that in salt-impregnated structures, such as bridge decks and highways, corrosion quickly extends across the entire rebar lattice so that the need to locate specific areas of attack may be moot. In these cases, it is more important to obtain a reliable measure of the polarization resistance, from which the corrosion rate may be calculated. The direct estimation of the "true" polarization resistance (R_p) of embedded metallic bars in concrete is not feasible because the distance that the electrical signal applied to the concrete-rebar system extends down the bar increases as the frequency is lowered. Accordingly, the area sampled is frequency dependent, and the measured polarization resistance yields erroneous estimates of the corrosion rate when used in the Stearn-Geary equation. Furthermore, embedded rebar is a dynamic system whose electrical characteristics change with time and as changes occur in the environment. Consequently, the concrete resistivity and the interfacial impedance (impedance between the concrete and the rebar) may themselves be time-dependent quantities. These factors must be taken into account when any electrochemical technique is attempted to measure R_p.

As noted above, the accurate determination of the polarization resistance is not a simple matter because the electrical perturbation becomes increasingly attenuated with distance from the point of application. Because the rebar can be described as an electrical transmission line, we have previously argued that the area of rebar sampled using any time- or frequency-dependent perturbation increases as the time from application of the signal increases or as the frequency decreases. Nonetheless, the possibility of estimating the polarization resistance, R_p, in a large reinforced concrete slab by means of simple, remote measurements is very attractive to engineers in the field because it would permit rapid,

nondestructive survey of corrosion damage to reinforced concrete structures. In this section, we describe a method for determining the polarization resistance, and hence the rebar corrosion rate, using ac impedance spectroscopy.

The proposed method is based on the transmission line model described in the previous section. Feliu et al[12,13] developed a similar approach, but they assumed that the rebar-concrete system could be represented by a completely nonreactive model. Their approach is valid only if the impedance of the rebar-concrete system can be measured at sufficiently *low* frequencies that the phase angle $\phi \rightarrow 0$. Our experience indicates that this is seldom the case (e.g., see Figure 8), so that we will explore the more general, reactive case for which the interfacial impedance is represented as a parallel combination of resistance and capacitance (Figure 39).

The technique developed in this work, which we refer to as ZSCAN®, makes use of our finding that the electrical properties of rebar in concrete can be described in terms of an electrical transmission line equivalent circuit (Figure 40). In reality we have chosen a bifurcated transmission line to recognize the fact that the rebar generally extends in two directions from the monitoring point (x = 0) and we recognize that the lengths of the two arms may not be equal. By applying Kirchoff's equations to a small increment of the line, as described elsewhere (see Final Technical Report), we are able to derive the following expression for the impedance of the rebar/concrete system

$$Z_T(\Omega) = \frac{V}{I}\Big]_{x=0} = \frac{-(R_c Z)^{1/2} + \left(e^{-2\alpha L} + 1\right)\left(e^{-2\alpha M} + 1\right)}{\left(e^{-2\alpha L} - 1\right)\left(e^{-2\alpha M} + 1\right) + \left(e^{-2\alpha L} + 1\right)\left(e^{-2\alpha M} - 1\right)} \qquad (14)$$

where R_c is the resistance per unit length of the concrete,

$$\alpha = \sqrt{R_c/Z} \qquad (15)$$

and Z is the impedance per unit length of the bar.

To complete the derivation, we describe the impedance of the steel/concrete interface in terms of the electrical equivalent circuit shown in Figure 39. Accordingly,

$$Z/dx = R_s + \frac{\hat{R}_p}{1+\omega^2 \hat{R}_p^2 \hat{C}_c^2} - j\frac{\omega \hat{R}_p^2 \hat{C}_c}{1+\omega^2 \hat{R}_p^2 \hat{C}_c^2} \qquad (16)$$

where R_s is a series resistance, ω is the circular frequency, and $\hat{R}_p$ and $\hat{C}_c$ are the polarization resistance and interfacial capacitance, respectively, per unit length of the rebar. These latter two quantities are related to the specific parameters as

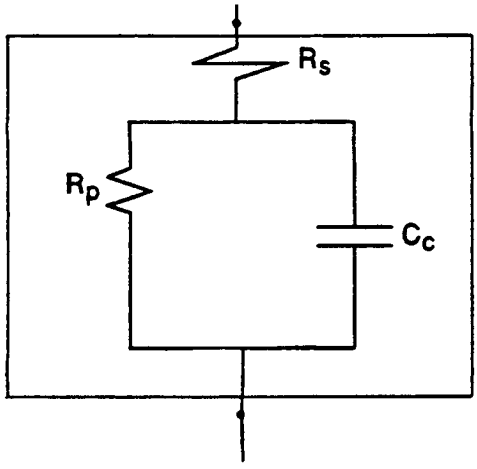

Figure 39. Electrical model for the specific interfacial impedance.

R_p = polarization resistance, C_c = interfacial capacitance, R_s = series resistance.

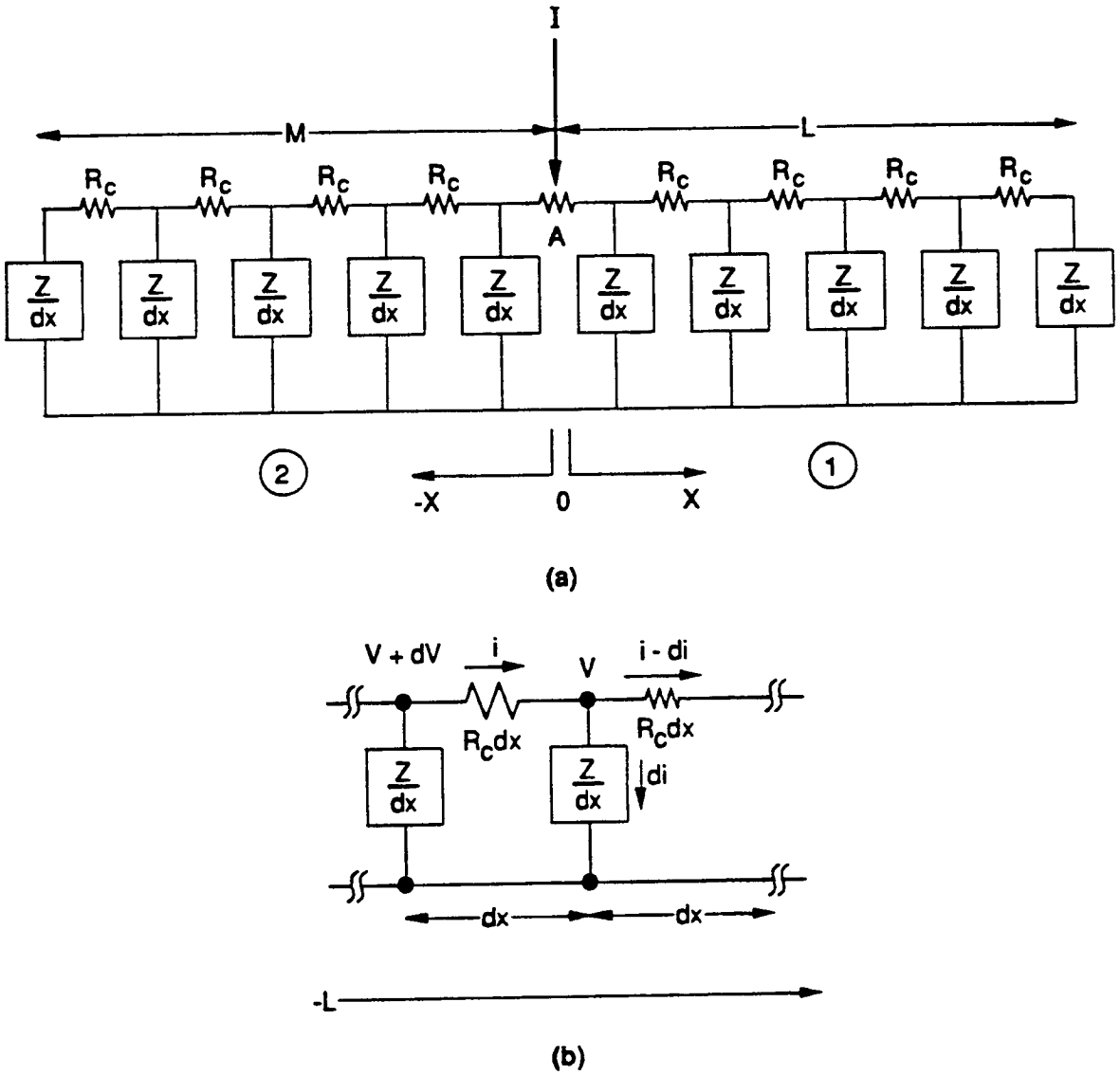

Figure 40. Equivalent circuit representation of a uniform-finite transmission line.

(a) Schematic representation of a finite transmission line where the current I is applied at the point A, distant L cm from the right end and M cm from the left end. (b) Detailed node analysis of an infinitesimally small element in the L branch.

$$\hat{R}_p = Rp/2\pi rdx \tag{17}$$

$$\hat{C}_c = 2\pi rdx.C_c \tag{18}$$

where r is the radius of the rebar. Our objective, then, is to fit the transmission line model to experimental impedance data to extract values for R_s, R_c, R_p, and C_c. The analytic problems that we faced were clearly ones of the desired quantities being deeply buried in the model and the nonlinear dependence of the impedance on the interfacial parameters.

The optimization procedure employed in this study is based on our previous work on the degradation of porous $Ni(OH)_2/NiOOH$ battery electrodes on cyclic charging/discharging in alkaline solutions.[23] In that study, we developed an optimization procedure for estimating the parameters of a transmission line that was used to represent the porous electrode after preselected numbers of cycles. In this regard, our present application is comparable to the previous one. The core of the optimization procedure makes use of OPTDES,[24] which is a software package used to perform fitting of data to a preconceived model involving several variables related in a linear or highly nonlinear manner. The fitting procedures are used to extract values for the variables when a function to be minimized is given and a set of constraints is listed. We defined the function to be minimized as

$$F = \sum_{i=1}^{N} \left(\frac{Z_c'(\omega_i) - Z_e'(\omega_i)}{Z_c'(\omega_i) + Z_e'(\omega_i)} \right)^2 + \sum_{i=1}^{N} \left(\frac{Z_c''(\omega_i) - Z_e''(\omega_i)}{Z_e''(\omega_i) + Z_c'(\omega_i)} \right)^2 \tag{19}$$

subject to the following two constraints:

$$F_i = \left(\frac{|Z_e(\omega_i)| - |Z_c(\omega_i)|}{|Z_e(\omega_i)| + |Z_c(\omega_i)|} \right)^2 \tag{20}$$

$$F_{i+N} = \frac{1}{\omega_i} \left(\frac{\theta_e(\omega_i) - \theta_c(\omega_i)}{\theta_e(\omega_i) + \theta_c(\omega_i)} \right)^2 \tag{21}$$

where Z' and Z" are the real and imaginary components of the impedance $|Z(\omega_i)|$ is the impedance magnitude, $\theta(\omega_i)$ the phase angle, w_i the circular frequency, and subscripts "c" and "e" designate calculated and experimental quantities, respectively. The constraints are that the individual differences between calculated and experimental impedance magnitude and phase angle at different circular frequencies w_i should not exceed 0.1.

As previously noted, the rebar/concrete interface is represented by a parallel combination of the polarization resistance and a capacitance in series with the concrete resistance in the direction perpendicular to the surface (Figure 39 and 41). The parameters that we wish to extract directly from the fitting procedure, when the function F is minimized, are the interfacial concrete resistance, R_c, the series resistance, R_s, the polarization resistance, $\hat{R}_p$, and interfacial capacitance, $\hat{C}_c$, all per unit length of the rebar. The input parameters for the minimization procedure are:

R_c (Ω/cm)	Concrete resistance per unit length
L (cm)	Distance between the point where the impedance is measured and the left end of the system
M (cm)	Distance between the point where the impedance is measured and the right end of the system
$Z(\omega) = Z'(\omega) - jZ''(\omega)(\Omega)$	Impedance of the concrete-rebar system
r (cm)	Radius of rebar
ω(rad/s)	Circular frequency

During our initial work on this problem, we found that multiple solutions (that is, different combinations of R_c, R_s, R_p, and $\hat{C}_c$) existed that appeared to represent the impedance characteristics equally well. However, the problem of selecting the most appropriate set is greatly eased by noting that at an effectively infinite frequency $Z = R_s dx$ and hence

$$Z_T(\omega \rightarrow \infty) = (R_c R_s dx)^{1/2} \tag{22}$$

or

$$R_s = Z_T^2(\omega \rightarrow \infty)/(R_c dx) \tag{23}$$

The problem is further eased by assuming that we know the resistance of the concrete per unit length, R_c, which we may estimate from the concrete resistivity and the geometry of the system.

If the impedance data can be measured at sufficiently high and low frequencies or can be extrapolated so that the impedance locus intercepts the real axis at both limits, then from Equation (16), we may write

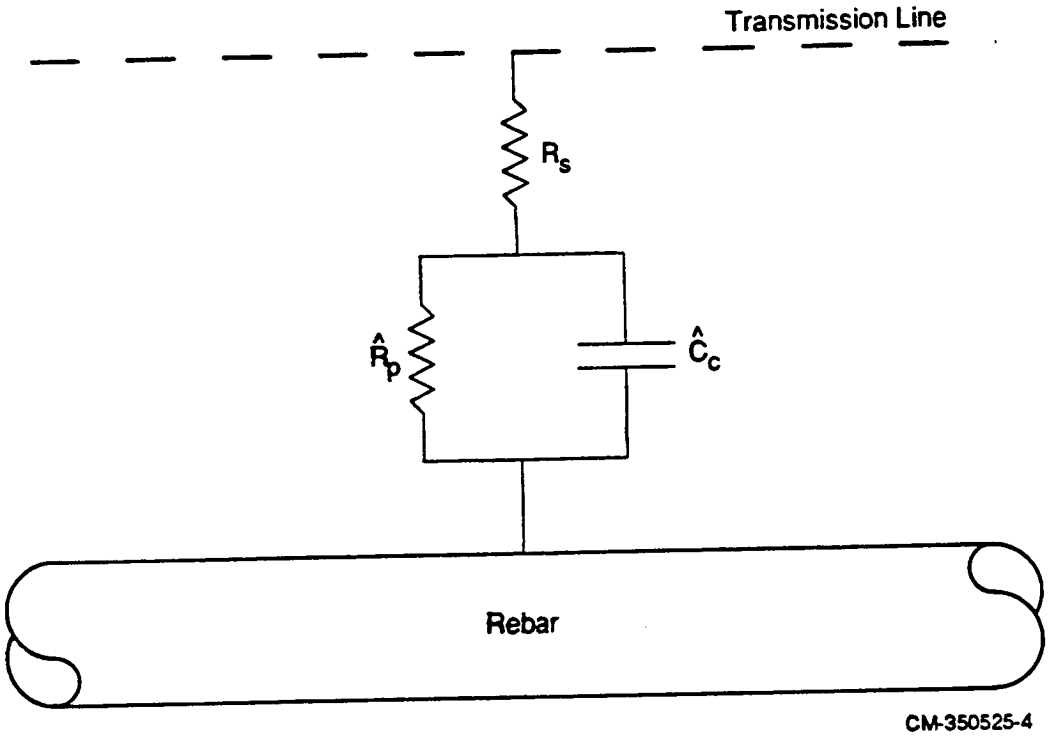

Figure 41. Equivalent circuit assumed for the concrete/rebar interface.

$$Z'_{T\infty} = (R_c R_s dx)^{1/2} \quad (24)$$

and

$$Z'_{T0} = (R_c R_s dx + \hat{R}_p R_c dx)^{1/2} \quad (25)$$

and, hence

$$\hat{R}_p = [(Z'_{T0})^2 - (Z'_{T\infty})^2]/(R_c dx) \quad (26)$$

Note that this procedure for estimating an initial value for $\hat{R}_p$ applies strictly to an infinite transmission line and requires an *a priori* estimate of R_c. However, Equation (24) has proved to be most useful for estimating an initial value for R_p for the optimization procedure described in this paper.

Any physically realistic model fitted to experimental data using well-formulated minimization and constraint functions will yield not only a calculated impedance that emulates the experimental data but also physically sensible and accurate values of the variables R_s, R_p, and C_c. Since no *a priori* method exists for determining the accuracy of parameter values calculated from the experimental data (because we have no independent knowledge of these values), we tested the fitting procedure using synthetic impedance data by comparing the calculated parameters with those initially used to generate the "experimental" impedance using the transmission line model. Numerous trials using synthetic data yielded excellent results, with the theoretical values for the parameters R_s, R_p, and $\hat{C}_c$ being retrieved regardless of the initial guesses employed in the optimization procedure with $1 < R_s < 1000\ \Omega$, $100 < R_p < 100{,}000\ \Omega \cdot cm^2$, and $0.000005 < C_c < 0.1$ F/cm^2. These values are considered to be representative of those that are found for corroding rebar in concrete. The numerical analyses summarized above demonstrate that the analytical procedures developed in this work are capable of yielding accurate values for the polarization resistance as well as the corrosion capacitance and series resistance, provided the electrical properties of the rebar/concrete system can be adequately modeled by the transmission line shown in Figure 40.

Because the method requires independent knowledge of the concrete resistivity, it is important to assess the sensitivity of the values obtained for R_s, R_p and $\hat{C}_c$ to the value assumed for R_c. This sensitivity relationship was explored by introducing systematic errors of +20%, +10%, -10%, and -20% into the value of R_c. The results are shown in Table 8. Clearly, we were able to retrieve the values for R_s and $\hat{C}_c$ exactly, regardless of the uncertainty in R_c, and the error in R_p is negligible. Therefore, moderate uncertainty in the concrete resistivity, as might be experienced in the field, can be tolerated by the analytical procedure developed in this work.

We used the procedure developed in this work to extract corrosion parameters from impedance data obtained on actual rebar/concrete slabs employed in this study. While the experimental configuration is not ideal, in that the counter and reference electrodes were not coincident (i.e. concentric) as depicted in the transmission line model shown in Figure 40, we obtained $\hat{R}_p$ values ranging from 1×10^2 to $1 \times 10^9\ \Omega$, R_s values ranging from 0 to 100 Ω, and $\hat{C}_c$ values ranging from 1000 to 5000 μF for rebar in concrete that does not

Table 8

CALCULATED VALUES OF POLARIZATION RESISTANCE (R_p), CORROSION CAPACITANCE (C_c) AND SERIES CONCRETE RESISTANCE (R_s) (SEE FIGURE 37) AS A FUNCTION OF THE ERROR INTRODUCED IN THE VALUE OR THE CONCRETE RESISTIVITY (R_c)

% Error in Concrete Resistivity, R_c	Concrete Resistivity, R_c (Ω/cm)	Polarization Resistance, R_p (Ω-cm^2)	Series Concrete Resistance, R_s (Ω)	Corrosion Capacitance, C_c (μF/cm^2)
		Obtained from OPTIDES		
-20	400	6004	30.09	69.90
-10	450	6004	30.09	69.90
+10	550	6003	30.09	69.90
+20	600	6003	30.09	69.90
		Actual Values[a]		
		6000	30	70
		Initial Guesses[b]		
		3640	55	10^4

[a]These values were used for calculating the synthetic data.
[b]The same initial guesses were used in conjunction with all concrete resistivity values.

contain $CaCl_2$. We consider these values to be reasonable. The value for $\hat{R}_p$ may then be used to calculate the true polarization resistance, R_p, by inserting the radius of the rebar (r) and the increment length (dx) into Equation (17). Subsequently, R_p may be used to estimate the corrosion rate using the Stern-Geary equation.

$$i_{corr} = \beta_a\beta_c/2.303\, R_p(\beta_a + \beta_c) \tag{27}$$

where the corrosion current (rate) is in units of amperes per square centimeter and β_a and β_c are the Tafel constants for the anodic and cathodic reactions, respectively. Equation (27) may be integrated to yield the damage function (weight loss) between times t_1 and t_2 $(\Delta W]_{t_1}^{t_2})$ as

$$\Delta W]_{t_1}^{t_2} = \frac{M\beta_a\beta_c}{2.303\ nF(\beta_a + \beta_c)} \int_{t_1}^{t_2} \frac{1}{R_p}\, dt \quad (gm/cm^2) \tag{28}$$

where M is the atomic weight of iron (56 gms/mol), n is the oxidation charge (n = 2 for iron in concrete), and F is Faraday's constant (F = 96,487 C/equiv.). Assuming uniform attack, the depth of penetration of corrosion into the rebar over the period t_1 to t_2 is then simply given as

$$\Delta L]_{t_1}^{t_2} = \frac{M\beta_a\beta_c}{2.303\ nF\rho(\beta_a + \beta_c)} \int_{t_1}^{t_2} \frac{1}{R_p}\, dt \tag{29}$$

where ρ is the density of iron (ρ = 7.8 gm/cm^3 at 20°C).

To illustrate how these equations may be applied, consider the case of rebar of 1/2-inch diameter (1.27 cm) corroding in concrete. Assuming that the polarization resistance corresponds to that for the most corrosive conditions explored in this work (R_p = 1000Ω•cm^2) and that $\beta_a\beta_c/(\beta_a + \beta_c) \sim 0.06$ V, which is considered to be realistic for corroding rebar, we obtain

$$\Delta W]_{t_1}^{t_2} = \frac{56 \times 0.06}{2.303 \times 2 \times 96{,}487 \times 1000} (t_2 - t_1) = 7.56 \times 10^{-8}(t_2 - t_1) \ (gm/cm^2) \tag{30}$$

and

$$\Delta L]_{t_1}^{t_2} = 9.69 \times 10^{-9}\ (t_2 - t_1) \quad (cm) \tag{31}$$

Thus, for a period of one year (3.15×10^7 s) the specific weight loss and penetration depth are found to be 0.24 gm/cm^2 and 0.31 mm (12 mils), respectively. For non-corroding rebar (that in chloride-free concrete), polarization resistance values several orders of magnitude higher than that noted above were found corresponding to negligible weight loss and penetration.

We end this discussion by commenting on the significance of measuring corrosion rates of rebar in concrete with respect to the type of damage that is observed. As stated at the beginning of this report, the principal damage arises from spalling of the concrete cover rather than loss of structural strength of the rebar. Spalling occurs because concrete has poor tensile strength and the conversion of iron into corrosion product result in the generation of tensile stresses at the rebar/concrete interface. Indeed, the volume change resulting from corrosion is best expressed in terms of the Pilling-Bedworth ratio

$$\text{PBR} = \frac{\text{Volume of corrosion products}}{\text{Volume of metal corroded}} \tag{32}$$

which ranges from ~2.5 to 3.5 for the corrosion of iron in aqueous media, depending on the exact corrosion products formed. In principle, it should be possible (on purely mechanical grounds) to estimate the maximum volume change (V_m) that can be tolerated at the rebar/concrete interface without spalling the concrete. Accordingly, by combining Equations (29) and (32) we obtain an expression for the service life (t_f) of the structure

$$\int_0^{t_f} \frac{1}{R_p} dt = \frac{2.303nF\rho(\beta_a + \beta_c)V_m}{M\beta_a\beta_c(\text{PBR-1})} \tag{33}$$

Solution of this integral equation is rendered simple by assuming that the polarization resistance (corrosion rate) remains constant with time, in which case

$$t_f = \frac{2.303nF\rho(\beta_a + \beta_c)V_m R_p}{M\beta_a\beta_c(\text{PBR-1})} \tag{34}$$

Substitution for the constants and for the parameters for iron yields

$$\begin{aligned} t_f &= 1.03 \times 10^6 \, V_m R_p/(\text{PBR-1}) \qquad \text{(s)} \\ &= 0.033 \, V_m \, R_p/(\text{PBR-1}) \qquad \text{(year)} \end{aligned} \tag{35}$$

By way of illustration, assume that V_m is 20%* of the volume of the rebar. In this case, for a rebar of 1/2-inch diameter, we obtain $V_m = 0.25$ cm^3 per centimeter length so that the service life becomes

$$t_f = 4.29 \times 10^{-4} R_p \qquad \text{(Year)}$$

assuming a Pilling-Bedworth ratio of 3 for the corrosion products. For rapidly corroding concrete, R_p is of the order of 10^3-10^4 Ω•cm$_2$ in which case spalling might be expected within five years after construction whereas chloride free reinforced concrete ($R_p > 10^6$ Ω•cm^2) is not expected to fail by spalling within the design life of the structure.

The calculations presented above are necessarily approximate because some of the quantities are poorly defined. Nevertheless, the analysis provides considerable insight into the causes of failure and identifies those parameters that have the greatest influence on the service life of a structure. Thus, for failure to occur, PBR > 1, which is always the case for iron (or for any other metal of interest). Clearly, the service life of the structure depends upon the increase in volume of the corrosion products over the metal lost and hence upon the thickness and porosity of that concrete cover and the mechanical properties of the matrix. However, it is difficult to see how V_m may be changed by more than a factor of two for most structures so that changes in structure design and concrete properties are likely to yield only modest increases in the service life. On the other hand, the polarization resistance may change by many orders of magnitude implying that the most fruitful avenue for life extension lies in better corrosion control. However, this will not be possible without developing an accurate method for the *in situ* measurement of the rebar polarization resistance, which was one of the goals of the present work.

* This value will depend on the porosity of the concrete, the thickness of the concrete cover, and on the concrete mechanical properties.

5

FUTURE TECHNOLOGY TRANSFER TO THE FIELD

While much of the work reported here is fundamental in nature, in that we sought to develop an understanding of the physical and electrochemical nature of the corrosion of rebar in concrete, we have solved the problem of extracting the polarization resistance from impedance data and hence we have developed a more accurate and reliable method (ZSCAN®) for measuring corrosion rate. This development is most important for the engineer in the field because we can offer, for the first time, a practical technique, soundly based on theory, for nondestructively surveying rebar with respect to corrosion rate. We believe that relatively simple, cost- effective instrumentation can be developed to provide this important capability to surveying crews. However, the practicality and ultimate accuracy of ZSCAN® can only be assesssed and demonstrated by developing and evaluating the instrumentation and software in cooperation with engineers in the field on actual concrete structures.

The ZSCAN® instrument package would consist of five components: (1) counter and reference electrode assembly, (2) a controlled current oscillator that can generate a sinusoidal current of suitable amplitude over a wide frequency range, (3) data aquisition hardware/software including a transfer function analyzer driven by a microcomputer, (4) data analysis software based on the OPTDES optimization algorithm, and (5) a-four electrode probe for measuring concrete resistivity. It is too early to estimate the cost of such a package, but we note that inexpensive transfer function analyzers, such as that offered by CPCIS/Voltech Instruments Ltd., UK, for £1800 (~$2900), are now becoming available. We envisage that the entire instrument package including the computer and operator station could be accommodated in a small utility van. In this way, the instrument would be highly mobile and could be used to survey a large number of structures over a wide geographical area efficiently and cost effectively.

6

REFERENCES

1. Proc. Symp. Corrosion Steel Reinf. Concr. Constr., Soc. Chem. Ind. London (1979).

2. J. E. Slater, "Corrosion of Metals in Association with Concrete," ASTM STP 818, ASTM, Philadelphia, PA (1983).

3. Proc. Conf. Cath. Prot. Reinforced. Concr. Bridge Decks, NACE, Houston, TX (1985).

4. D. D. Macdonald, M.C.H. McKubre, and M. Urquidi-Macdonald, Corrosion-NACE, **44**, 2 (1988).

5. J. L. Dawson, J. A. Richardson, L. M. Callow and K. Hladky, "Electrochemical Impedance Measurements Applied to the Corrosion of Reinforced Steel in Concrete," CORROSION/78, Paper 125, NACE, Houston, TX (1978).

6. D. G. John, P. C. Searson, and J. L. Dawson, Br. Corrosion J., **16**, 102 (1981).

7. P. Lay, P. F. Lawrence, N. J. Wilkins, and D. E. Williams, J. Appl. Electrochem., **15**, 755 (1985).

8. K. Matsuoka, "Monitoring of Corrosion of Reinforcing Bar in Concrete," CORROSION/87, Paper 121, NACE, Houston, TX (1987).

9. A. A. Sagues, "Corrosion Measurements of Reinforcing Steel in Concrete Exposed to Various Aqueous Environments," CORROSION/87, Paper 118, NACE, Houston, TX (1987).

10. D. G. John et al, "Corrosion Measurements on Reinforcing Steel and Monitoring of Concrete Structures," CORROSION/87, Paper 136, NACE, Houston, TX (1987).

11. S. Feliu, J. A. Gonzalez, M. C. Andrade, and V. Feliu, "On-site Determination of the Polarization Resistance in a Reinforced Concrete Beam," CORROSION/87, paper 145, Houston, TX (1987).

12. S. Feliu, J. A. Gonzalez, M. C. Andrade, and V. Feliu, Corrosion Eng., **44**, 761 (1988).

13. S. Feliu, J. A. Gonzalez, M. C. Andrade, and V. Feliu, Corrosion Sci., **29**, 105 (1989).

14. J. J. Coleman, Trans. Electrochem. Soc., **90**, 545 (1946).

15. R. de Levie, Electrochim. Acta, **9**, 1231 (1964).

16. R. de Levie, Electrochim. Acta, **10**, 113 (1965).

17. R. de Levie, in *Advances in Electrochemistry and Electrochemical Engineering*, Vol. 6, P. Delahay and C. W. Tobias, Eds., Interscience, New York, 1967, pp. 329-397.

18. M.C.H. McKubre, "An Impedance Study of the Membrane Polarization Effect in Simulated Rock Systems," Ph.D. Thesis, Victoria University, Wellington, New Zealand (1976).

19. S. Atlung and T. Jacobsen, Electrohim. Acta, **21**, 575 (1976).

20. J. R. Park and D. D. Macdonald, Corrosion Sci., **23**, 295 (1983).

21. S. J. Lenhart, D. D. Macdonald, and B. G. Pound, "Restructuring of Porous Nickel Electrodes," Proc. 19th IECEC Conference, San Francisco, (1984), p. 875.

22. H. W. Bode, *Network Analysis and Feedback Amplifier Design*, Van Nostrand, New York, 1945.

23. D. D. Macdonald and M. Urquidi-Macdonald, J. Electrochem. Soc., **132**, 2316 (1985).

24. M. Urquidi-Macdonald, S. Real, and D. D. Macdonald, J. Electrochem. Soc., **133**, 2018 (1986).

25. M. Stern and A. L. Geary, J. Electrochem. Soc., **104**, 56 (1957).

26. S. J. Lenhart, D. D. Macdonald, and B. G. Pound, J. Electrochem. Soc., **135**, 1063 (1988).